NASA Technical Memorandum 4710
ATCOM Technical Report 96-A-005

Wind Tunnel Test Results of a 1/8-Scale Fan-in-Wing Model

John C. Wilson
Joint Research Program Office, Aeroflightdynamics Directorate
U.S. Army Aviation and Troop Command
Langley Research Center • Hampton, Virginia

Garl L. Gentry
Langley Research Center • Hampton, Virginia

Susan A. Gorton
Joint Research Program Office, Aeroflightdynamics Directorate
U.S. Army Aviation and Troop Command
Langley Research Center • Hampton, Virginia

National Aeronautics and Space Administration
Langley Research Center • Hampton, Virginia 23681-0001

May 1996

Available electronically at the following URL address: http://techreports.larc.nasa.gov/ltrs/ltrs.html

Printed copies available from the following:

NASA Center for AeroSpace Information
800 Elkridge Landing Road
Linthicum Heights, MD 21090-2934
(301) 621-0390

National Technical Information Service (NTIS)
5285 Port Royal Road
Springfield, VA 22161-2171
(703) 487-4650

Summary

A 1/8-scale model of a fan-in-wing concept was tested in the Langley 14- by 22-Foot Subsonic Tunnel. The concept is a design (identified as the model 755) which Grumman Aerospace Corporation (now Northrup Grumman) considered for development for the U.S. Army. Hover testing was conducted in a model preparation area near the tunnel. Height above a pressure-instrumented ground plane, angle of pitch, and angle of roll were varied for a range of fan thrust. In the tunnel, angles of attack and sideslip, height above the tunnel floor, and wind speed were varied for a range of fan thrust. The air loads and surface pressures on the model were measured for several configurations in the model preparation area and in the tunnel. The major configuration change was that of varying the vane angles that were attached to the exit of the fans to produce propulsive force. As the model height above the ground was decreased in the hover testing, there was a significant variation of thrust-removed normal force with constant fan rpm. The greatest variation was generally for the ratio of height to fan exit diameter of less than 2.5. A substantial reduction of that variation was obtained by deflecting fan exit flow outboard with the vanes. In the tunnel many vane angle configurations were tested for roll, yaw, and lift control. Other configuration features such as flap deflections and tail incidence were evaluated as well. Though the V-tail empennage provided an increase in static longitudinal stability, the total model configuration remained unstable.

Introduction

The *fan-in-wing* concept is being reconsidered for vertical or short takeoff and landing (VSTOL) aircraft application. The particular design consists of a fuselage-mounted turbojet and a single, large wing-mounted lift fan in each wing semispan. For low flight speeds, diverter valves in the turbojet exhaust stream direct the gases through ducting to the tip-driven fans. Deflector vanes in the efflux from the lift fans provide pitch, roll, yaw, and height control during vertical flight operation and transition from fan lift to wing lift. For higher flight speeds the valves are opened to permit straight-through flow to conventional jet nozzles. The concept, which was initiated in 1961 (refs. 1, 2, and 3), was originally employed for the full-scale XV-5A aircraft.

Since that early development there have been advances in materials, structural design, turbojet performance, and flight-control systems which may be particularly advantageous for fan-in-wing aircraft applications. Therefore, the Grumman Aerospace Corporation (now Northrup Grumman) designed a configuration suitable for the future battlefield needs of the U.S. Army (ref. 4). Under a Cooperative Research and Development Agreement with the U.S. Army, Grumman developed the model 755 design. A Memorandum of Understanding with Langley was established to test a 1/8-scale model in the Langley 14- by 22-Foot Subsonic Tunnel. These tests of the model 755 were to provide some initial design assessments.

Although all fixed-wing aircraft development programs require wind tunnel testing, it is especially necessary for the fan-in-wing configuration. Large amounts of air, which affect the pressures on both the upper and lower surfaces of the wing, are drawn through the fan-in-wing location. Also, when operated near the ground, additional significant pressure changes occur on the fuselage and wing. These pressures and resulting air loads are not predicted easily by current computational fluid dynamics analyses.

This report documents the wind tunnel test program and includes a description of the model, the test variables, and some significant results. Some of the data are considered proprietary by Grumman and are not available.

Symbols

The axis system for the data is shown in figure 1. The moment reference center is midway between the fans at fuselage station 40.14 in. (321.1 in.) and waterline station 11.75 in. (94.0 in.) (fig. 2). The numbers in parentheses are the full-scale dimensions as defined by Grumman.

A	fan (one) exit area, 0.4466 ft^2
A_F	fan axial force (parallel to wing chord plane), lb
b	wing span, 4.3875 ft
c	wing mean aerodynamic chord, 2.0075 ft
C_D	drag coefficient, $D_s/(qS)$
C_l	rolling-moment coefficient, $l_s/(qSb)$
C_L	lift coefficient, $L_s/(qS)$
C_m	pitching-moment coefficient, $m_s/(qSc)$
C_n	yawing-moment coefficient, $n_s/(qSb)$
C_Y	side-force coefficient, $Y_s/(qS)$
C_{ZT}	coefficient of thrust-removed normal force, $C_{ZT} = (-Z - 2 * N_F)/(2 * T)$
D	fan exit diameter, 8.75 in.
D_s	drag, lb
H	height of model above ground plane (measured to underside of fuselage at fuselage station 40.14 in. (321.1 in.))

H/D	ratio of model height to fan exit diameter
i_t	incidence of tail surfaces, deg
l_s	rolling moment, ft-lb
L_s	lift, lb
m_s	pitching moment, ft-lb
n_s	yawing moment, ft-lb
N_F	fan normal force (perpendicular to wing chord plane), lb
q	tunnel dynamic pressure, $(\rho * V^2)/2$, psf (in hover q was defined as $q = N_F/A$, psf)
S	wing area, 7.417 ft^2 (in hover S was defined as $S = 2A$ (0.8932 ft^2))
T	fan thrust, $T = (N_F^2 + A_F^2)^{0.5}$
V	wind speed, ft/sec
V_K	wind speed, knots
Y_s	side force, lb
Z	normal force, lb
α	angle of attack (in hover, angle of pitch), deg
β	angle of sideslip, deg
ϕ	angle of roll, deg
ρ	density of air, slugs/ft^3

Abbreviations:

BL	lateral butt-line station, in.
FS	longitudinal fuselage station, in.
RTC	rotor test cell
Sta.	tunnel station
V/STOL	vertical or short takeoff and landing aircraft
WL	vertical waterline station, in.

Test Facilities and Model

Rotor Test Cell

The model preparation area, the rotor test cell (RTC), is adjacent to the Langley 14- by 22-Foot Subsonic Tunnel and was used to prepare the model for tunnel testing and to conduct the majority of the hover tests. The RTC is a large chamber 69 ft high by 42 ft wide by 48 ft long. As such, the chamber provides an area free of aerodynamic interference such as boundary-induced recirculation. The model was mounted on a sting (fig. 3) that permitted variation of height, angle of pitch, and angle of roll above a pressure-instrumented ground board. There were 90 static pressure taps on the surface of the ground board and 10 small total pressure rakes with 7 ports, each used for the measurement of wake velocities near the surface of the ground board. After the hover testing in the RTC, the model and the forward part of the sting mount were removed as a unit and installed in the tunnel (so that the air line bridging the balance within the model would not be disturbed).

Wind Tunnel

Tests of the model were conducted in the closed-throat test section (fig. 4) of the Langley 14- by 22-Foot Subsonic Tunnel where the model was mounted on a different sting. The sting permitted variation of height, angle of attack, and angle of sideslip, but not angle of roll as in the RTC. The tunnel is an atmospheric pressure, closed circuit with a test section measuring 14.5 ft high by 21.75 ft wide (ref. 5). Wind speed can be varied from 0 to 200 knots. A floor boundary layer suction system at the test section entrance was operated throughout the wind tunnel tests to reduce the boundary layer. Another capability, used briefly, was a laser light sheet for flow visualization to illuminate fan exit flow patterns.

Model Description

The model was constructed primarily of aluminum and steel with some minor components of fiberglass and wood. Drawings of the model components are shown in figure 5. The major dimensional values used in the determination of the aerodynamic parameters are given in the symbol list. Table 1 lists the dimensions and other characteristics of the model. Additional details of the model can be found in reference 6. There were two leading-edge configurations: one with zero deflection and the other with a droop of 25°. Also, the trailing-edge flaps and ailerons could be deflected 30°, trailing edge down. The tail configuration had two surfaces in a V shape, with each positioned 40° above the horizontal. The tail configuration had elevator components, although these were not deflected during this test program. However, the incidence of the tail surfaces was varied. A tip-driven fan was located in each wing semispan panel, and both fans rotated in the same direction: clockwise as viewed from above the model. One fan was mounted in the wing on strain gage elements (i.e., the fan balance) that measured four force and moment load components: normal force, axial force, pitching moment, and rolling moment. The fans were driven with air pressure up to 150 psi (conducted through a pipe which bridged the six-component force and moment measuring balance that supported the model). The balance was mounted to a sting. Both balances had been calibrated with the air line connected and pressurized to account for the influence of the air line.

Fan exit deflection vanes, fuselage strakes, and fan inlet doors were tested. Vanes with various deflection angles could be attached to the underside of the fans.

Figure 5(b) shows a sketch of the vanes with various angle settings. The vane assemblies were flat plates welded to a mounting ring. The two longitudinal strakes were attached to the chines of the flat-bottomed fuselage, and two different lengths of these were tested (fig. 2). Throughout most of the testing, fan inlet doors, which would cover the fans in high-speed flight, were mounted in the open position, i.e., vertical and parallel to the fuselage centerline on the upper side of the wing.

There were five primary vane assemblies: EV0, EV7.5, EV15, EV30, and EV45. The deflected orientation (trailing edge aft) of the vanes provided propulsive force. However, they could also be turned 90° so that the vanes provided side force. The EV0, EV7.5, and EV15 assemblies were tested with both orientations during the program. In addition, the EV15 assembly was mounted on the right fan with a 180° orientation (trailing edge forward, i.e., −15°), which resulted in a force aft rather than forward for some runs. There were also assemblies that had half the vanes vertical and half with a 15° deflection, and there were assemblies that had half the vanes deflected 15° forward and the other half deflected 15° aft (resulting in a reduction of thrust without a net propulsive force). Various combinations of these assemblies were tested for their effectiveness in providing roll and yaw control as well as fan thrust modulation. Thrust of the fans was varied also, by varying fan rpm (fig. 6).

In addition to balance measurements of the air-induced loads, there were up to 160 pressure-measuring ports on the model. Some of these ports were total pressure-measuring rakes in the inlet of one fan. Small-diameter tubing connected these ports to transducers in the model nose. Fan rpm and thermocouple measurements of fan-bearing temperatures were obtained as well.

Throughout most of the testing, grit (no. 80) was glued to the wing and tail surfaces in strips approximately 0.10 in. wide and approximately 1 in. behind and parallel to the leading edge of each wing and tail surface. The purpose was to fix the boundary layer transition point, a standard practice at the Langley 14- by 22-Foot Subsonic Tunnel.

Test Procedures

The first phase of the testing was conducted in the rotor test cell (RTC) adjacent to the Langley 14- by 22-Foot Subsonic Tunnel. The model is shown (fig. 2) mounted on a sting that offered vertical height variation (i.e., above the ground board) and variation of angles of pitch and roll. Typically, the model was set at angles of pitch or roll, and the height above the ground board was varied from the maximum possible (H/D = 7.4) until the landing gear almost made contact with the ground board. For the hover tests the fans were generally operated at approximately 15000, 18000, or 22000 rpm. The angle-of-pitch range was −10° to 10°. The angle-of-roll range was 0° to 10°. The forces, moments, and pressures were recorded at each scheduled height.

In the tunnel the model angle of pitch or sideslip was varied at a scheduled height location, wind speed, and fan rpm. Fan rpm settings were varied from 0 to 23000. The fan rpm for most testing was approximately 22000, which was below the maximum allowable rpm of 23000. Adjustments were made to airflow to each of the tip-driven fans to make both fans operate at the same rpm with the expectation that both would have the same thrust.

The sting support in the tunnel was not the same as that used in the RTC. Whereas the sting support in the RTC could vary the angles of pitch and roll in addition to height, the tunnel support system could not provide the angle of roll variation or the same height or pitch range as that in the RTC. The height range was less than that in the RTC, varying from an H/D of 5.8 to 1.3 because of a sting support travel limitation. The angle-of-attack range was 0° to 20°. The sideslip angle range was −4° to 16°. For most testing, the wind speed was approximately 170 fps or had an approximate pressure of 35 psf. There was some testing at lower dynamic pressures. The tunnel boundary layer removal system was used throughout the testing in the tunnel with resulting boundary layer thickness of approximately 2 in. at the model location without the moving ground plane.

Data Accuracy

The main balance data were corrected for weight tares, tunnel wall effects, differential balance cavity pressures, and pressure tares. Blockage corrections were not applied to correct the data since the model was small compared to the size of the tunnel test section. The ratio of model wing span to tunnel width was 0.204. Corrections for tunnel boundary interference for the effect of the jet wake were small. The fan balance data were corrected for weight tares and pressure tares.

The balance supporting the model was calibrated with the air line in place and was pressurized and treated as a normal balance. Typically, the accuracy of such balances is considered to be ±0.5 percent of the maximum load capability of the balance. Force and moment capability and the associated accuracy is listed in table 2. Repeatability of balance measurements is believed to be between 0.1 and 0.2 percent of balance capabilities. The fan balance had been calibrated at Grumman, but check loads were applied at the beginning of both test phases. These check loads established that the accuracy was approximately ±0.5 percent.

Presentation of Data

Representative data are plotted in this report to illustrate notable characteristics of the fan-in-wing model. Data obtained from the fan balance and the pressure data are not included. Table 3 provides the configuration nomenclature that is used in the figures and in tables 4 and 5. Tables 4 and 5 list the test runs for both the hover and forward flight phases of testing, respectively.

The graphs presented herein are as follows:

Discussion of Results

Static Tests

The static model testing in the RTC was conducted with the fans operating predominantly at 22000 rpm and sometimes operating at 18000 and 15000 rpm. Figure 6 shows the variation of thrust with fan rpm for the five primary vane configurations: no vanes, EV0, EV15, EV30, and EV45 at $H/D = 7.0$ and an angle of pitch of 0°. Also, figure 7 shows the effects of those vane configurations on the variation of coefficients C_m, C_{ZT}, and C_D with fan rpm. It is notable that the EV45 vanes result in a lift loss ($C_{ZT} \approx -0.10$) throughout the range of fan rpm. The model configuration with the EV45 vanes (W5 B6 D1 T FS2 EV45) differed from the configurations with the other vanes in that the leading edge and flaps were not deflected.

The primary data (as obtained in the RTC) for the fan-in-wing configurations with a fan rpm of 22000 are presented in figures 8, 9, and 10 (for the EV0, EV15, and EV30 vanes, respectively) as a function of the height (H/D) of the model. The change in the thrust-removed normal force coefficient (C_{ZT}) is as much as approximately –0.15 for $H/D < 2$. As the vane angles increase to 30°, the effects of angle of pitch increase for $H/D < 4.0$ as well. Pitching-moment coefficient and drag coefficient (approximately equal to propulsive-force coefficient) vary in a consistent manner. The only data obtained at 22000 rpm for the EV45 vanes are compared at $\alpha = 0°$ with those of the other three vanes in figure 11. For the EV45 vanes, C_{ZT} varies little with H/D and reflects the greatest loss of thrust throughout the H/D range.

There is also a loss in C_{ZT} effected by roll angle as shown in figure 12 for the EV0(90) vane configuration. The data indicate that the variation of lift loss for $H/D < 2.5$ may present major flight-control problems. At full scale, a roll angle of 9° would result when a wing tip drops (and the other rises) 2.75 ft, which to a pilot may not appear to be a significant change in roll attitude. Of course, when there is a roll angle, especially near the ground, the effect of height differs for each fan because one is higher above the ground than the other.

In an attempt possibly to reduce the variation of C_{ZT} with H/D, the EV15 vane was rotated 90° (vane configuration EV15(90)). As shown in figures 13 and 14, by rotating the EV15 vanes 90° so that vane-induced propulsive thrusting is directed outboard rather than forward, there is significant reduction of the variation of C_{ZT} with H/D. Since the EV15(90) vane reduces the lift loss at low H/D, a set of vanes with 7.5° deflection was made and tested with the outboard orientation (EV7.5(90)). Figure 15 shows that there is improvement, though not as much as for the EV15(90) vanes. There is, of course, a loss of propulsive thrusting capability with the outboard orientation, but if the fans themselves were canted, the same effect could be achieved and the vanes once again could be used for the primary function of providing longitudinal propulsive force, roll, and yaw control.

The four basic vane configurations were tested with the long strakes mounted on the fuselage chines (the bottom corners of the fuselage cross section). Figure 16 compares the effect of variation of H/D on coefficients C_m, C_L, and C_D for long (FS2) and short (FS1) strakes (though for a configuration without exit vanes). It is evident that the long strakes do increase C_{ZT} for $H/D < 2.5$ whereas the short strakes are relatively ineffective. Deflecting the flaps or wing leading edge did not affect the variation of C_m, C_{ZT}, and C_D with H/D (fig. 17) in the hover testing.

Wind Tunnel

Though there was some hover testing in the tunnel, the major part of the testing was conducted with $q = 35$ psf ($V \approx 172$ fps or $V_K \approx 103$ knots). This wind speed is representative of the flight speed ($V_K \approx 103$ knots) at which transition from fan-lift-supported flight to wing-lift-supported flight occurs. There was also limited testing at intermediate values of dynamic pressure: $q = 17.0$ psf ($V \approx 120$ fps), $q = 5.0$ psf ($V \approx 65$ fps), and $q = 3.0$ psf ($V \approx 51$ fps).

Figure 18 shows the effect of the EV0, EV15, and EV30 vane configurations on C_m, C_L, and C_D as fan rpm is varied. In figure 18 the fan speeds are 22000, 20300, and 17800 rpm, which are approximately equivalent to 100, 90, and 75 percent of *maximum* thrust (fig. 6). The lift is attenuated and propulsive force is increased; that is, C_D becomes less positive as expected with the increase in vane angle. At the lowest rpm level of 17800, pitching moment C_m is more affected (fig. 18(c)) than at the other two rpm levels. That effect may be attributable to reduced entrainment of flow over the forward portion of the wing and results in decreased pitching moment and greater sensitivity to vane angle changes.

Figure 19 presents the effect of fan rpm on the performance parameters for a much wider range of fan rpm for the three vane configurations. The variation of all three coefficients with rpm is, of course, far greater than is shown in figure 18, especially at rpm values less than approximately 17000. These data are all shown for a constant $H/D \approx 5.4$.

The effect of H/D variation for each vane configuration is shown in figure 20. At $H/D \approx 1.3$, the effect on

C_m is pronounced; the EV0 vane also shows that the pitching-moment coefficient is apparently affected by ground proximity at *H/D* of 2.1. It appears that as the vane angle increases, C_m is less affected by height. The EV15 and EV30 vanes show a reasonable attenuation of C_L and C_D with increased vane angle.

There should be little variation in lateral characteristics for the EV0, EV15, and EV30 vanes, but as shown in figure 21 (varying *H/D*) and in figure 22 (varying rpm), that is not the case. The positive rolling moment suggests that the thrusts of both fans differed even though the fan speeds were nearly the same. The left fan may have had a higher thrust than the right fan, which would have resulted in the positive rolling moment. Adjustments had been made with the valves that controlled the airflow to the tip-driven fans to obtain similar fan speeds. However, a second fan balance (one for each fan) would have been better for equalizing thrust than the present method of using fan speed to equalize thrust. The negative yawing moment in figures 21 and 22 is more difficult to explain. It may be that the sets of left and right vanes were not identical. That the fans rotated in the same direction (clockwise when viewed from the upper side of the model) may have contributed a friction torque. The nonsymmetric fan rotation could have resulted in nonsymmetric flow patterns that contributed to the variations in the lateral characteristics, C_l, C_n, and C_Y, with angle of attack.

Varying the thrust of the fans by varying rpm in the the full-scale aircraft may not yield adequate rapid control of attitude. By throttling fan exit flow and simultaneously staggering the vane deflection (deflecting half the vanes forward and half the vanes aft), fan-generated lift is attenuated and a faster control response can be obtained. Figure 23 shows the results for a deflection of 15° (EV(15/15)). A comparison of figure 23(a) with figures 18 and 19 shows that lift is reduced. As with the EV0, EV15, and EV30 vanes, the variation of C_m with α is affected by low height above ground, *H/D* = 1.3 (fig. 23(d)).

The EV(15/15) vanes have the same problem of variation of lateral characteristics with height and fan rpm (fig. 24) as that shown in figures 21 and 22 for EV0, EV15, and EV30 vanes. At the lowest height, *H/D* = 1.3, there is much greater C_l variation as angle of attack increases. The possible causes cited for the sensitivity of lateral characteristics to height, fan rpm, and fan rotation of the other vanes may apply to the EV(15/15) vanes as well.

Yawing and roll control can be obtained by deflecting vanes in several configurations. The longitudinal and lateral characteristics are shown for four vane configurations: EV[*L*(0), R(–15)], EV[*L*(15), R(–15)], EV[*L*(15/0), R(–15/0)], and EV[*L*(15/15), R(0)] in figures 25–28. Of the four configurations, the EV[*L*(15), R(–15)] reasonably offers the greatest yawing-moment contribution, though with some rolling moment (fig. 26(b)). Rolling-moment control can be obtained by reducing the net thrust of one fan, and the resultant rolling moment that is obtained is shown for vane configuration EV[*L*(15/15), R(0)] in figure 28(b). All six coefficients are provided in figures 25–28 for judgment of cross-coupling effects, which must be considered when control capabilities and penalties of the various vane configurations are being defined.

The effectiveness of the empennage (V-tail) in pitch is shown in figures 29 and 30. As *H/D* decreases to the lowest level, there is slight increase in stability for fans not operating (fig. 29). The V-tail provides an improvement in pitch stability but not enough for the desired level of stability (negative $dC_m/d\alpha$). There is little or no significant difference between fans not operating (fig. 29) and those operating at 22000 rpm (fig. 30).

Tail effectiveness in sideslip is shown in figures 31–34. The V-tail contributes some stability in yaw along with some rolling-moment variation. As sideslip increases, the increment in C_n and the decrement in C_Y with the addition of the tail are approximately the same for the fans covered (fig. 31) or operated at 22000 rpm (fig. 32). The decrement in C_l, however, is moderately greater with fan rpm. The possible reasons for the nonzero values for C_l, C_n, and C_Y at $\beta = 0°$ in figure 32 were reviewed in the discussion regarding figures 21 and 22. Changing the angle of attack from 0° (fig. 33) to 15° (fig. 34) does not change C_n or C_Y versus β, but it does affect C_l versus β for tail off and on.

The effectiveness of two nonsymmetrical vane configurations in sideslip for roll and yaw control are shown in figure 35. Generally, linear variations of rolling moment, yawing moment, and side force (with sideslip angle) indicate that sideslip does not diminish roll control offered by EV[*L*(15/15), R(0)] or yaw control offered by EV[*L*(15/0), R(–15/0)].

The long strakes (FS2) show only a minor effect on side force (fig. 36). Their primary attribute is the thrust recovery in hover near the ground as shown earlier in figure 16.

At the conclusion of testing, a comparison was made of the two means for fixing boundary layer transition on the wing panels. The technique used in the Langley 14- by 22-Foot Subsonic Tunnel is to glue no. 80 grit by sprinkling the grit on an adhesive in a band 0.1 in. wide along the span of the wing, approximately 1 in. behind

the leading edge. The technique used at the Grumman Low-Speed Tunnel is to use serrated plastic tape approximately 0.25 in. wide along the span and about 1 in. behind the leading edge. Figure 37 shows the differences in lift, drag, and pitching-moment characteristics. There was no testing of the configuration without either treatment at that time.

Concluding Remarks

Tests of a 1/8-scale model of a fan-in-wing concept developed by Grumman Aerospace Corporation (now Northrup Grumman) were conducted in the Langley 14- by 22-Foot Subsonic Tunnel and in the adjacent rotor test cell (RTC). In hover testing the variation of the coefficient of thrust-removed normal force C_{ZT} is as much as –0.15 when the ratio of model height above the ground to fan exit diameter $H/D < 2.5$. When the model was rolled up to 9°, there was a similar variation of C_{ZT}. When the 15° vanes (EV15) are rotated 90° (EV15(90)) so that jet efflux is outboard, the C_{ZT} variation with roll at low H/D is reduced. The long strakes on the bottom of the fuselage also are effective in reducing C_{ZT} variation at low H/D in hover.

In the wind tunnel, vane configurations that were tested in forward flight demonstrated the means of providing lift, roll, and yaw control. The V-tail improves pitch stability, but not enough to show that the tested model configuration is stable. The results for the lateral characteristics of rolling and yawing moment are obscured by possible mismatch of the thrust of the two fans. Although keeping the fan speeds roughly the same was attempted, testing would have benefited if both fans had been mounted on balances to match fan thrusts rather than rotor speeds. The V-tail configuration does offer yaw stability, but with some induced rolling moment.

NASA Langley Research Center
Hampton, VA 23681-0001
November 28, 1995

References

1. Starkey, H. B.; and True, H. C.: Design and Development of the XV-5A V/STOL Aircraft and Its Pneumatically-Coupled Lift-Fan Propulsion System. *Proceedings of the 19th American Helicopter Society Annual National Forum*, 1963, pp. 102–110.

2. Everett, W. L.: Pilot Report on XV-5A Fan Mode Handling Qualities. *Proceedings of the 21st American Helicopter Society Annual National Forum*, 1965, pp. 223–232.

3. Baldwin, R. L.; and La Plant, P., II: *Flight Evaluation of the XV-5A V/STOL Aircraft.* FTC-TR-66-30, U.S. Air Force, Mar. 1967.

4. Peterein, Wayne F., Sr.; Zaleski, Alfred J.; Lind, George W.; and Brittingham, Michael L.: An Advanced Counter Air System (ACAS)—Conceptual Formulation. AIAA Paper 89-2136, July 1989.

5. Gentry, Garl L., Jr.; Quinto, P. Frank; Gatlin, Gregory M.; and Applin, Zachary T.: *The Langley 14- by 22-Foot Subsonic Tunnel: Description, Flow Characteristics, and Guide for Users*. NASA TP-3008, 1990.

6. Maerki, Glenn: *Post Test Report of a Series II Low Speed Wind Tunnel Test on a 1/8 Scale Model of an Advanced Fan-In Wing Aircraft Configuration*. Grumman Report FAAV-380-TR-9401, Sept. 1994.

Table 1. Model Dimensions and Characteristics

[Full-scale dimensions are in parentheses]

Wing:		
Area, ft^2	7.417	(474.7)
Span, ft	4.3875	(35.06)
Mean aerodynamic chord, ft	2.0	(16.05)
Tip chord, ft	0.424	(3.395)
Root chord (center of fuselage), ft	2.958	(23.66)
Flap chord, ft	0.317	(2.53)
Leading-edge chord, ft	0.25	(2.00)
Leading-edge sweep angle, deg	30	
Trailing-edge sweep angle, deg	–30	
Dihedral angle, deg	5.0	
Airfoil thickness, percent	15	
V-tail:		
Area (total), ft^2	1.71	(109.6)
Semispan (one panel), ft	1.087	(8.69)
Tip chord, ft	0.308	(2.43)
Root chord (butt line Sta. 5.15 (3.43)), ft	1.269	(10.14)
Leading-edge sweep, deg	23.52	
Trailing-edge sweep, deg	–23.52	
Center of tail area (fuselage Sta.), ft	5.608	(44.87)
General:		
Total planform area, ft^2	11.08	(709.0)
Profile area, ft^2	2.72	(174.2)
Frontal area, ft^2	1.29	(82.4)
Aircraft volume, ft^3	1.52	(776.8)
Total length, ft	5.48	(43.84)
Balance center:		
FS, in.	41.70	(333.64)
WL, in.	10.18	(81.45)
BL, in.	0.0	(0.0)
Reference center:		
FS, in.	40.14	(321.1)
WL, in.	11.75	(94.0)
BL, in.	0.0	(0.0)
Lift fan centers:		
FS, in.	41.70	(333.64)
WL, in.	10.70	(85.6)
BL, in.	±8.95	(71.6)
Fuselage nose:		
FS, in.	10.26	(82.1)
WL, in.	10.18	(81.46)
BL, in.	0.0	(0.0)
Strakes:		
Height, mounted at butt lines, in. (1.5) (12.0)	±(3.2)	(±25.6)

Table 2. Primary Balance Load Capability and Accuracy

[Langley balance 843]

Component	Maximum load	Accuracy	Approximate coefficients at q = 35.0 psf
Normal force, lb	800	±4.0	$C_L \approx 0.0154$
Axial force, lb	250	±1.25	$C_D \approx 0.0048$
Pitching moment, in-lb	2500	±12.5	$C_m \approx 0.0020$
Rolling moment, in-lb.	1000	±5.0	$C_l \approx 0.0004$
Yawing moment, in-lb.	1000	±5.0	$C_n \approx 0.0004$
Side force, lb	500	±2.5	$C_Y \approx 0.0096$

Table 3. Model Nomenclature

B6	Design 755 body with no canopy (i.e., faired over)
B*	B* = W5 B6 FAI(30) LED(25)
D1	Upper wing surface fan doors (open, i.e., vertical)
D1(c)	Upper wing surface fan doors closed with inlet fairing
EV0	Fan exit vanes, left and right undeflected
EVX	Left and right vane assemblies similar and vanes deflected X° aft (negative if deflected forward, i.e., assembly rotated 180°)
EVX(90)	Left and right vane assemblies similar and vanes deflected X° outboard (X = 0°, or 7.5°, or 15°)
EV(15/0)	Both left and right vane assemblies similar with half the vanes undeflected and other half deflected 15° aft. If negative, assembly is rotated 180°
EV(15/15)	Both left and right vane assemblies similar with half the vanes deflected 15° forward and half deflected 15° aft (for zero net propulsive force)
EV(L( ), R( ))	Left and right assemblies differ but combinations are as listed above
FAI(30)	Flaps and ailerons deflected 30° trailing edge down
FS1	Short strakes from 30.11 in. (240.9 in.) to 54.15 in. (433.2 in.)
FS2	Long strakes from 21.05 in. (168.4 in.) to 63.25 in. (506.0 in.)
G	Landing gear on (nose and main gear extended; doors open)
LED(25)	Wing leading edge dropped 25°
T	Baseline V-tail. *T*(X) both surfaces deflected X°, i.e., incidence, positive trailing edge down
W5	Large design 755 wing

Table 4. Static Test Runs for Fan-in-Wing Model

[Hover test in rotor test cell]

Run	Configuration	α, deg (approximate)	ϕ, deg	rpm, (approximate)	*H/D*	Comments
139	B* G D1	0	0	Vary	7.0	
140				18000	7.0	Several repeat points
141				18000	Vary	
142				22000		Left landing gear failed
143				22000		Repeat of 142
144		Vary		22000		
145	B* G D1 T	0		18000		V-tail on
146	B* G D1 T			22000		
147	B* G D1 T FS1			18000		FS1 strake on
148				22000		
149		2				
150		5				
151		10				
152		–2				
153		–5				
154		–10				
156	B* G D1 T FS1	0	0	22000	Vary	Repeat of 148
157	B* G D1 T FS1			18000		Repeat of 147
158	B* G D1 T FS2			18000		FS2 strake on
159				22000		
160		–2				
161		–5				
162		–10				
163		2				
164		5				
165		10				
166	B* G D1 T FS2 EV15(90)	0		18000		EV15(90) vanes
167		0		22000		
168		2				
169		5				
170		10				
171		–2				
172		–5				
173		–10				
175	B* G D1 T FS2 EV0	0	0	Vary	7.0	EV0 vanes on
176		0		22000	Vary	
177		2				
178		5				
179		10				
180		–2				
181		–5				
182		–10				

Table 4. Continued

Run	Configuration	α, deg (approximate)	ϕ, deg	rpm, (approximate)	*H/D*	Comments
183	B* G D1 T FS2 EV15	0	0	Vary	7.0	EV15 vanes on
184		0		22000	Vary	
185		2				
186		5				
187		10				
188		–2				
189		–5				
190		–10				
191		0				Repeat of 184
192	B* G D1 T FS2 EV30			Vary	7.0	EV30 vanes on
193				22000	Vary	
194						Repeat of 193
195		2				
196		0				Repeat of 193
197						Repeat of 193
198						Repeat of 193
199						Repeat of 193
200		5				
201		10				
202		–2				
203		–5				
204		–10				
205		0				Repeat of 193
206		0				Repeat of 193
209	B* G D1 T FS2 EV45	0	0	22000	Vary	EV45 vanes on
210	B* G D1 T FS2 EV45	2		22000	Vary	
211	B* G D1 T FS2	0		Vary	7.0	No vanes
212	B* G D1 T FS2			22000	Vary	
213	B* G D1 T FS2 EV15/15			Vary	7.0	EV15/15 vanes on
214	B* G D1 T FS2 EV15/15			22000	Vary	
215	B* G D1 T FS2 EV15/0			Vary	7.0	EV15/0 vanes on
216				22000	Vary	
217		2				
218		5				
219		10				
220		–2				
221		–5				
222	B* G D1 T FS2 EV0	0				Repeat of 176
223	B* G D1 T FS2 EV15					Repeat of 184
224	B* G D1 T FS2 EV30					Repeat of 205
225	B* G D1 T FS2 EV0(90)			Vary	7.0	EV0(90) vanes on
226				22000	Vary	
227				18000	Vary	
228				15000	Vary	

Table 4. Concluded

Run	Configuration	α, deg (approximate)	ϕ, deg	rpm, (approximate)	*H/D*	Comments
229	B* G D1 T FS2 EV0(90)	0	3	22000	Vary	
230	B* G D1 T FS2 EV0(90)	0	6	22000	Vary	
231	B* G D1 T FS2 EV0(90)	0	9	↓	↓	
232	W5 B6 G D1 T FS2 EV0(90)	0	0	↓	↓	Flaps and leading edge undeflected
233	W5 B6 G D1 T FS2 EV0(90)	5	0	↓	↓	
234	W5 B6 G D1 T FS2 EV0(90)	0	6	↓	↓	
235	W5 B6 D1 T FS2 EV0(90)	0	0	↓	↓	Landing gear off
236	W5 B6 D1 T FS2 EV45	0	↓	18000	↓	EV45 vanes on
237	↓	2	↓	↓	↓	
238	↓	5	↓	↓	↓	
239	↓	–10	↓	↓	↓	
240	↓	–5	↓	↓	↓	
241	↓	10	↓	↓	↓	
242	W5 B6 D1 T FS2 EV30	0	↓	↓	↓	EV30 vanes on
243	↓	5	↓	↓	↓	
244	↓	10	↓	↓	↓	
245	↓	–5	↓	↓	↓	
247	W5 B6 D1 T FS2 EV30	–10	0	18000	Vary	
248	W5 B6 D1 T FS2 EV30	0	↓	18000	Vary	
249	W5 B6 D1 T FS2 EV30	↓	↓	Vary	7.0	Repeat 192
250	W5 B6 D1 T FS2 EV45	↓	↓	Vary	7.0	
252	W5 B6 D1 T FS2	↓	↓	Vary	7.0	No vanes
263	W5 B6 D1 T FS2	0	0	18000	7.0	
264	W5 B6 D1 T FS2	↓	↓	22000	↓	
265	W5 B6 D1 T FS2 EV0	↓	↓	18000	↓	EV0 vanes on
266	W5 B6 D1 T FS2 EV0	↓	↓	22000	↓	
267	W5 B6 D1 T FS2 EV7.5(90)	↓	↓	18000	↓	EV7.5(90) vanes on
268	↓	↓	↓	22000	↓	
269	↓	–5	↓	18000	↓	
270	↓	–10	↓	↓	↓	
271	↓	5	↓	↓	↓	
272	↓	10	↓	↓	↓	
273	↓	0	↓	↓	↓	

Table 5. Test Runs for Fan-in-Wing Model in 14- by 22-Foot Subsonic Tunnel

Run	Configuration	α, deg (approx.)	β	*q*	rpm, (approx.)	*H/D*	Comments
300	B* G D1 FS2 EV0	0	0	0	Vary	5.8	Repeat of 175
301					Vary	5.8	Repeat of 300
302					22000	Vary	
303					22000		Repeat of 302
304					20000		Flow visualization
305	B* G D1 FS2 EV15(90)				20000		Flow visualization
306	B* G D1 FS2 EV0			35.0	22000		Repeat of 303
307	B* G D1 EV0	Vary			0	5.8	Strakes off
308	B* G D1 EV0	Vary			0	5.0	
309	B* G D1 EV0	Vary			0	4.0	
311	B* G D1 EV0	Vary	0	35.0	0	5.8	Boundary layer system off
312						5.0	Boundary layer system off
313						4.0	Boundary layer system off
314						4.0	Boundary layer system on
315						5.8	Boundary layer system on
316							Transition grit applied
317					22000		
318			5				
319			10				
320			15				
321		0	Vary			5.4	
322		15	Vary			5.4	
323		0	0		Vary	5.8	
324		Vary			22000	4.0	
325						3.0	
326						2.5	
327						2.0	
328						1.3	
329	B* G D1 T EV0					5.4	V-tail on
330			5				
331			10				
332			15				
333		0	Vary				
334		15	0				
335		Vary	0			4.0	
336	B* G D1(c) T		0		0	5.4	Fans covered
337			5				
338			10				
339			15				
340		0	Vary				
341		15	Vary				
342		Vary	0			4.0	
343		Vary	0			3.0	
344		Vary	0			2.5	

Table 5. Continued

Run	Configuration	α, deg (approx.)	β	*q*	rpm, (approx.)	*H/D*	Comments
345	B* G D1(c) T	Vary	0	35.0	0	2.0	
346	B* G D1(c) T	Vary	0			1.3	
347	B* G D1(c)		0			5.4	Tail off
348			5				
349			10				
350			15				
351		0	Vary				
352		15	Vary				
353		Vary	0			4.0	
354						3.0	
355						2.5	
356						2.0	
357						1.3	
358	B* G D1(c) T(–10)					5.4	V-tail on at –10°
359						4.0	
360						3.0	
361						2.5	
362						2.0	
363						1.3	
364	B* G D1(c) T(5)					5.4	V-tail on at 5°
365						4.0	
366						3.0	
367						2.5	
368						2.0	
369						1.3	
370	B* G D1(c) T FS2					5.4	FS2 strakes on
371			5				
372			10				
373			15				
374		0	Vary				
375		15	Vary				
406	B* D1(c)	Vary	0	35.0	0	5.4	V-tail, gear, and strakes off
407	B* D1(c) T		0		0		V-tail on
408	B* G D1 T EV0		0		22164		Gear and EV0 vanes on
409			5		22164		
410			10		22164		
411		0	15		22000		
412		0	Vary				
413		15	Vary				
414		Vary	0			4.0	
415						3.0	
416						2.5	
417						2.1	
418						1.3	

Table 5. Continued

Run	Configuration	α, deg (approx.)	β	*q*	rpm, (approx.)	*H/D*	Comments
419	B* G D1 T EV0	Vary	0	35.0	20246	5.4	
420					17780		
421					14115		
422					11061		
423					8174		
424					6086		
425				17.5	22000		
426				8.5	22000		
427				3.05	22000		
428				35.0	1515		
429		0		0	22000		
430	B* G D1 T(−10) EV0	Vary		35.0			V-tail on at −10°
431						4.0	
432						2.5	
433						2.0	
434						1.3	
435	B* G D1 T(5) EV0					5.4	V-tail on at 5°
436						4.0	
437						2.5	
438						2.0	
439						1.3	
440	B* G D1 T FS2 EV0					5.4	FS2 strakes on
441			5				
442			10				
443			15				
444		0	Vary				
445		15	Vary				
446	B* G D1 EV0	0	0	0	Vary		Static thrust varied
447		Vary	0	35.0	22000		
448			5				
449			10				
450			15				
451		0	Vary				
452		15	Vary				
453		Vary	0			4.0	
454						2.5	
455						2.0	
456						1.3	
457	B* G D1 EV(15/15)					5.4	EV(15/15) vanes on
458			10				
459		0	Vary				
460		15	Vary				
461	B* G T D1 EV(15/15)	Vary	0		22146		V-tail on
462	B* G T D1 EV(15/15)	Vary	10		22000		
463	B* G T D1 EV(15/15)	0	Vary		22000		

Table 5. Continued

Run	Configuration	α, deg (approx.)	β	q	rpm, (approx.)	H/D	Comments
464	B* G T D1 EV(15/15)	15	Vary	35.0	22000	5.4	
465		Vary	0		20307		
466					17830		
467					14100		
468					8100		
469				17.5	22000		
470				3.0			
471		0		0			
472	B* G D1 T(–10) EV(15/15)	Vary		35.0			V-tail on at –10°
473	B* G D1 T(5) EV(15/15)						V-tail on at 5°
474	B* G D1 T EV[L(15/15), R(0)]						EV[L(15/15), R(0)] vanes on
475			10				
476		0	Vary				
477		15	Vary				
478		Vary	0		20300		
479					17800		
480					20300		Repeat of 478
481					17800		Repeat of 479
482					14100		
483					8100		
484				17.5	22000		
485				3.0			
486		0		0			
487	B* G D1 T EV(15/0)	Vary		35.0			EV(15/0) vanes on
488		Vary	10				
489		0	Vary				
490		Vary	0		20300		
491					17800		
492					14100		
493					8100		
494				17.5	22000		
495				3.0			
496		0		0			
497	B* G D1 T(–10) EV(15/0)	Vary		35.0			V-tail on at –10°
498	B* G D1 T(5) EV(15/0)	Vary					V-tail on at 5°
499	B* G D1 EV(15/0)	Vary					V-tail off
500	B* G D1 EV(15/0)	0	Vary				
501	B* G D1 T EV[L(15/0), R(–15/0)]	Vary	0				EV[L(15/0), R(–15/0)] vanes
502		0	Vary				
503		Vary	0		20300		
504		Vary			17800		
505		Vary			14100		
506		0		0	22000		
507	B* G D1 T EV15	Vary		35.0	21066		EV15 vanes
508	B* G D1 T EV15	0	Vary	35.0	21066		

Table 5. Continued

Run	Configuration	α, deg (approx.)	β	*q*	rpm, (approx.)	*H/D*	Comments
509	B* G D1 T EV15	Vary	0	35.0	20453	5.4	
510					17630		
511					14228		
512					8192		
513				17.5	22000		
514				3.0			
515		0		0			
516	B* G D1 T EV[L(15), R(−15)]	Vary		35.0			EV[L(15), R(−15)] vanes
517		0	Vary				
518		Vary	0		20300		
519					17800		
520					14100		
521					8100		
522				17.5	22000		
523				3.0	22000		
524		0		0	22000		
525	B* G D1 T EV30	Vary		35.0	21320		EV30 vanes
526		Vary	10				
527		0	Vary				
528		15	Vary				
529		Vary	0		20252		
530					17768		
531					14309		
532					8145		
533				17.5	22000		
534				3.0			
535		0		0			
536	B* G D1 T EV[L(0), R(−15)]	Vary		35.0			
537		0	Vary				
538		Vary	0		20300		
539					17800		
540					14100		
541					8100		
542				17.5	22000		
543				3.0	22000		
544		0		0	22000		
551	W5 B6 D1(c)	Vary	0	35.0	0	5.4	Fans covered, tail off
552	W5 B6 D1(c)	Vary	10				
553	W5 B6 D1(c)	0	Vary				
554	W5 B6 D1(c) T	Vary	0				V-tail on
555	W5 B6 D1(c) T	0	Vary				
556	W5 B6 D1(c) T(−10)	Vary	0				V-tail on at −10°
557	W5 B6 D1(c) T(5)	Vary	0				V-tail on at 5°
558	W5 B6 D1 T(5) EV0	Vary	0		22000		EV0 vanes on

Table 5. Continued

Run	Configuration	α, deg (approx.)	β	*q*	rpm, (approx.)	*H/D*	Comments
559	W5 B6 D1 T(–10) EV0	Vary	0	35.0	22000	5.4	V-tail on at –10°
560	W5 B6 D1 T EV0	Vary	0				V-tail on at 0°
561	W5 B6 D1 T EV0	0	Vary				
562	W5 B6 D1 EV0	Vary	0				V-tail off
563	W5 B6 D1 EV0	0	Vary				
593	B* G D1 EV0	Vary	0	35.0	22000	5.4	Repeat of 447
594		Vary				3.0	
595		0				Vary	
596		6					
597		12					
598		0		10.0			
599		6		10.0			
600		12		10.0			
601		0		5.0			
602		6		5.0			
603		12		5.0			
604	B* G D1 T EV0	Vary		35.0		5.4	V-tail on
605	B* G D1 T(5) EV0					3.0	V-tail on at 5°
606	B* G D1 T(–10) EV0					3.0	V-tail on at –10°
607	B* G D1 T EV0					3.0	V-tail on at 0°
608	B* G D1 T EV15		5			5.4	EV15 vanes on
609			10			5.4	
610		15	Vary			5.4	
611		0	0	10.0		Vary	
612		12	0	10.0		Vary	
613		Vary	15	35.0		5.4	
614	B* G D1 T EV0	Vary	10			4.0	
615		0	Vary			4.0	
616		0	Vary			2.5	
617		0	Vary			1.3	
618		Vary	10			2.5	
619			10			1.3	
620			0		20300	4.0	
621					20300	2.5	
622					20300	1.3	
623					17800	2.5	
624					17800	1.3	
625					22000	1.3	Repeat of 418
626	B* G D1 T EV0 FS2					4.0	FS2 strakes on
627	B* G D1 T EV0 FS2					2.5	
628	B* G D1 T EV0 FS2					1.3	
629	B* G D1 EV0		10			4.0	V-tail and strakes off
630	B* G D1 EV0	0	Vary			4.0	
631	B* G D1 EV0	Vary	10			2.5	

Table 5. Continued

Run	Configuration	α, deg (approx.)	β	*q*	rpm, (approx.)	*H/D*	Comments
632	B* G D1 EV0	0	Vary	35.0	22000	2.5	
633	↓	Vary	10	35.0	22000	1.3	
634	↓	0	Vary	35.0	22000	1.3	
635	↓	0	0	0	Vary	5.4	
640	B* G D1 T EV(15/15)	Vary	0	35.0	21932	4.0	EV(15/15) vanes on
641	↓	↓	↓	↓	21902	2.5	
642	↓	↓	↓	↓	21931	1.3	
643	↓	↓	↓	↓	20226	4.0	
644	↓	↓	↓	↓	20274	2.5	
645	↓	↓	↓	↓	20275	1.3	
646	↓	↓	↓	↓	17815	2.5	
647	↓	↓	↓	↓	17806	1.3	
648	B* G D1 T EV[L(15/15), R(0)]	↓	↓	↓	22000	4.0	
649	↓	↓	↓	↓	↓	4.0	Repeat of 648
650	↓	↓	↓	↓	↓	2.5	
651	↓	↓	↓	↓	↓	1.3	
652	↓	↓	↓	↓	20300	4.0	
653	↓	↓	↓	↓	20300	2.5	
654	↓	↓	↓	↓	20300	1.3	
655	↓	↓	↓	↓	17800	2.5	
656	↓	↓	↓	↓	17800	1.3	
657	B* G D1 T EV(15/0)	↓	↓	↓	22000	4.0	EV(15/0) vanes on
658	↓	↓	↓	↓	22000	2.5	
659	↓	↓	↓	↓	22000	1.3	
660	↓	↓	↓	↓	20300	4.0	
661	↓	↓	↓	↓	20300	2.5	
662	↓	↓	↓	↓	20300	1.3	
663	↓	↓	↓	↓	17800	4.0	
664	↓	↓	↓	↓	17800	2.5	
665	↓	↓	↓	↓	17800	1.3	
666	B* G D1 T EV[L(15/0), R(–15/0)]	↓	↓	↓	22000	4.0	
667	↓	↓	↓	↓	↓	2.5	
668	↓	↓	↓	↓	↓	1.3	
669	↓	↓	↓	↓	↓	2.0	
670	↓	↓	↓	↓	↓	1.3	Repeat of 668
671	↓	↓	↓	↓	20300	4.0	
672	↓	↓	↓	↓	20300	2.5	
673	↓	↓	↓	↓	20300	1.3	
674	↓	↓	↓	↓	17800	4.0	
675	↓	↓	↓	↓	17800	2.5	
676	↓	↓	↓	↓	17800	1.3	
677	B* G D1 T EV15	↓	↓	↓	22000	4.0	EV15 vanes on
678	B* G D1 T EV15	↓	↓	↓	22000	2.5	
679	B* G D1 T EV15	↓	↓	↓	22000	1.3	

Table 5. Concluded

Run	Configuration	α, deg (approx.)	β	*q*	rpm, (approx.)	*H/D*	Comments
680	B* G D1 T EV15	Vary	0	35.0	20300	4.0	
681					20300	2.5	
682					20300	1.3	
683					17800	4.0	
684					17800	2.5	
685					17800	1.3	
686	B* G D1 T EV[L(15), R(−15)]				22000	4.0	EV[L(15), R(−15)] vanes on
687					22000	2.5	
688					22000	1.3	
689					20300	4.0	
690					20300	2.5	
691					20300	1.3	
692					17800	4.0	
693					17800	2.5	
694					17800	1.3	
695	B* G D1 T EV[L(0), R(−15)]				22000	4.0	EV[L(0), R(−15)] vanes on
696					22000	2.5	
697					22000	1.3	
698					20300	4.0	
699					20300	2.5	
700					20300	1.3	
701					17800	4.0	
702					17800	2.5	
703					17800	1.3	
704	B* G D1 T EV30				22000	4.0	
705					22000	2.5	
706					22000	1.3	
707					20300	4.0	
708					20300	2.5	
709					20300	1.3	
710					17800	4.0	
711					17800	2.5	
712					17800	1.3	
767	W5 B6 D1(c)	Vary	35.0	0	0	5.4	Serrated tape in place of transition grit

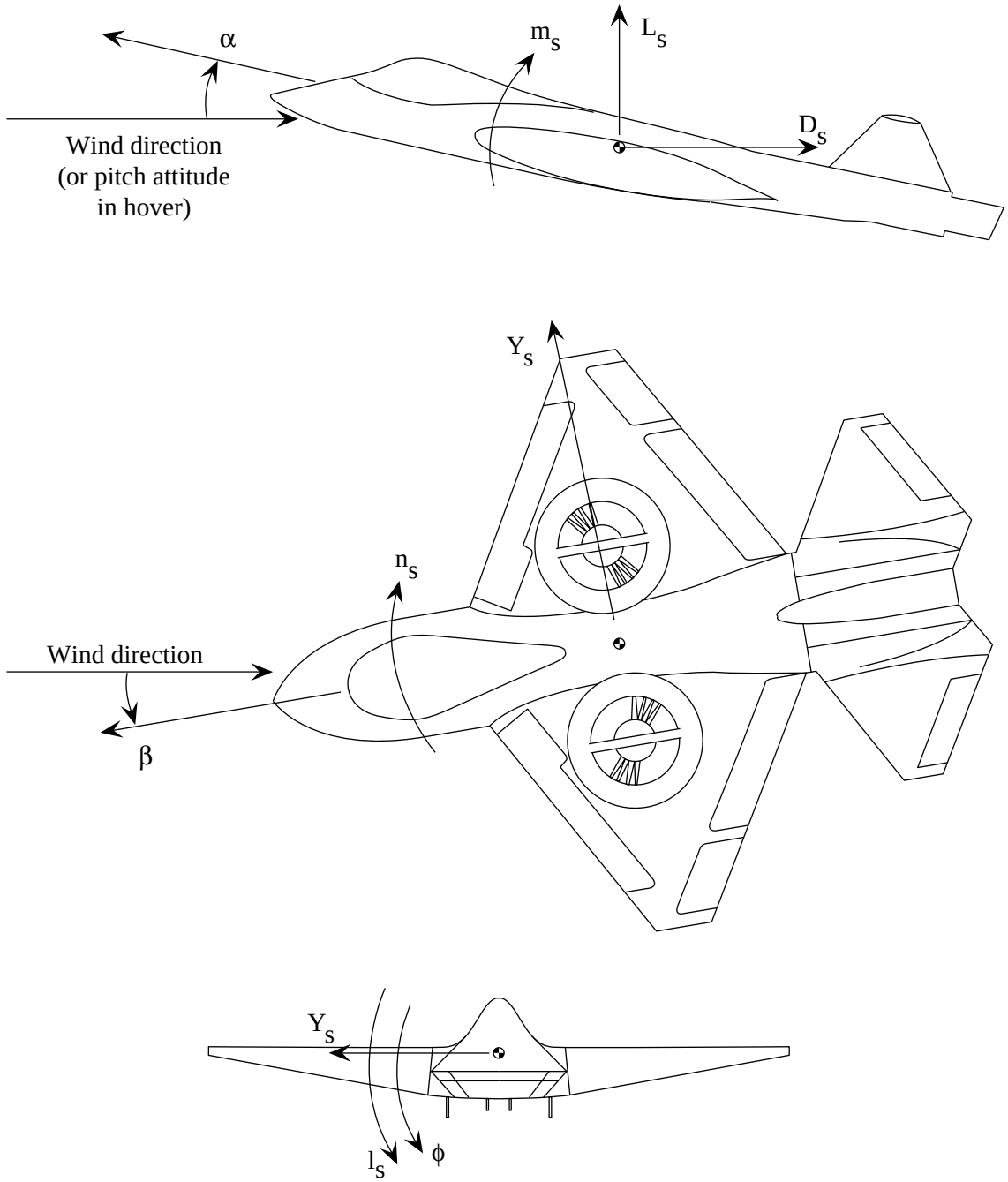

Figure 1. Axis system used in presentation of data. Arrows indicate positive direction of forces and moments.

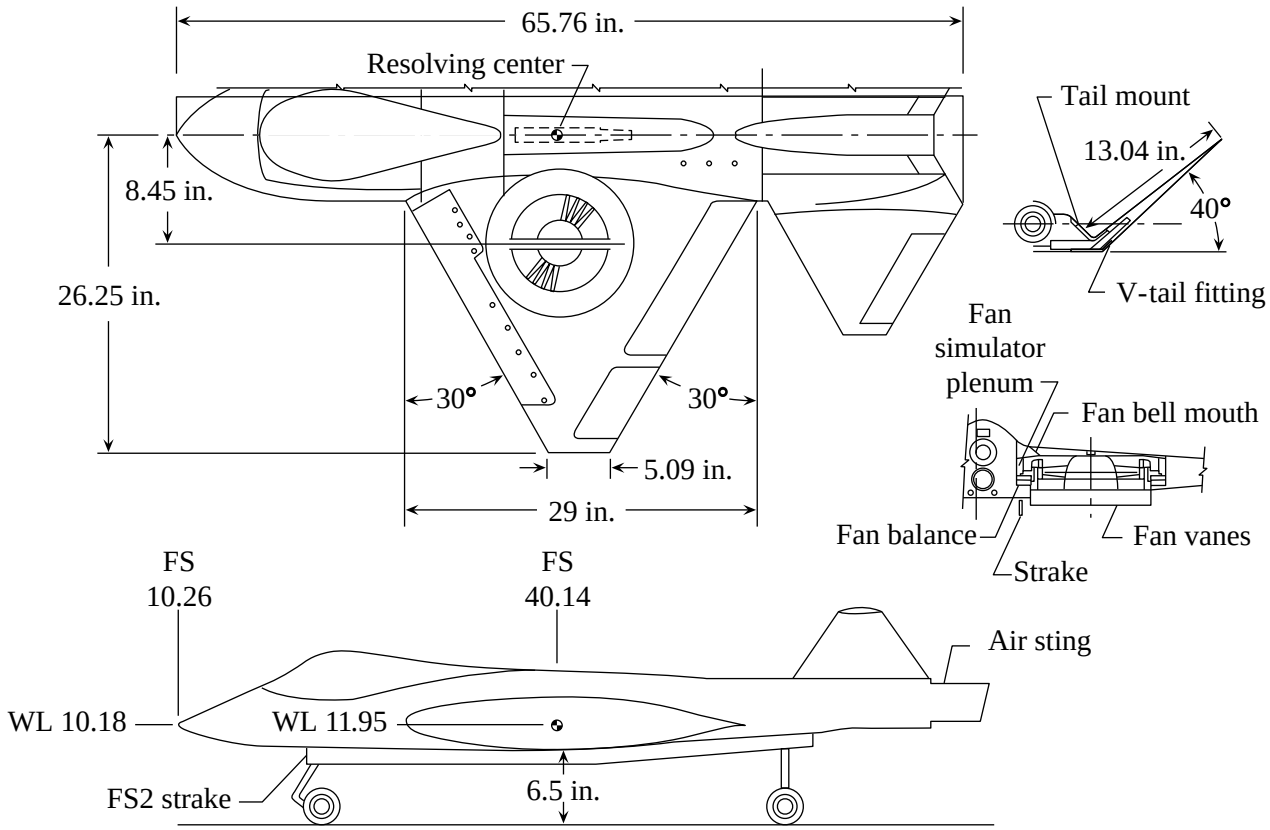

Figure 2. Planform, profile, and cross-section drawings of fan-in-wing model.

L-93-10308

Figure 3. Fan-in-wing model installation in rotor test cell at Langley 14- by 22-Foot Subsonic Tunnel.

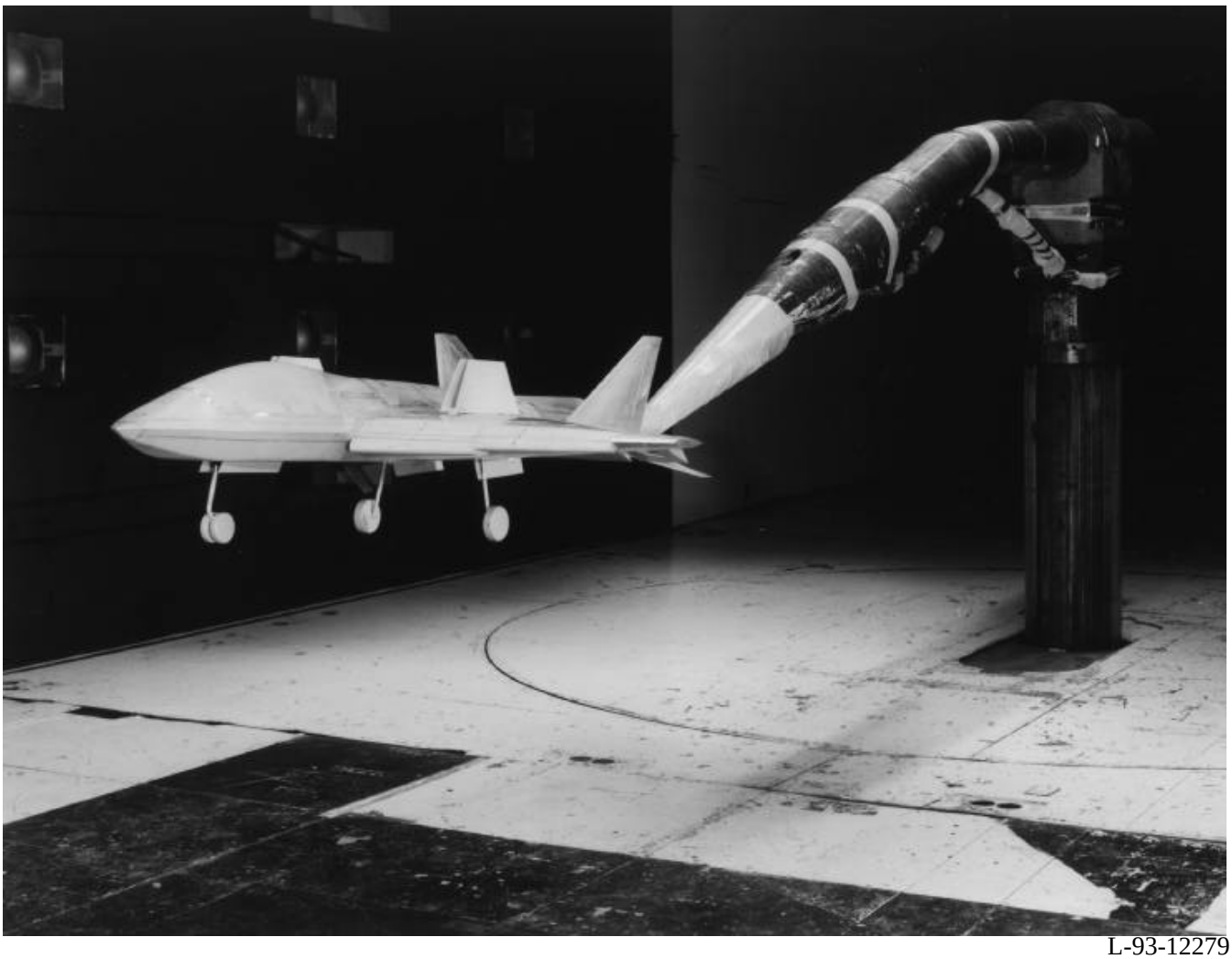

L-93-12279

Figure 4. Fan-in-wing model installation in test section of Langley 14- by 22-Foot Subsonic Tunnel.

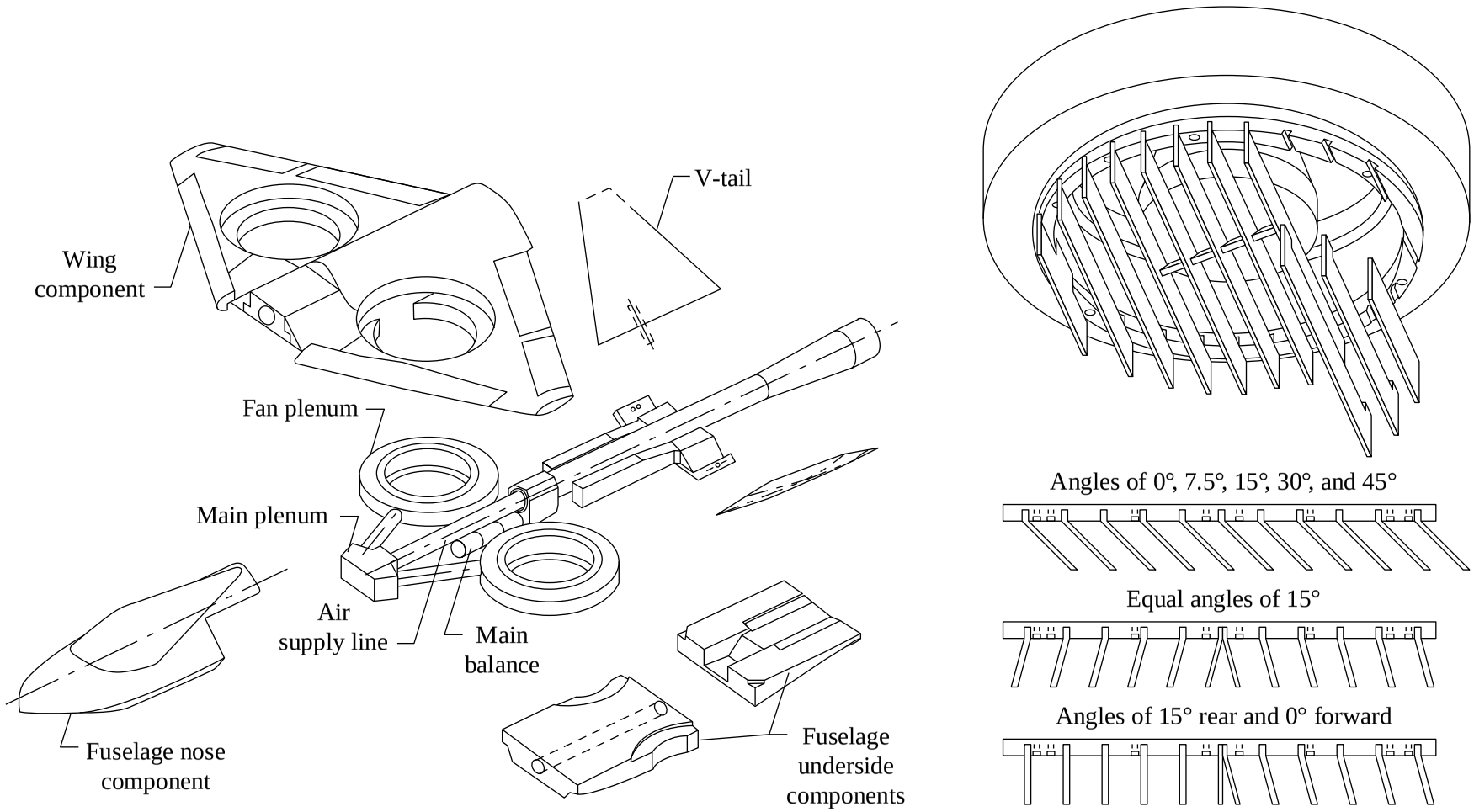

(a) Major components.

(b) Vane configurations.

Figure 5. Fan-in-wing model components.

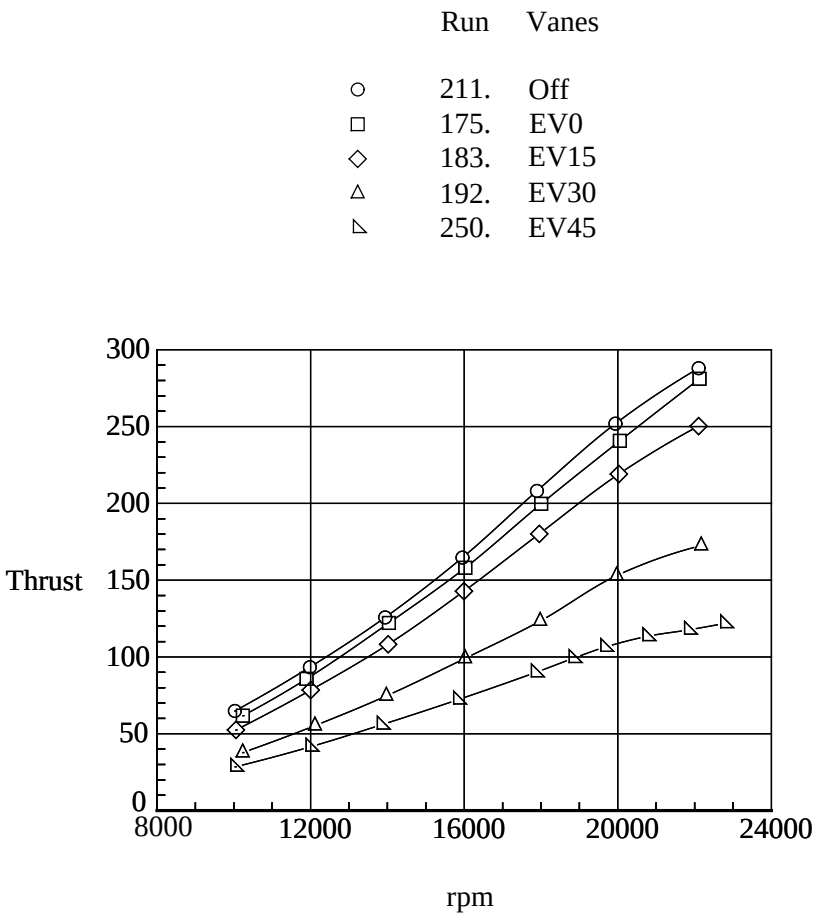

Figure 6. Effect of vane configuration (EV0, EV15, and EV30 with B* G D1 T FS2 and EV45 with W5 B6 D1 FS2) on variation of thrust with fan rpm (*H/D* = 7.0 and α = 0°).

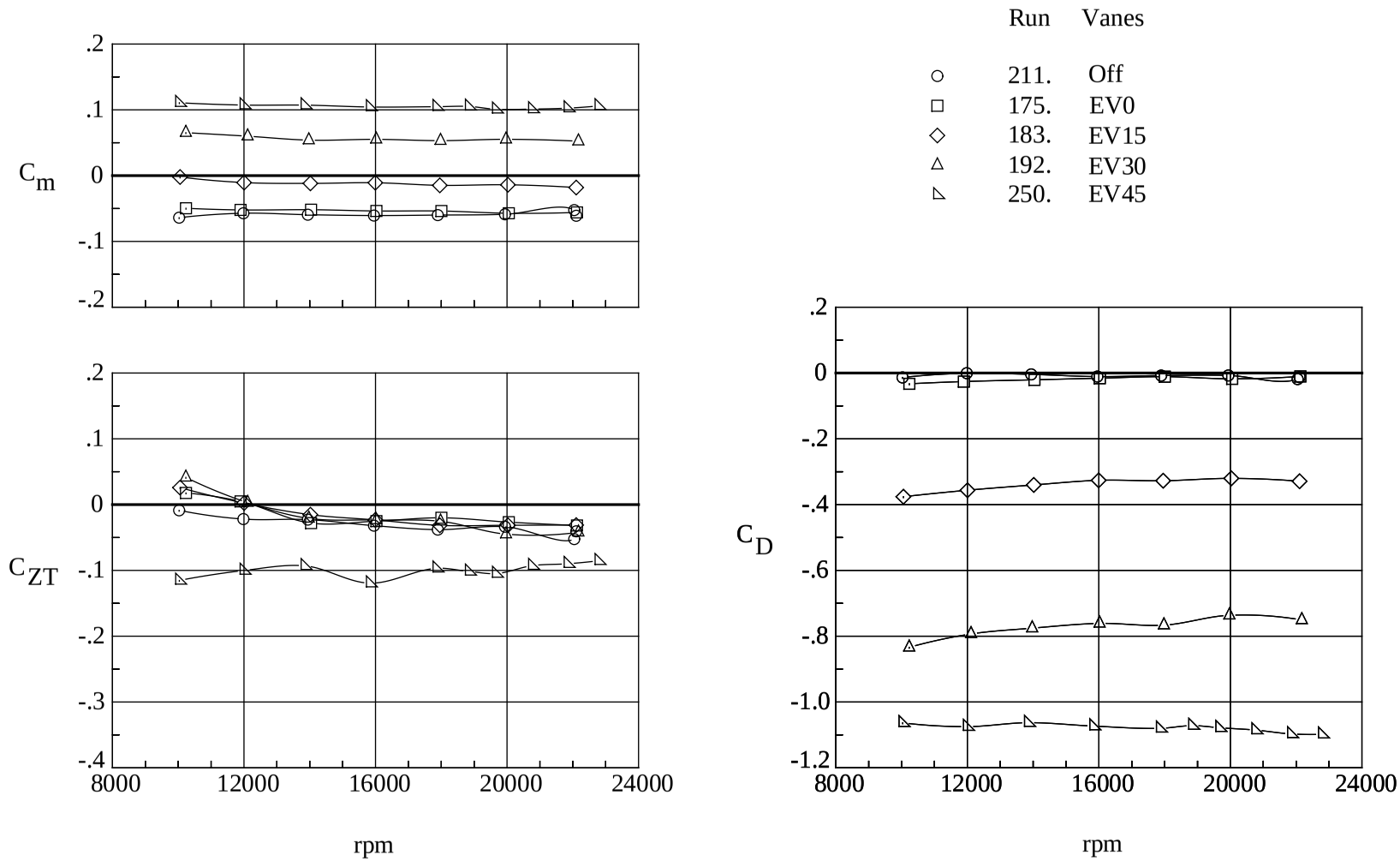

Figure 7. Effect of vane configuration (EV0, EV15, and EV30 with B* G D1 T FS2 and EV45 with W5 B6 D1 FS2) on variation of C_m, C_{ZT}, and C_D with fan rpm (H/D = 7.0 and α = 0°).

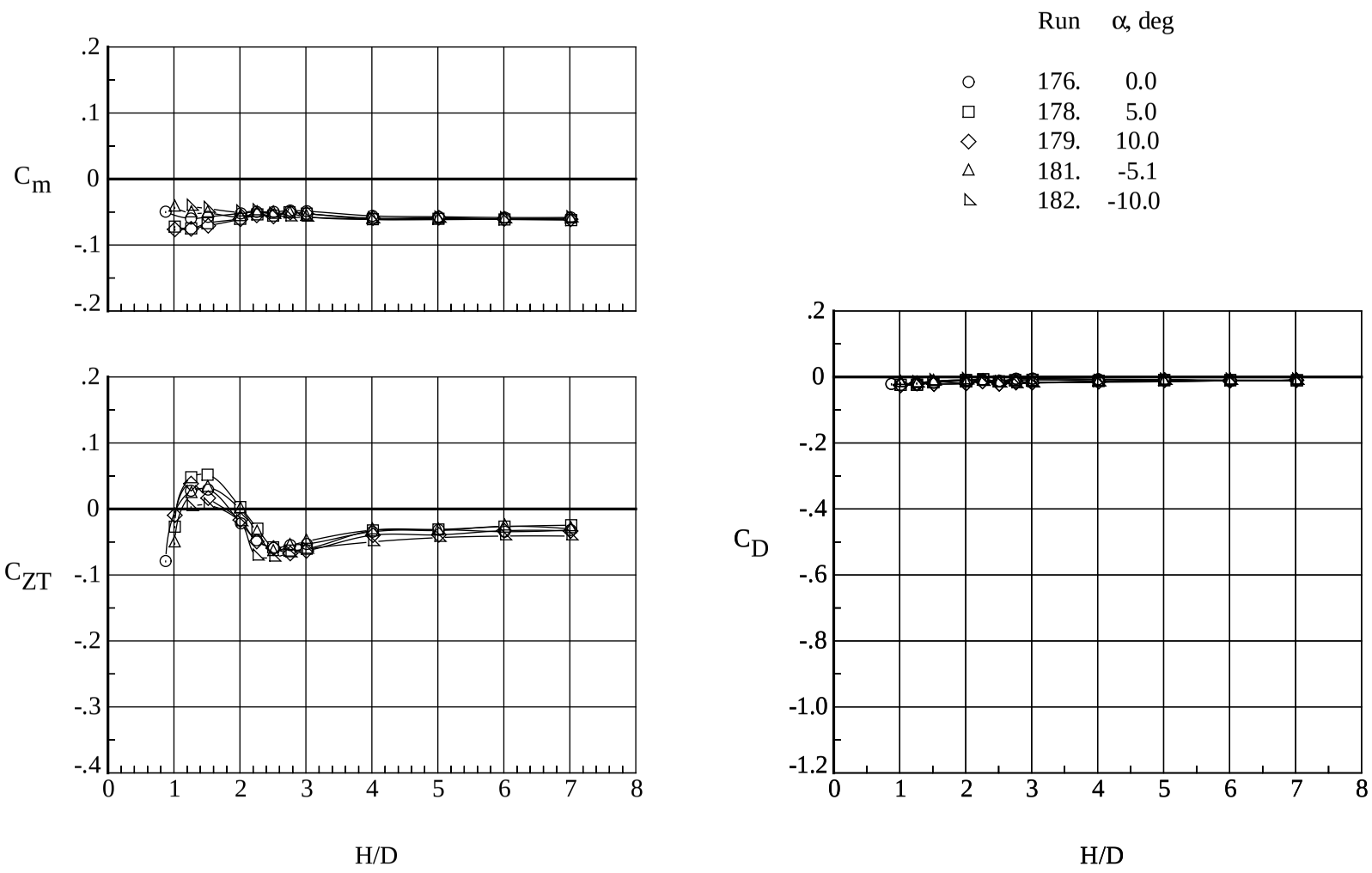

Figure 8. Effect of angle of pitch on variation of C_m, C_{ZT}, and C_D with *H/D* for B* G D1 T FS2 EV0 (22000 rpm).

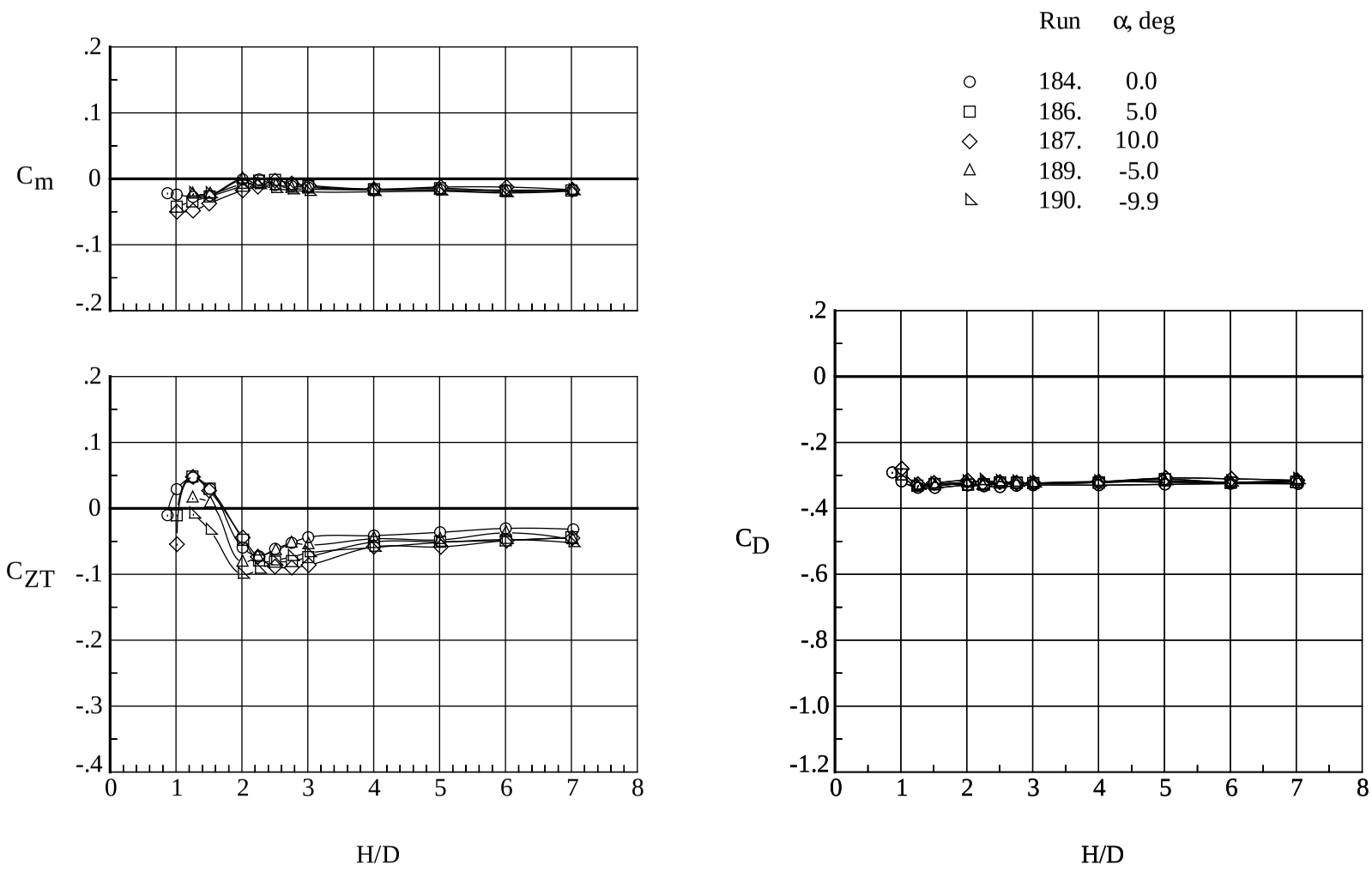

Figure 9. Effect of angle of pitch on variation of C_m, C_{ZT}, and C_D with *H/D* for B* G D1 T FS2 EV15 (22000 rpm).

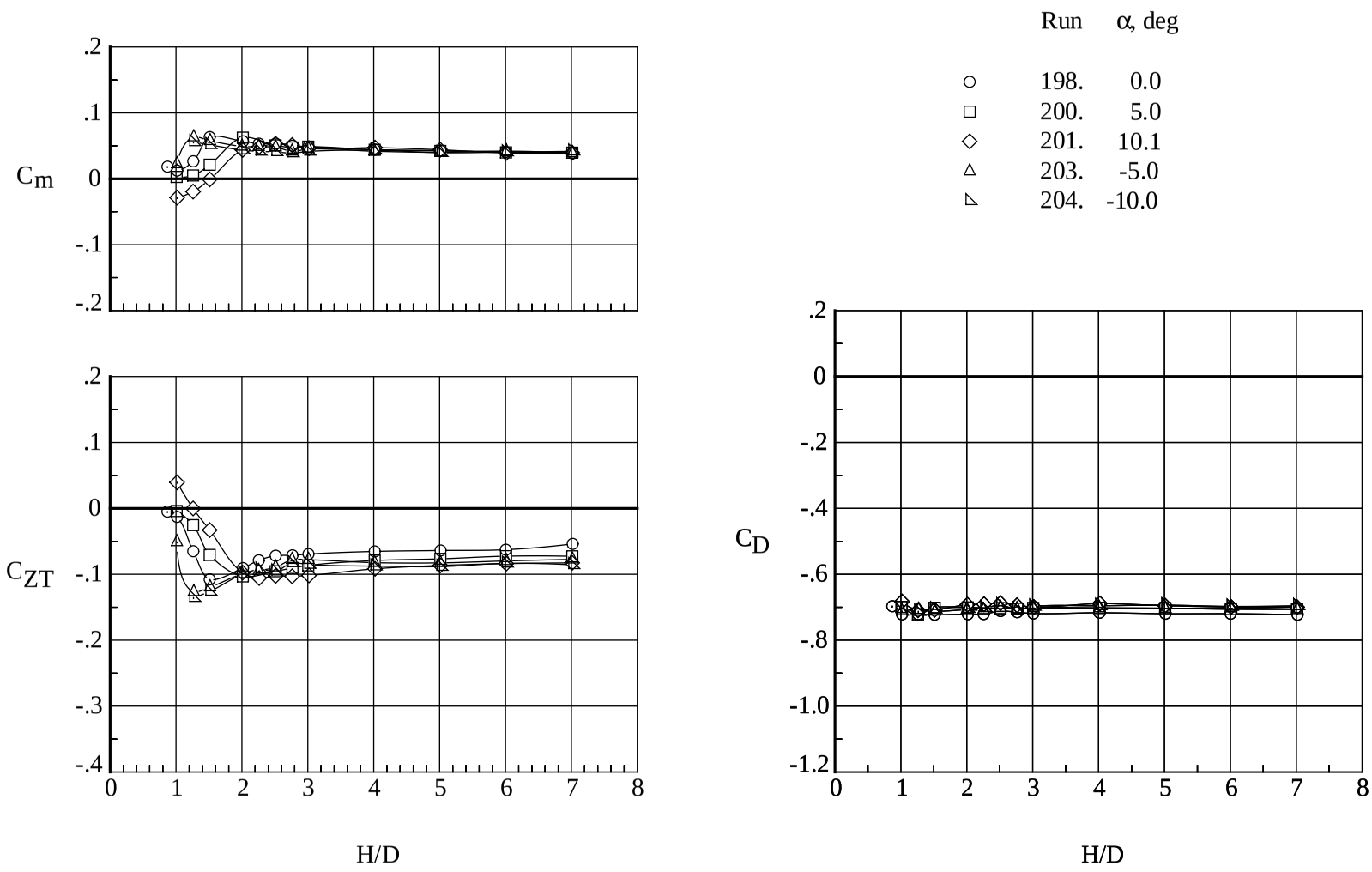

Figure 10. Effect of angle of pitch on variation of C_m, C_{ZT}, and C_D with *H/D* for B* G D1 T FS2 EV30 (22000 rpm).

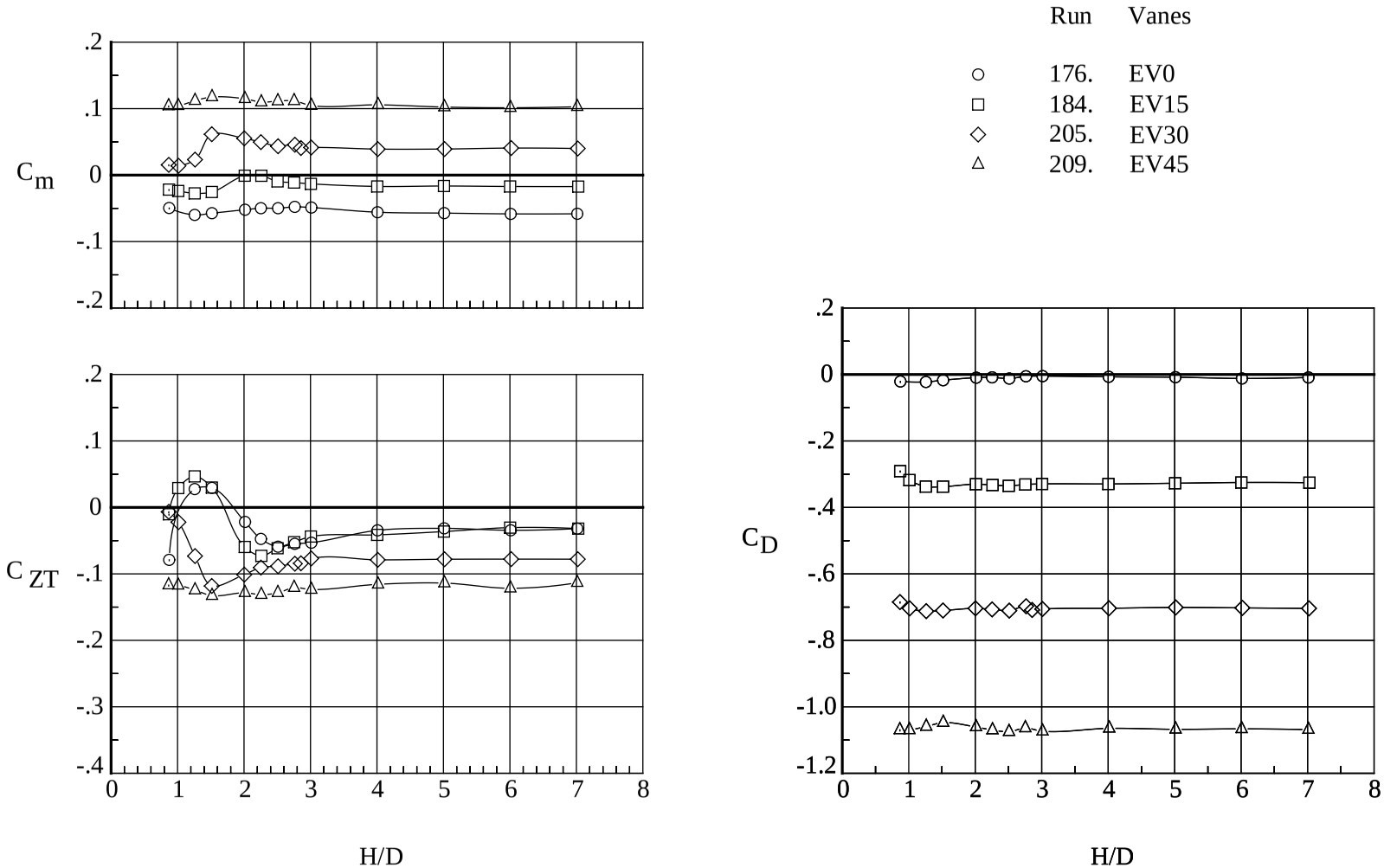

Figure 11. Effect of vane configuration (EV0, EV15, EV30, and EV45) on variation of C_m, C_{ZT}, and C_D with *H/D* for B* G D1 T FS2 (22 000 rpm and $\alpha = 0°$).

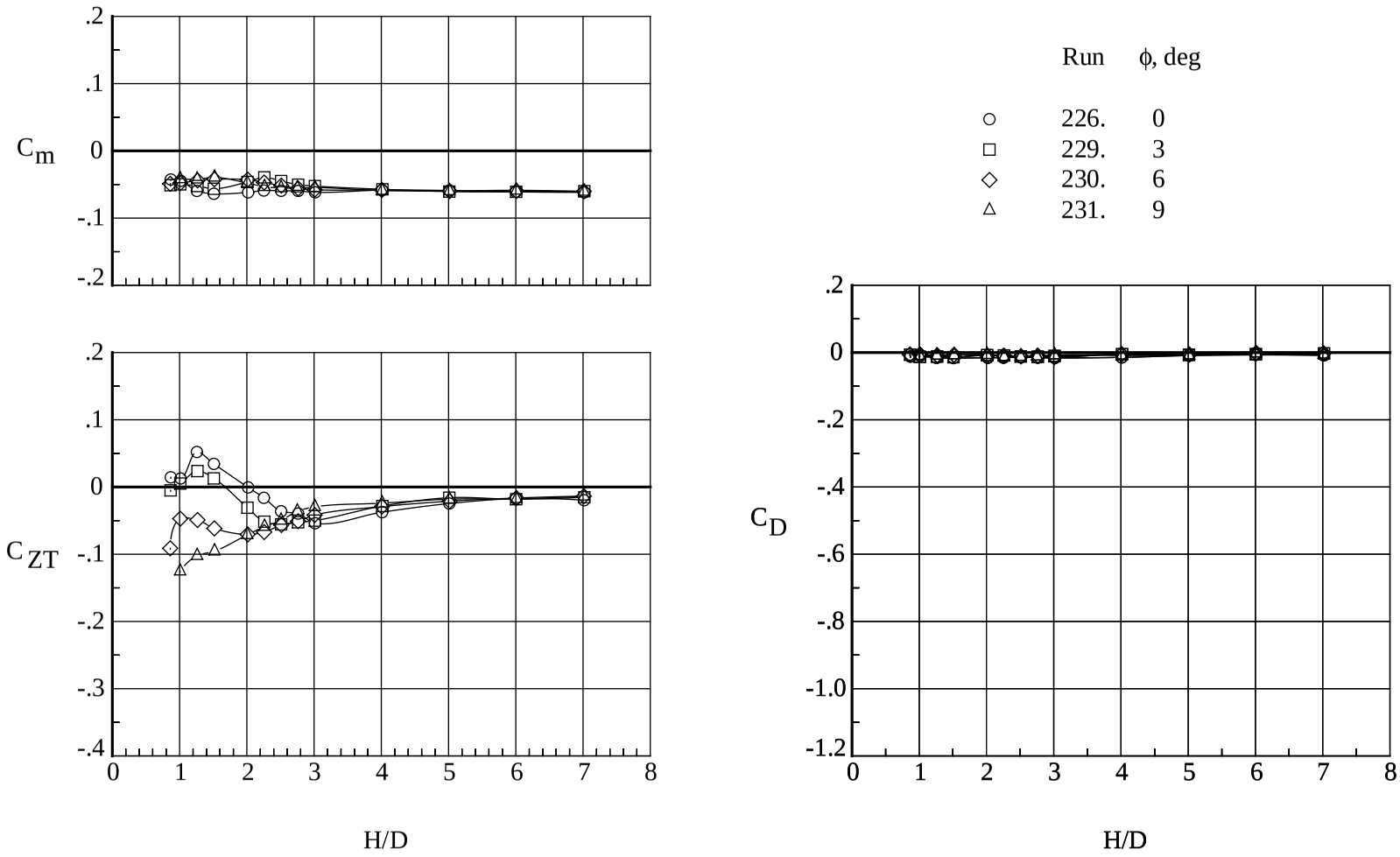

Figure 12. Effect of angles of roll on variation of C_m, C_{ZT}, and C_D with H/D for B* G D1 T FS2 EV0(90) (22000 rpm and $\alpha = 0°$).

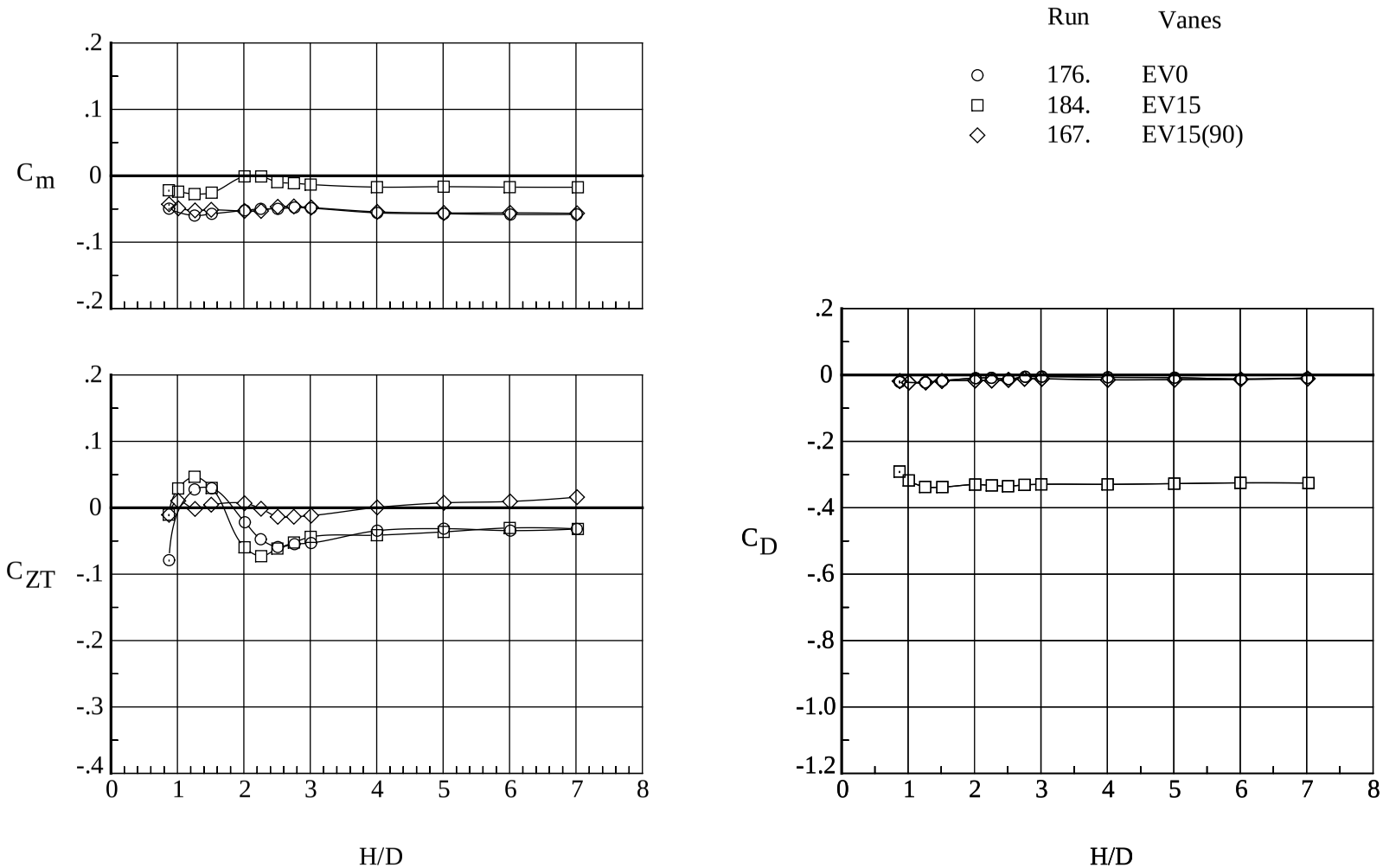

Figure 13. Effect of vane configurations (EV0, EV15, and EV15(90)) on variation of C_m, C_{ZT}, and C_D with *H/D* for B* G D1 T FS2 (22000 rpm and $\alpha = 0°$).

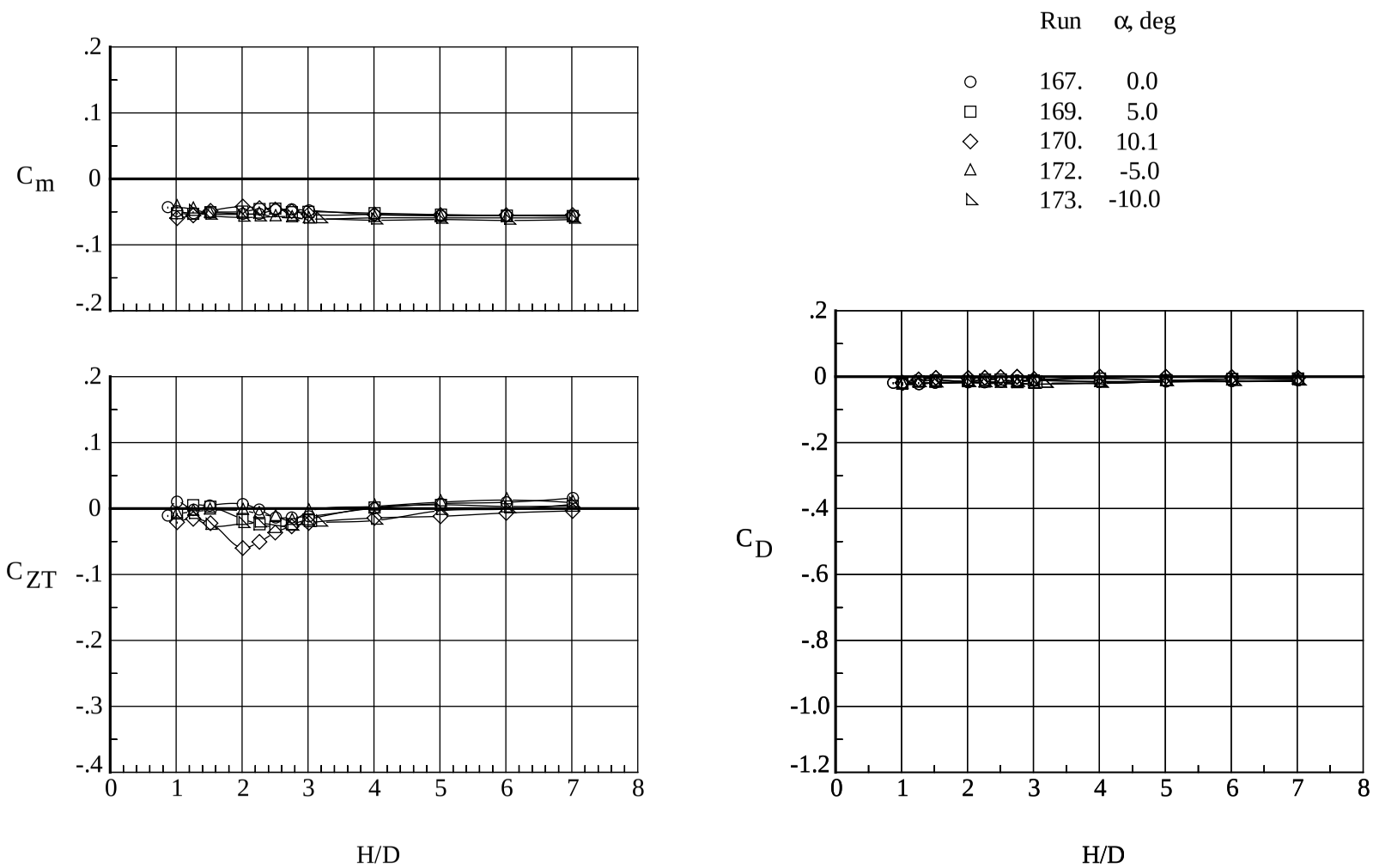

Figure 14. Effect of angle of pitch on variation of C_m, C_{ZT}, and C_D with *H/D* for B* G D1 T FS2 EV15(90) (22 000 rpm).

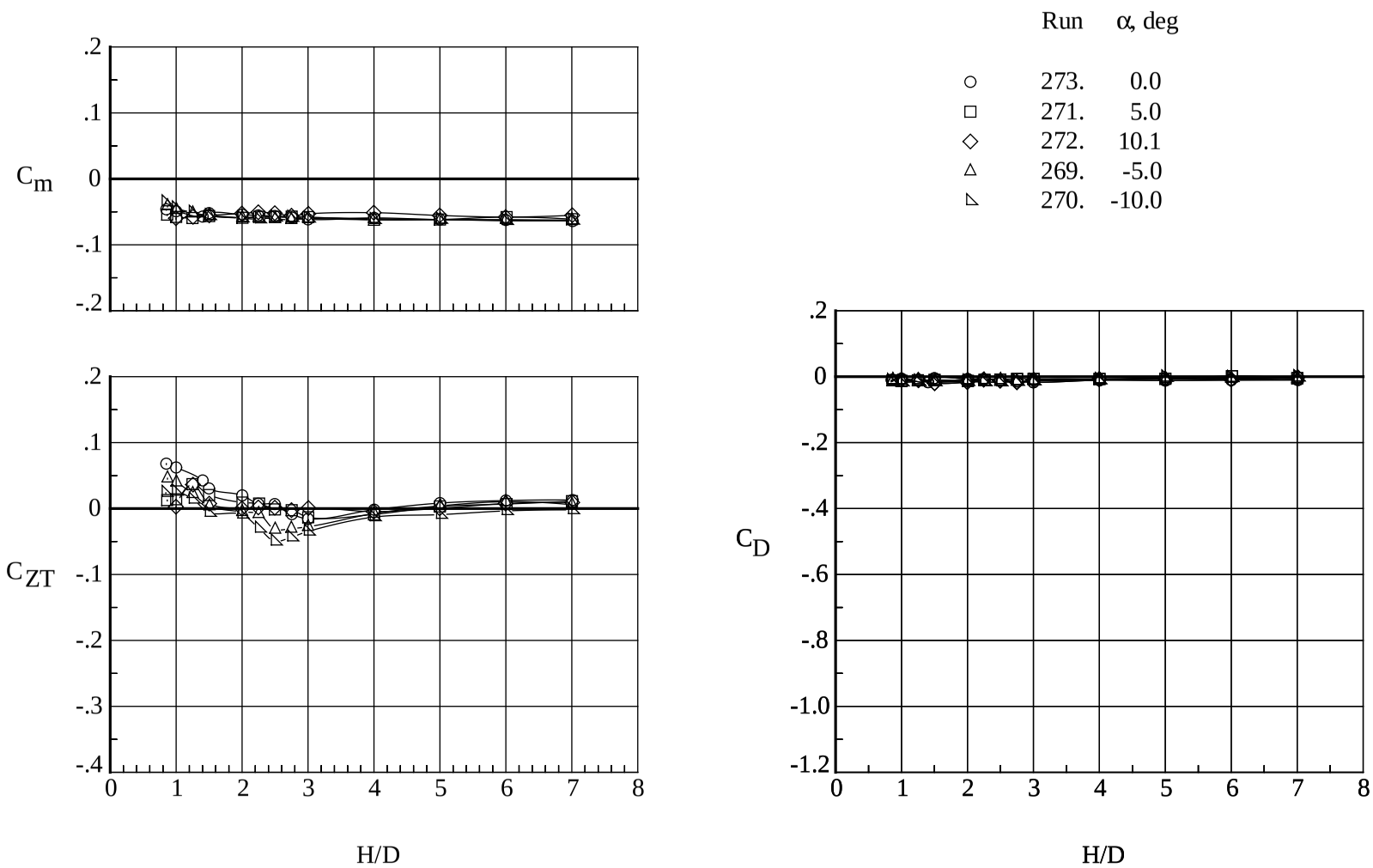

Figure 15. Effect of angle of pitch on variation of C_m, C_{ZT}, and C_D with *H/D* for W5 B6 D1 T FS2 EV7.5(90) (22000 rpm).

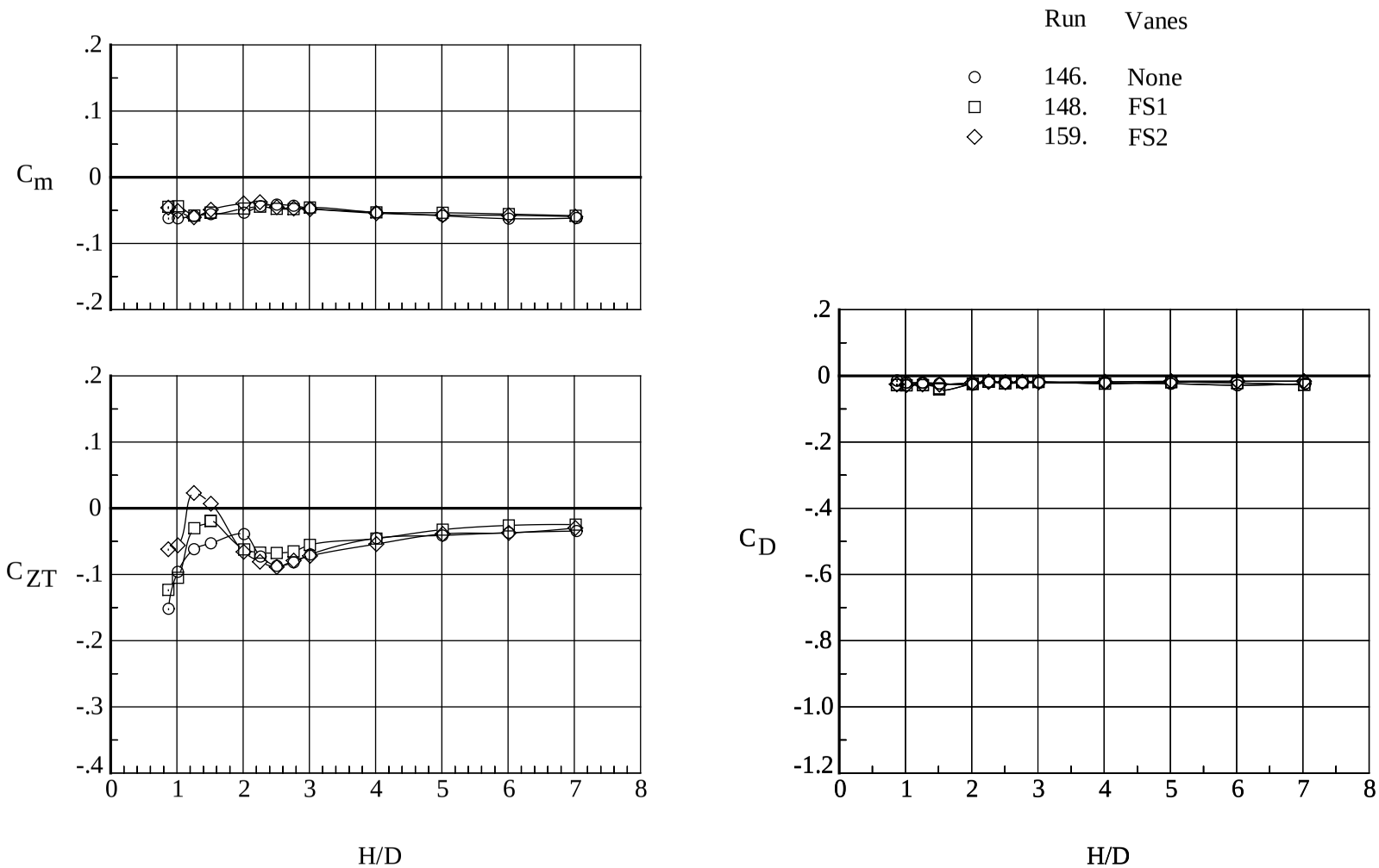

Figure 16. Effect of strake configuration (FS1 and FS2) on variation of C_m, C_{ZT}, and C_D with H/D for B* G D1 T (22000 rpm and $\alpha = 0°$).

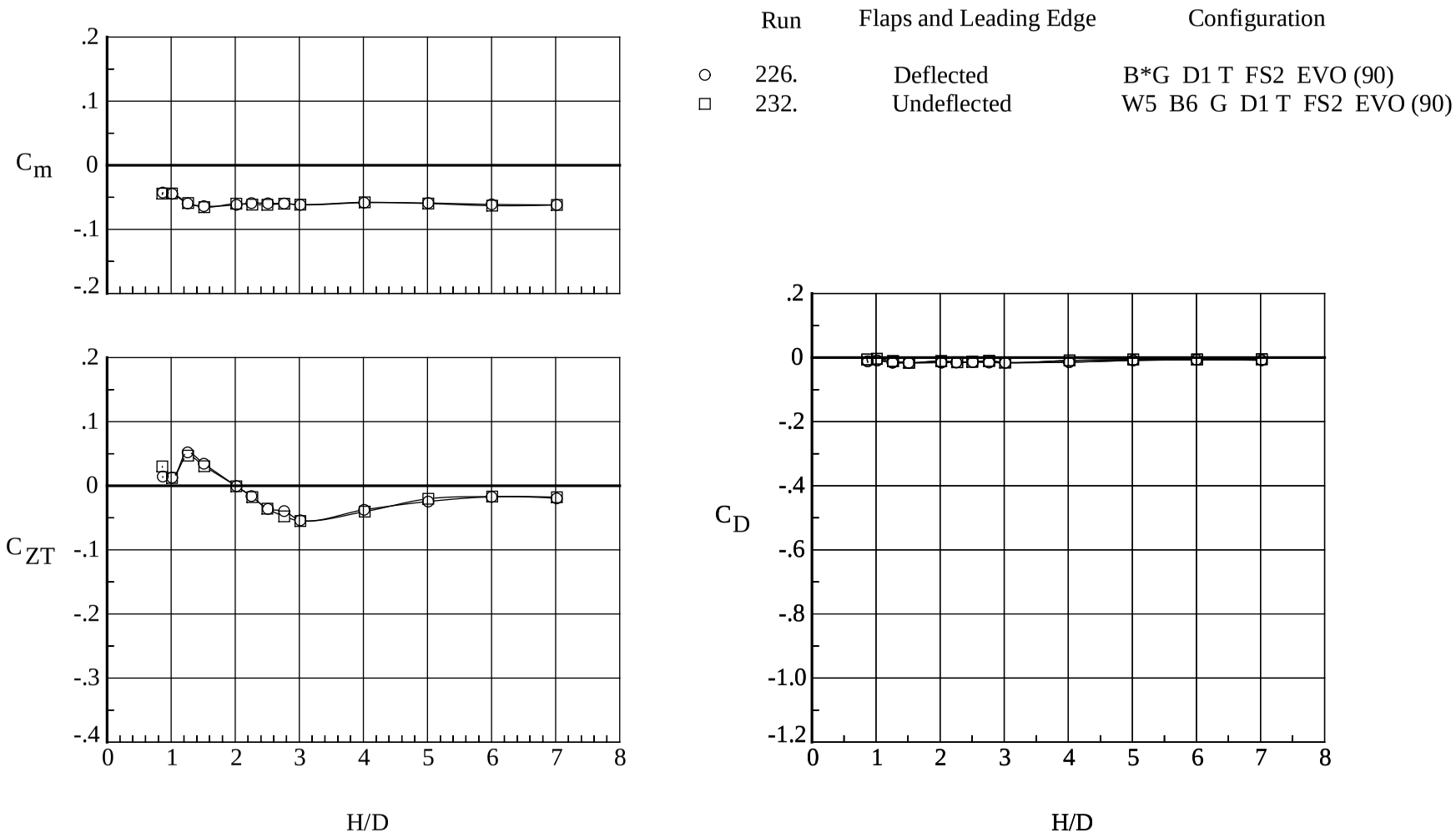

Figure 17. Effect of flap and leading-edge deflection on variation of C_m, C_{ZT}, and C_D with H/D (22 000 rpm and $\alpha = 0°$).

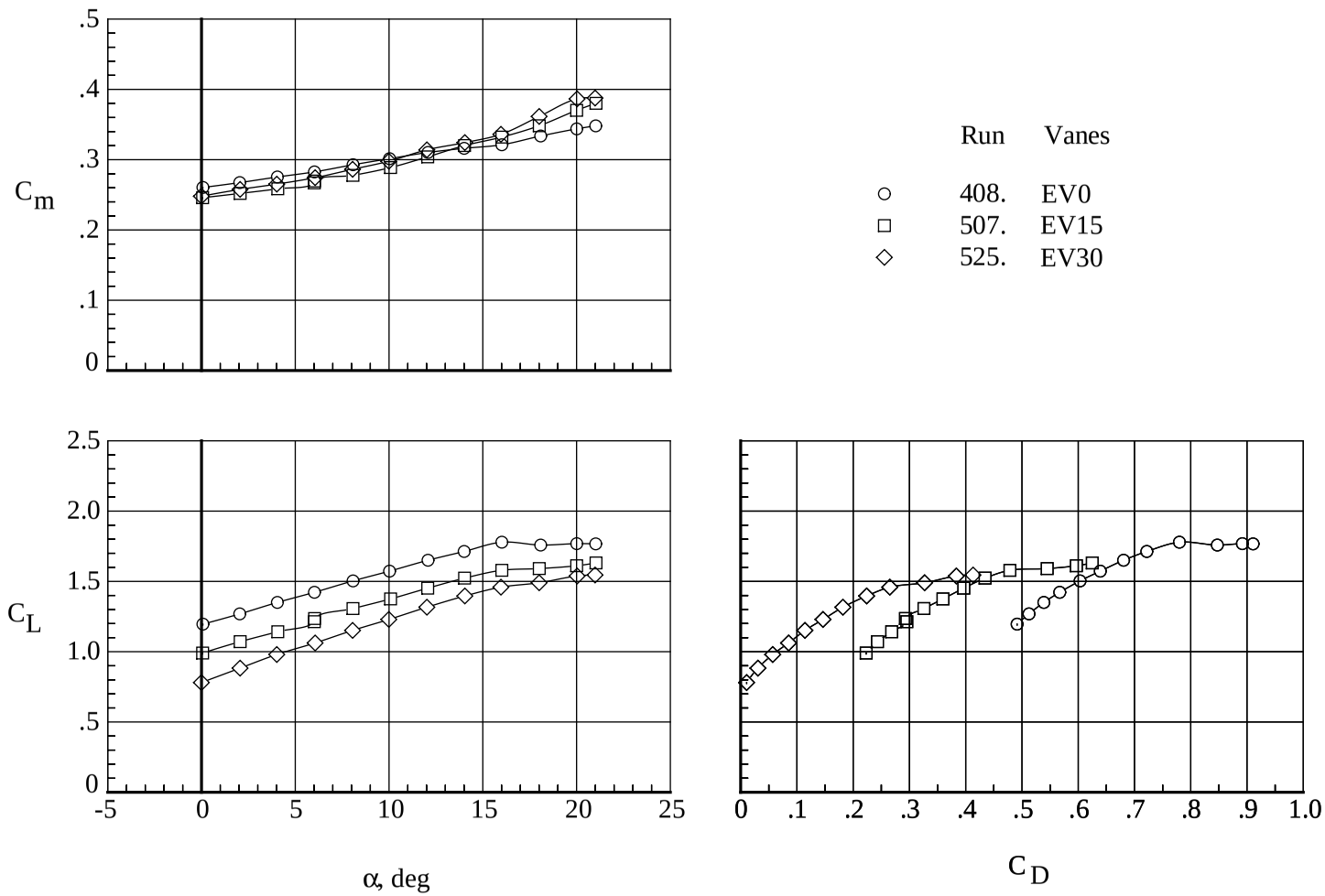

(a) rpm = 22 000.

Figure 18. Effect of vane configurations (EV0, EV15, and EV30) on variation of C_m and C_L with angle of attack and C_L with C_D for three levels of fan rpm for B* G D1 T (H/D = 5.4).

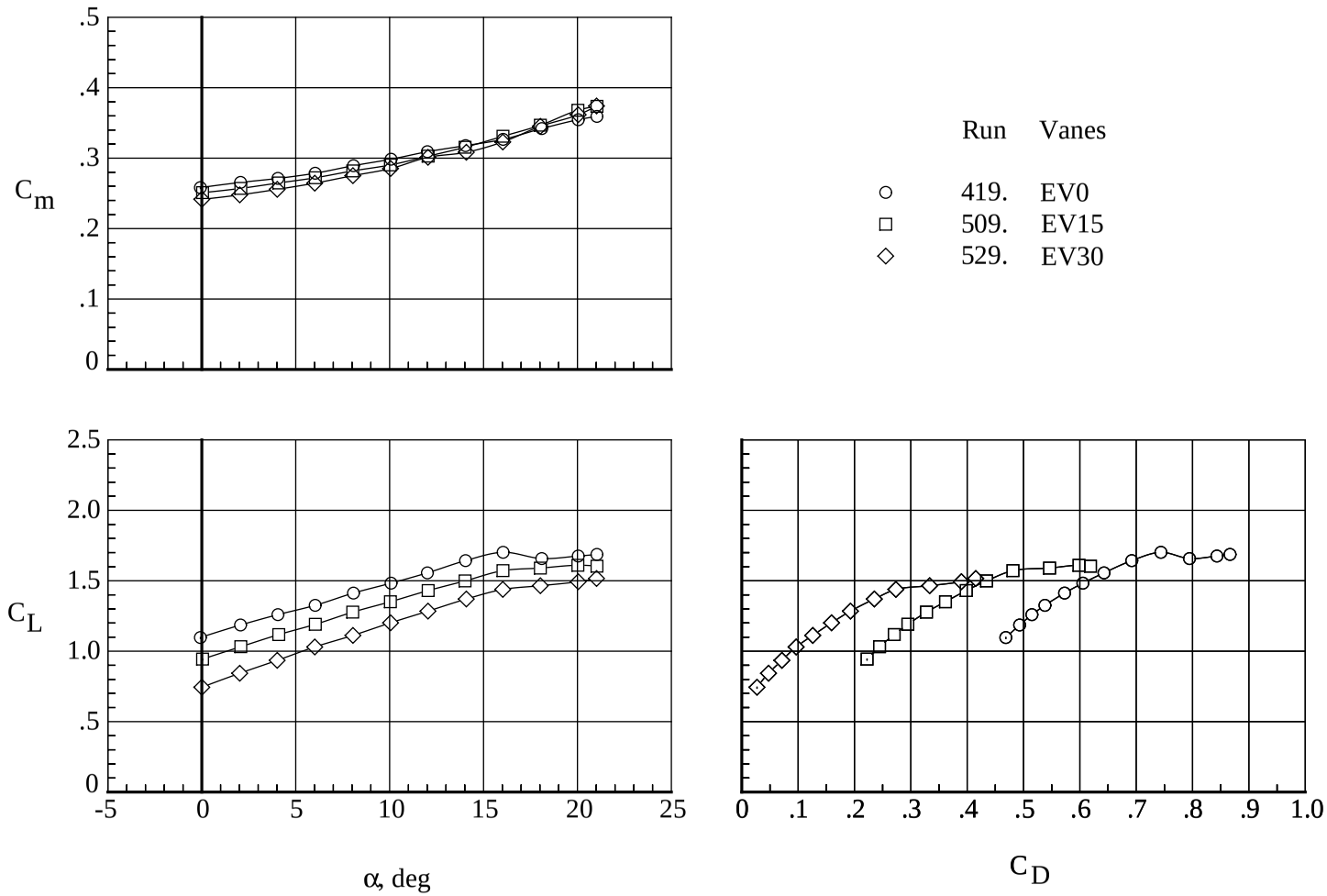

(b) rpm = 20300.

Figure 18. Continued.

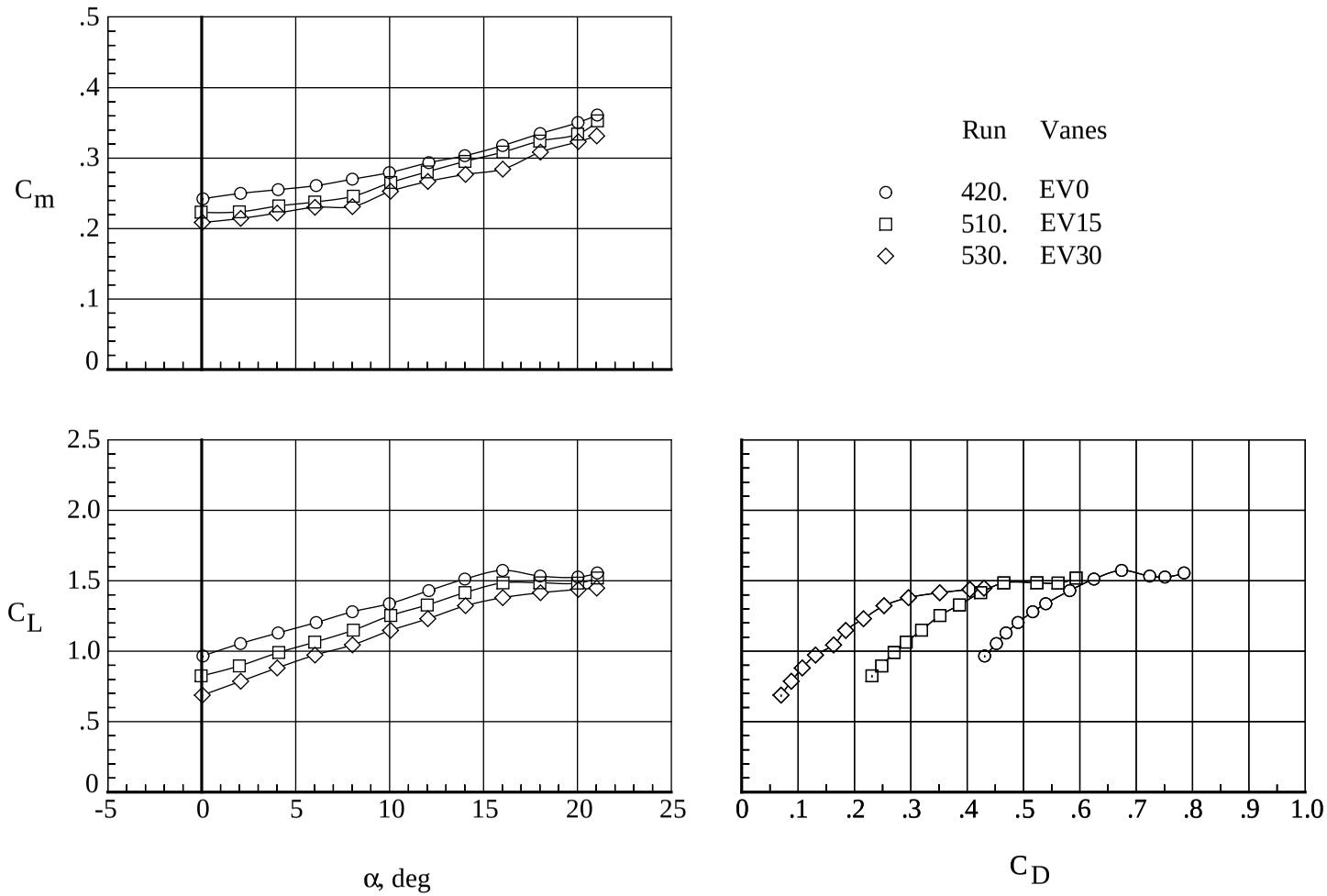

(c) rpm = 17 800.

Figure 18. Concluded.

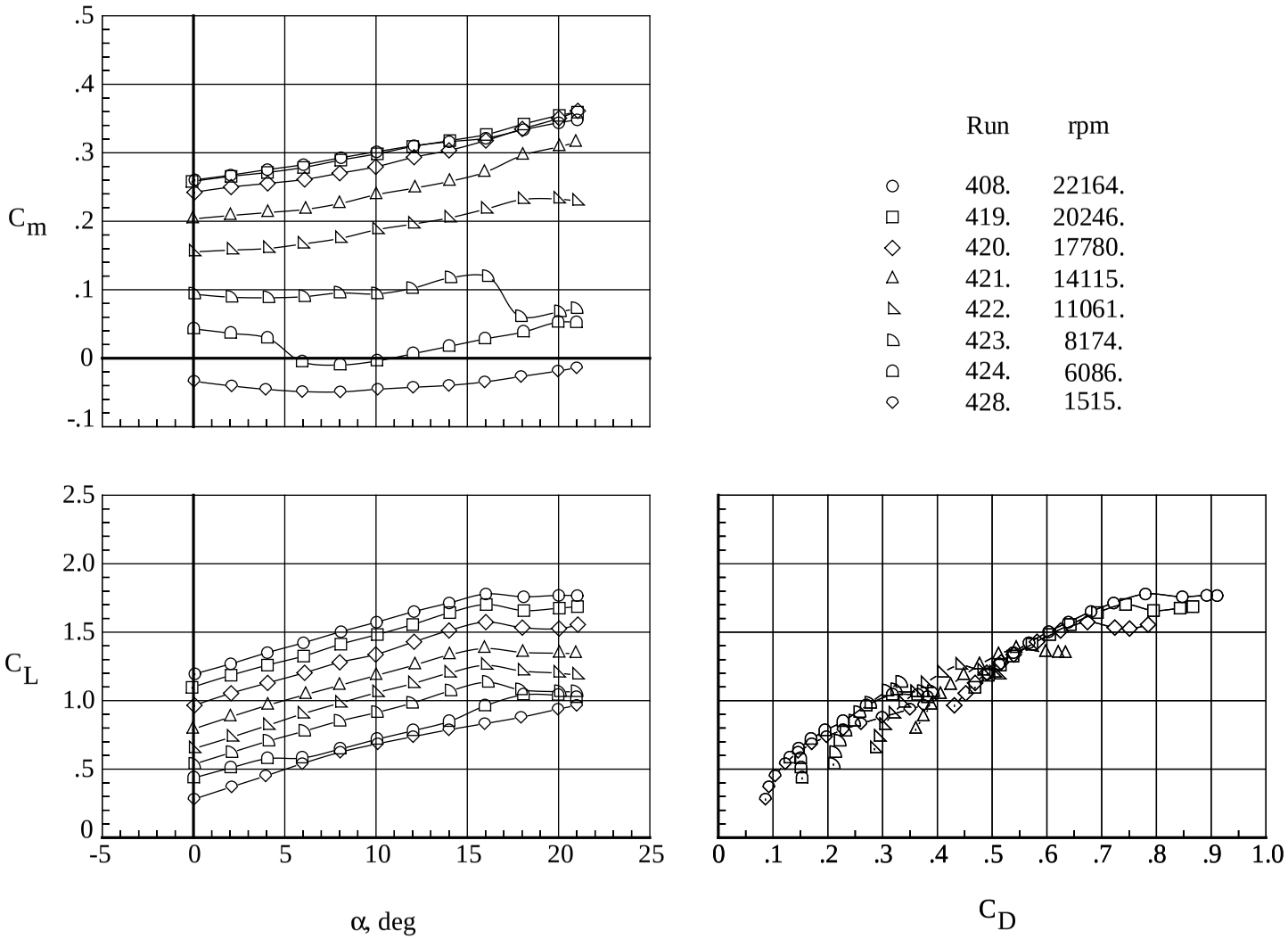

(a) EV0.

Figure 19. Effect of fan rpm on variation of C_m and C_L with angle of attack and C_L with C_D for B* G D1 T with EV0, EV15, and EV30 vanes (H/D = 5.4).

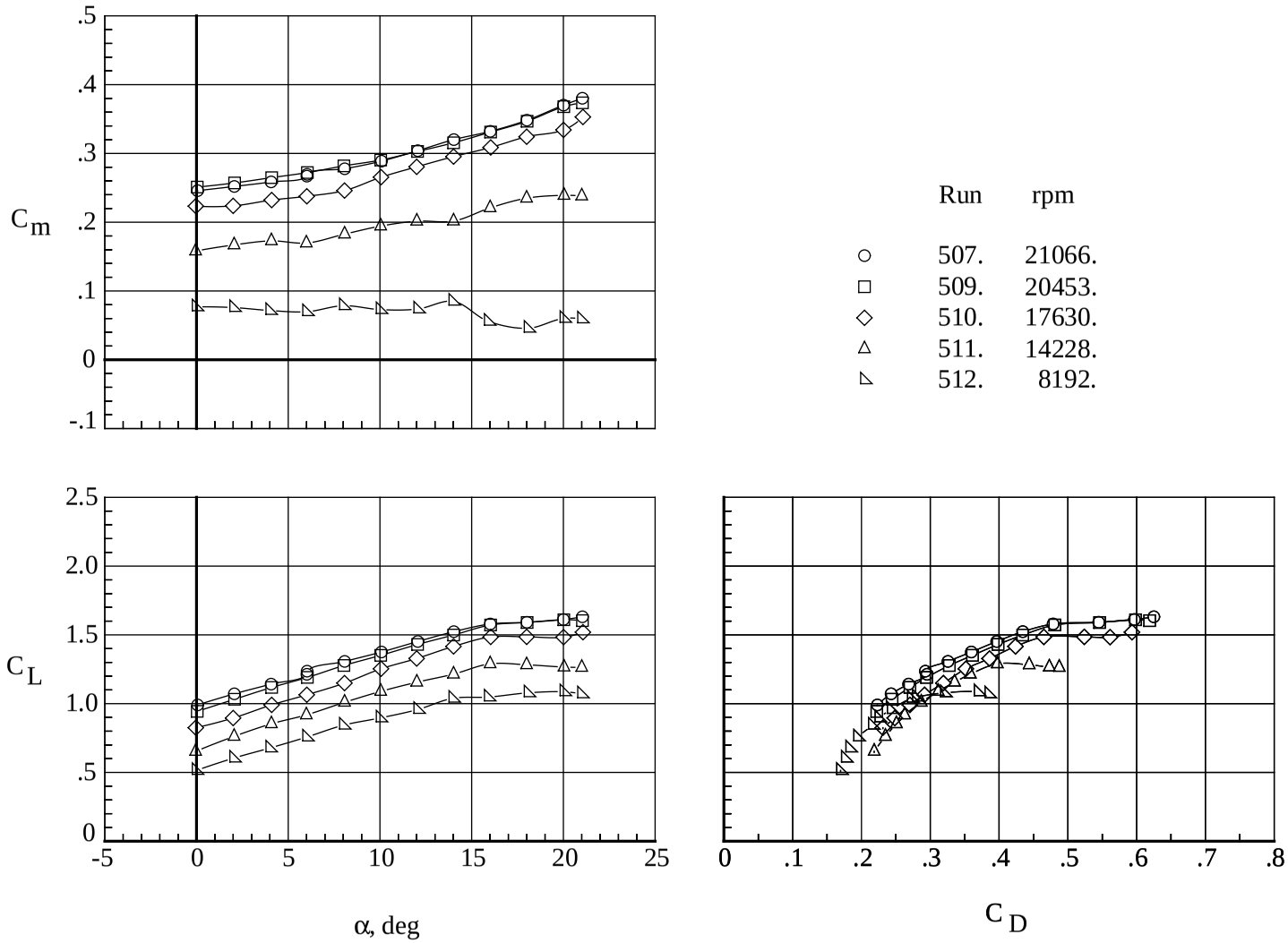

(b) EV15.

Figure 19. Continued.

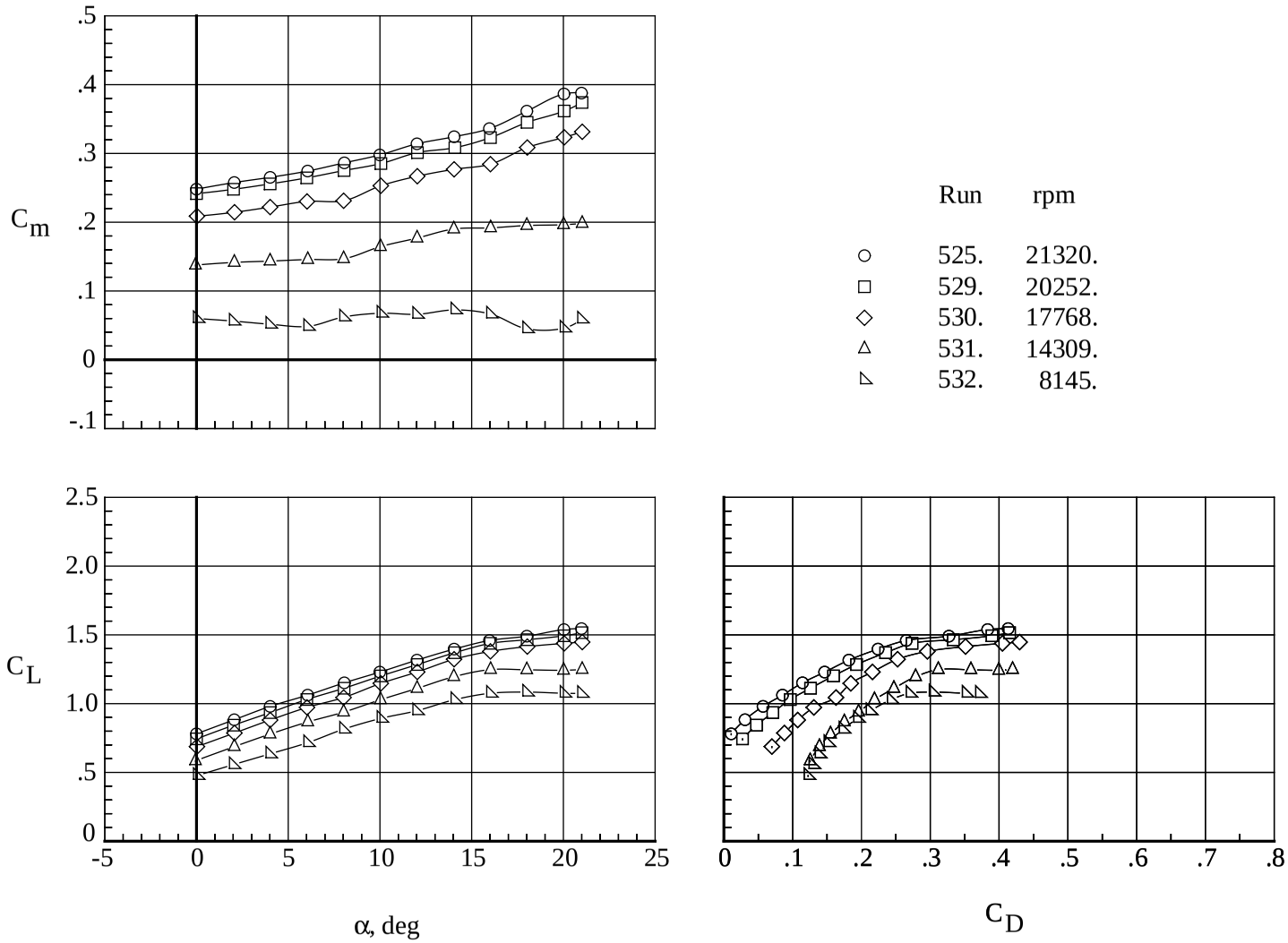

(c) EV30.

Figure 19. Concluded.

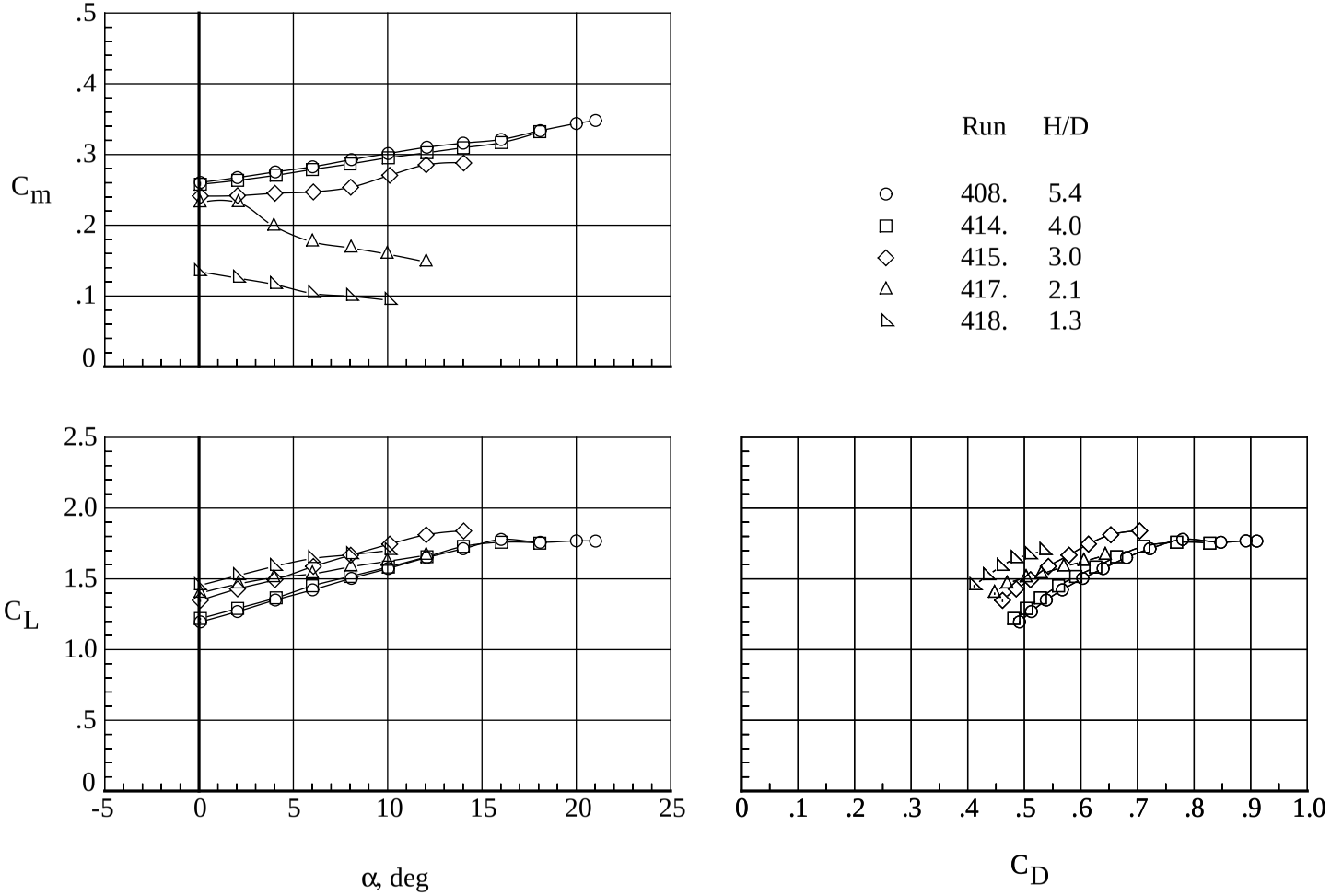

(a) EV0.

Figure 20. Effect of *H/D* on variation of C_m and C_L with angle of attack and C_L with C_D for B* G D1 T with EV0, EV15, and EV30 vanes (22000 rpm).

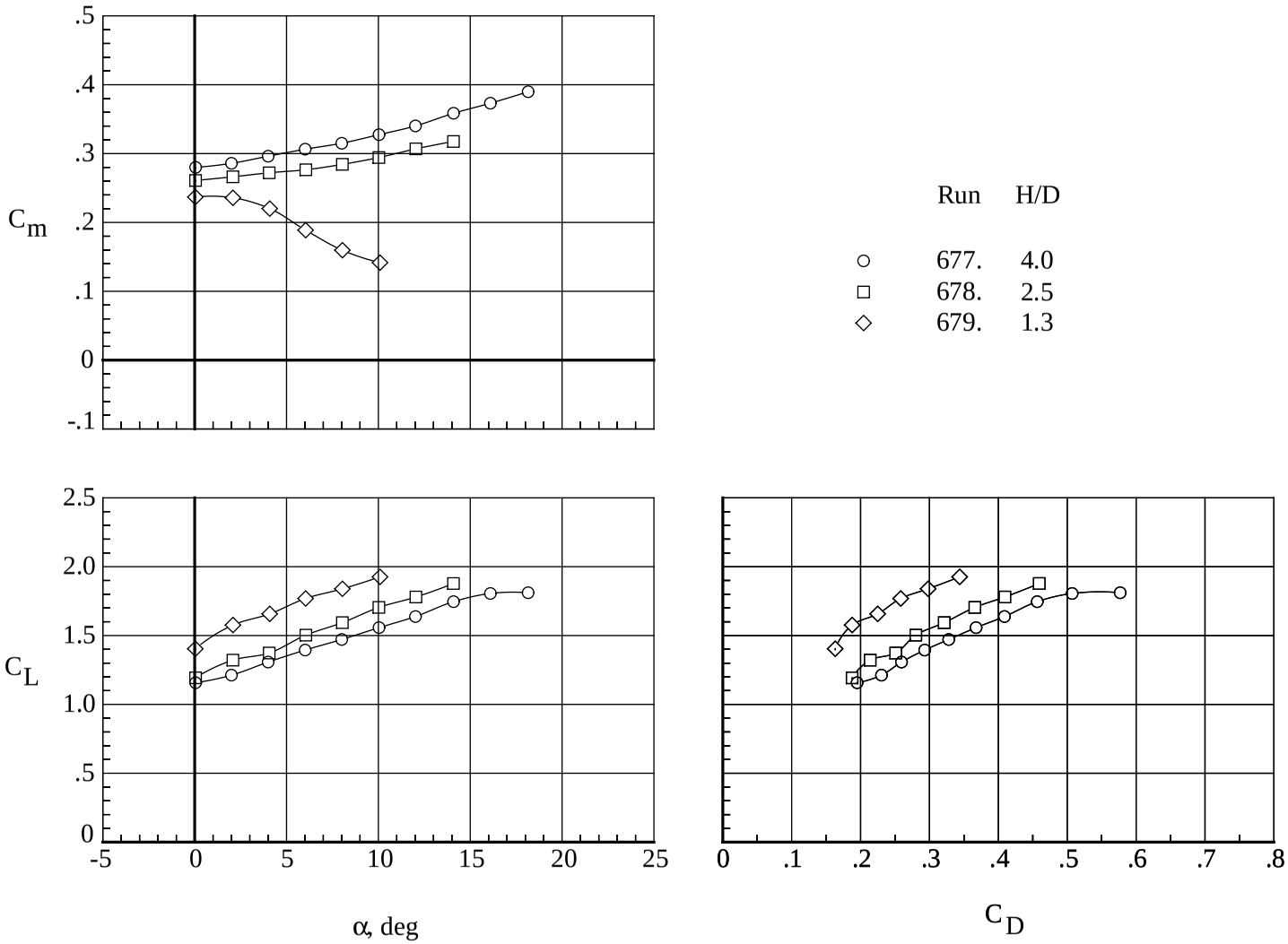

(b) EV15.

Figure 20. Continued.

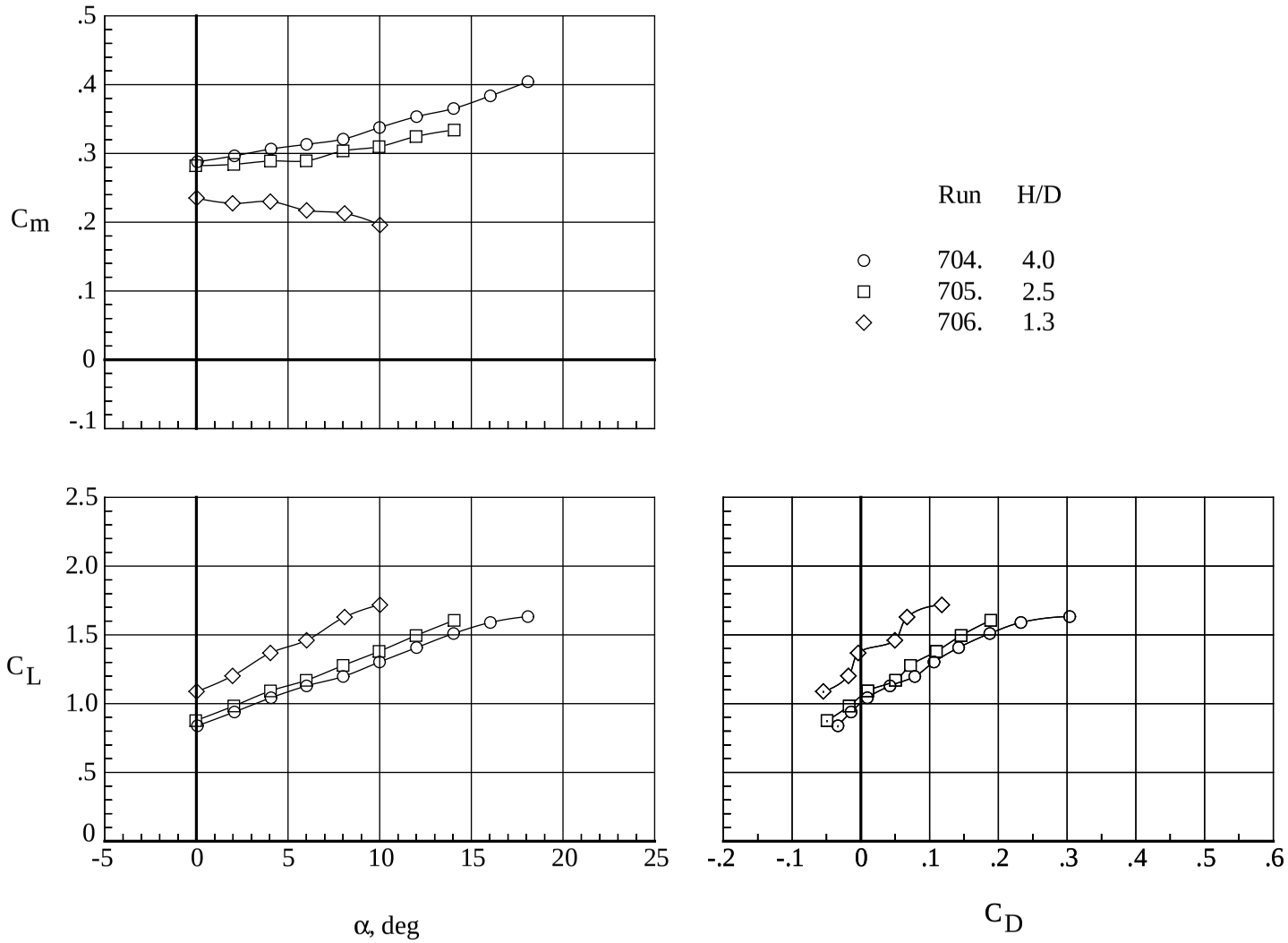

(c) EV30.

Figure 20. Concluded.

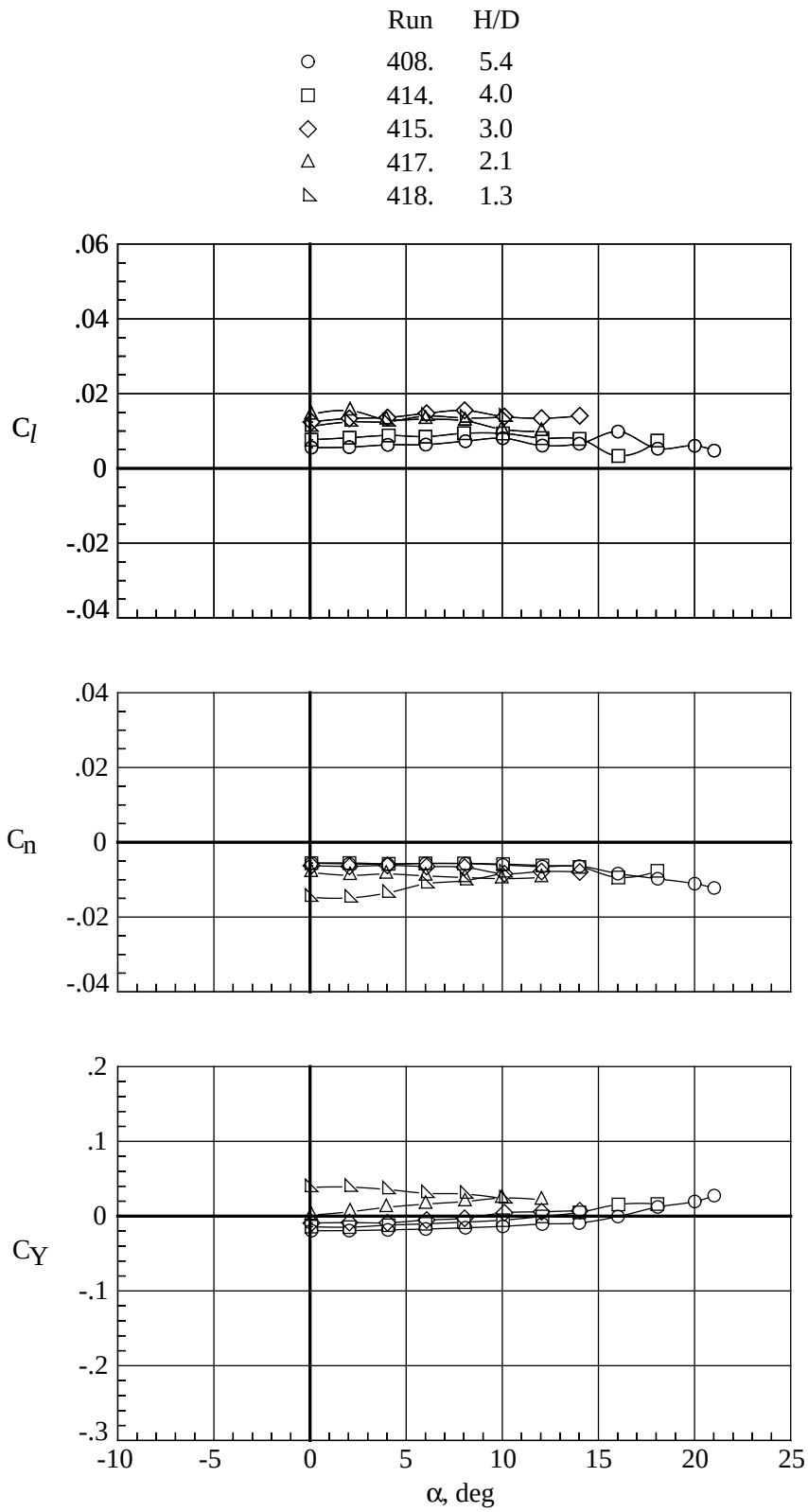

(a) EV0.

Figure 21. Effect of *H/D* on variation of C_l, C_n, and C_Y with angle of attack for B* G D1 T with EV0, EV15, and EV30 vanes (22000 rpm).

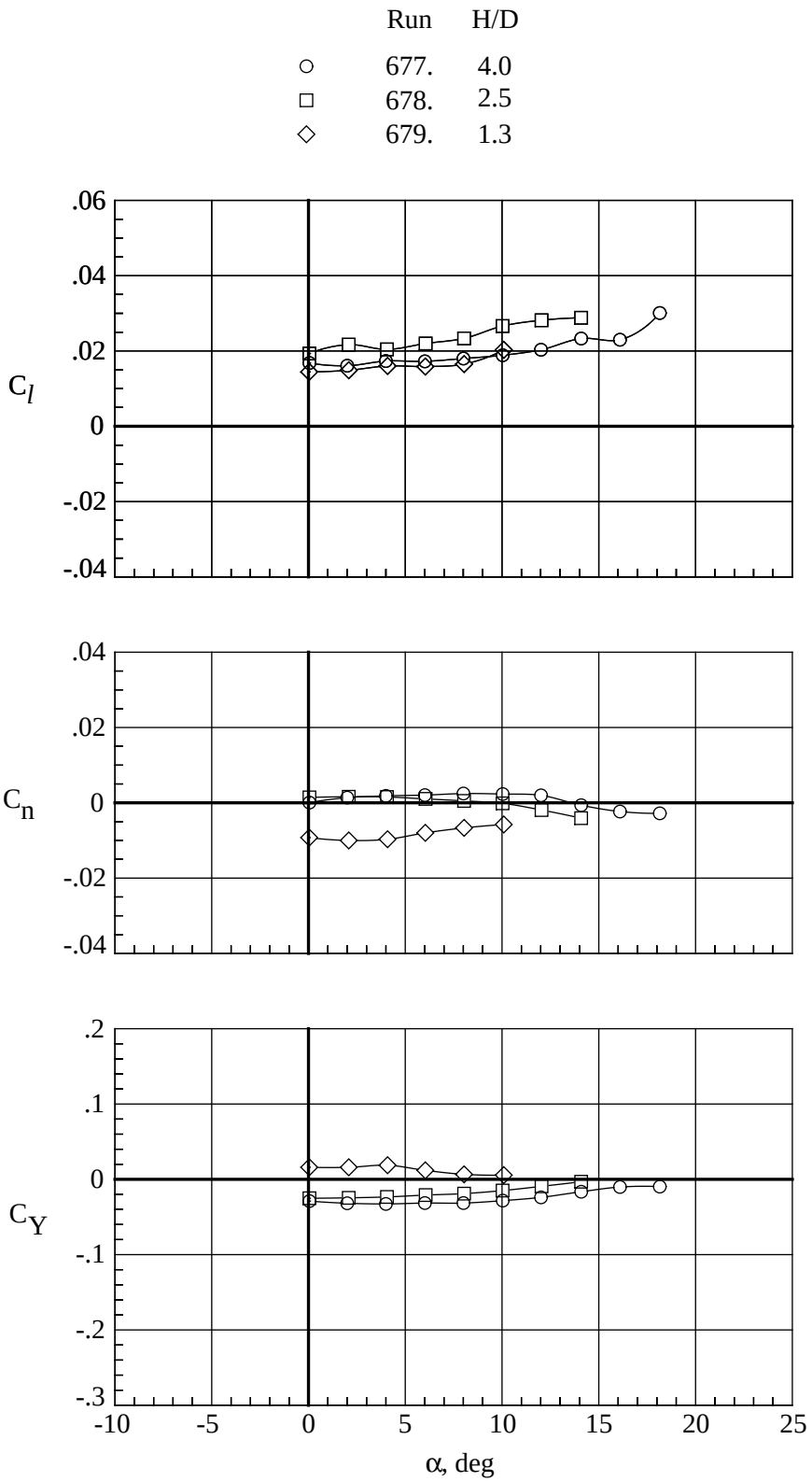

(b) EV15.

Figure 21. Continued.

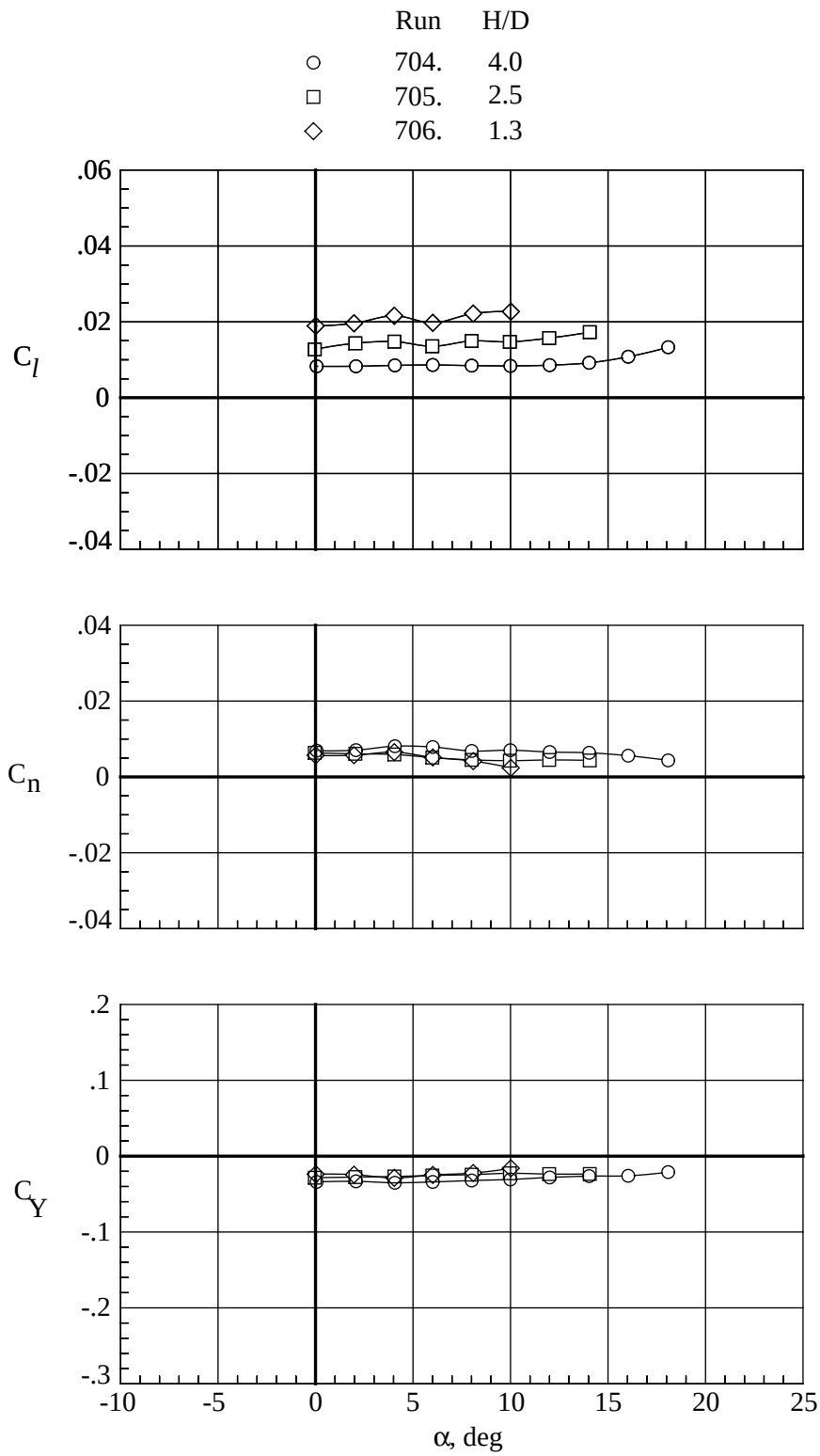

(c) EV30.

Figure 21. Concluded.

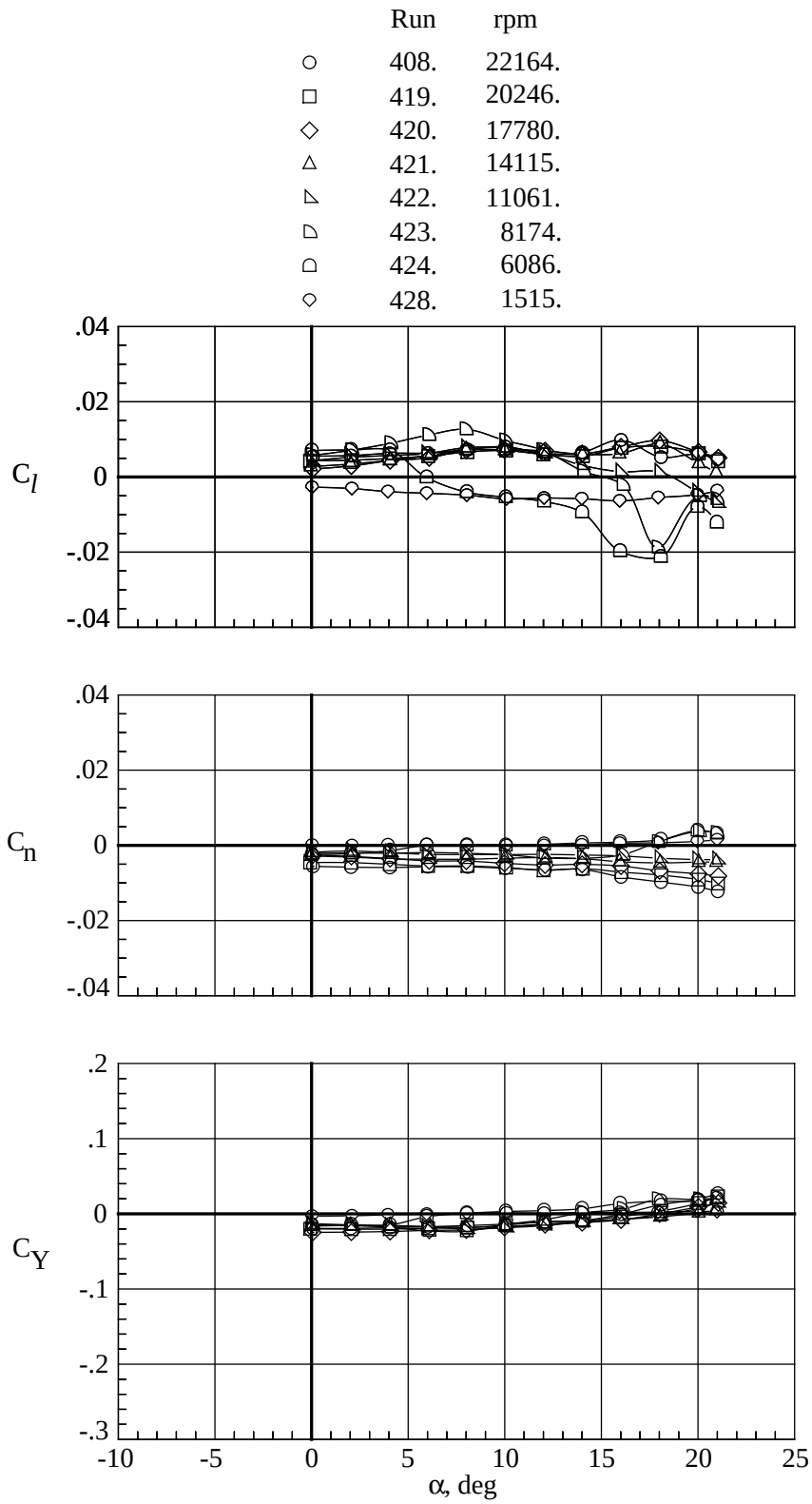

(a) EV0.

Figure 22. Effect of fan rpm on variation of C_l, C_n, and C_Y with angle of attack for B* G D1 T with EV0, EV15, and EV30 vanes (H/D = 5.4).

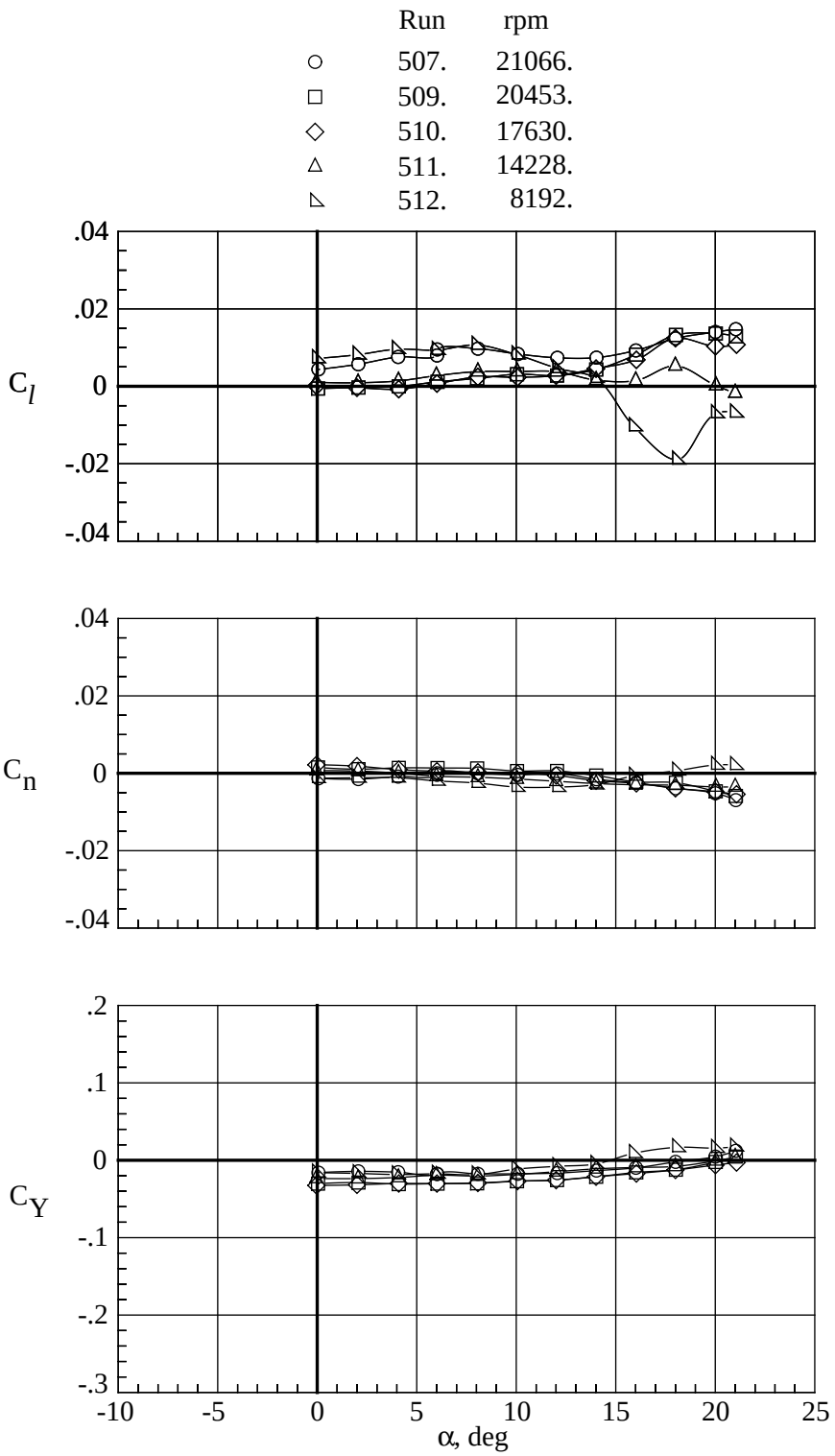

(b) EV15.

Figure 22. Continued.

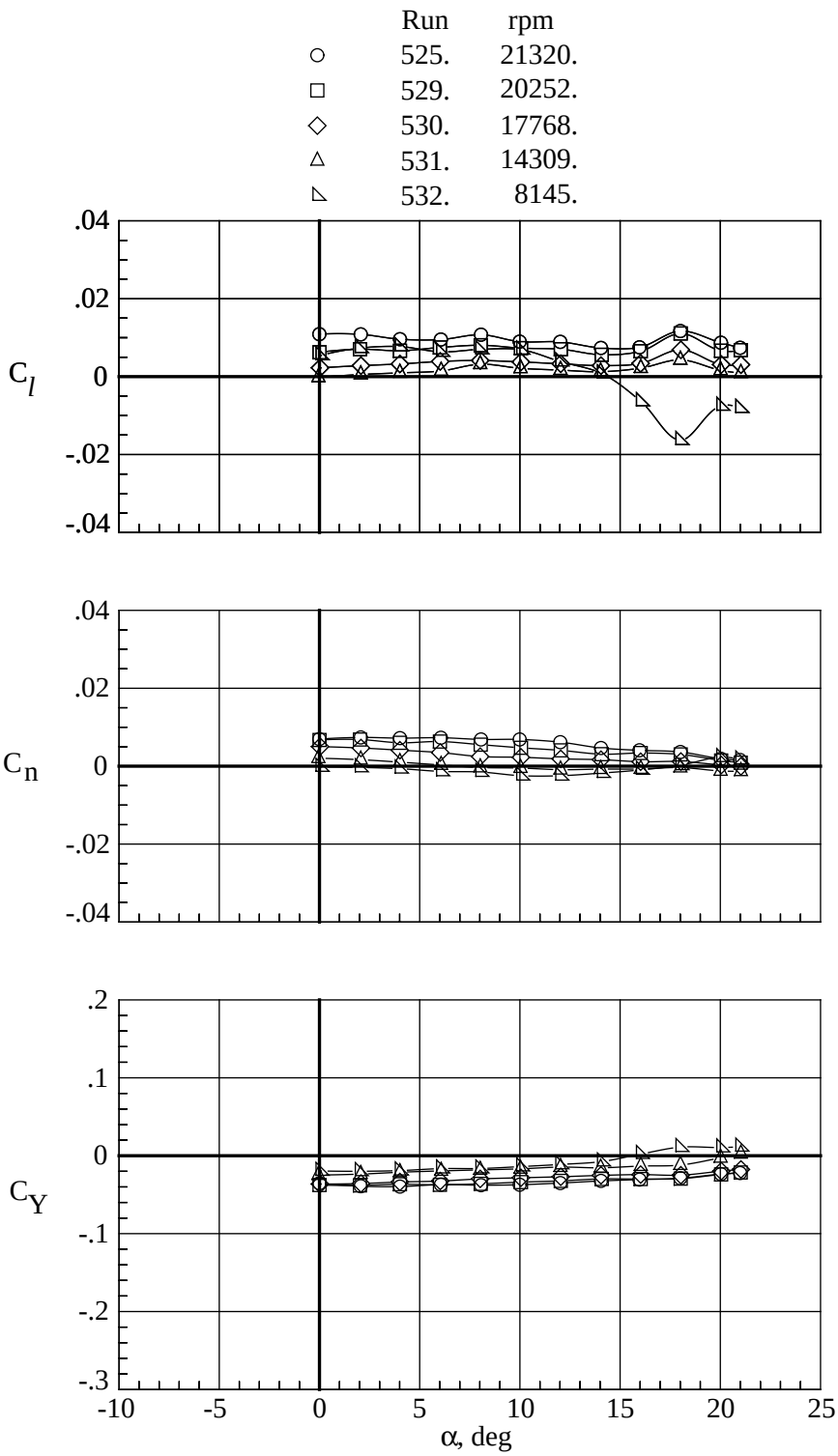

(c) EV30.

Figure 22. Concluded.

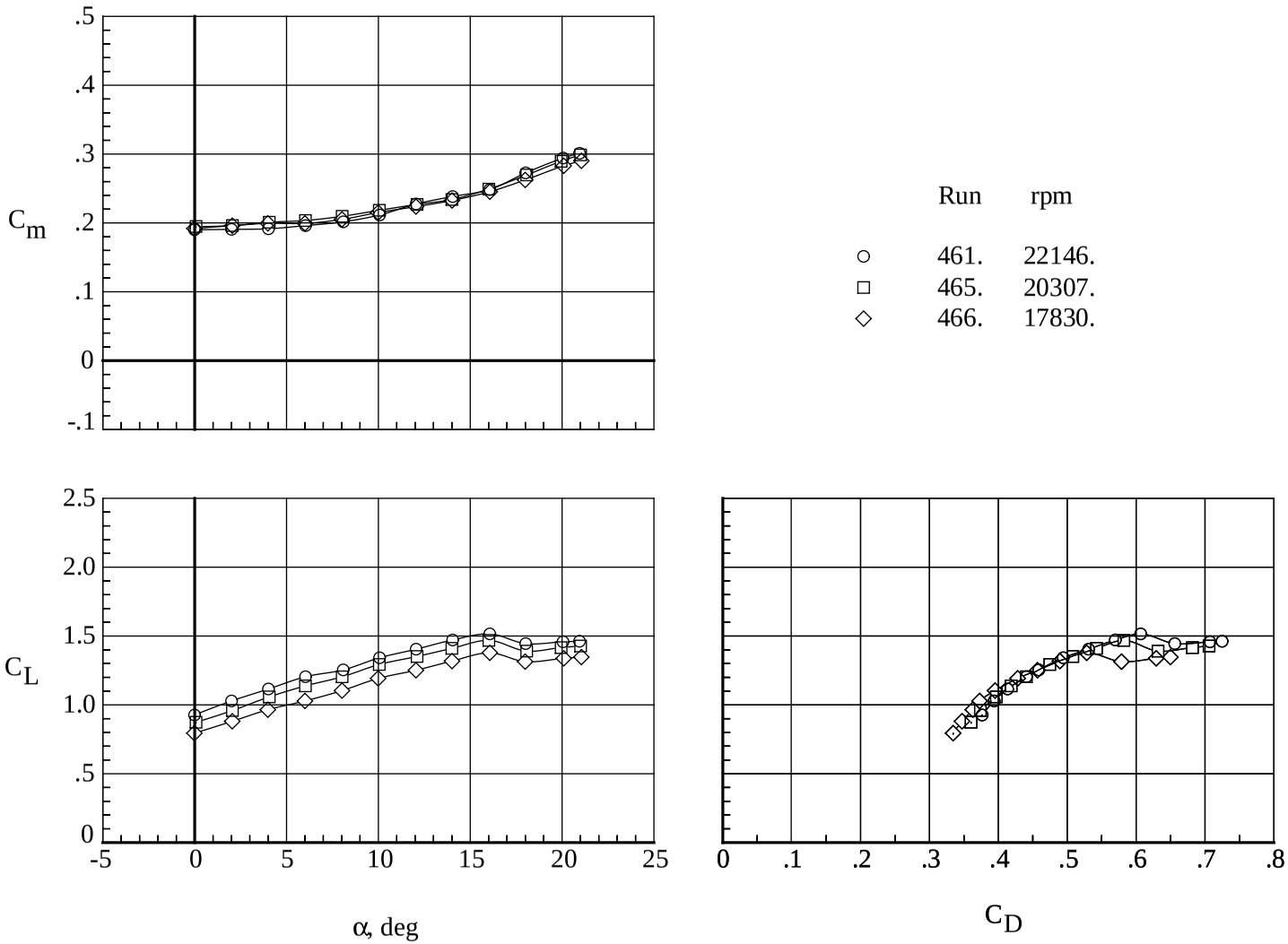

(a) *H/D* = 5.4.

Figure 23. Effect of fan rpm on variation of C_m and C_L with angle of attack and C_L with C_D for four values of *H/D* for B* G D1 T EV(15/15).

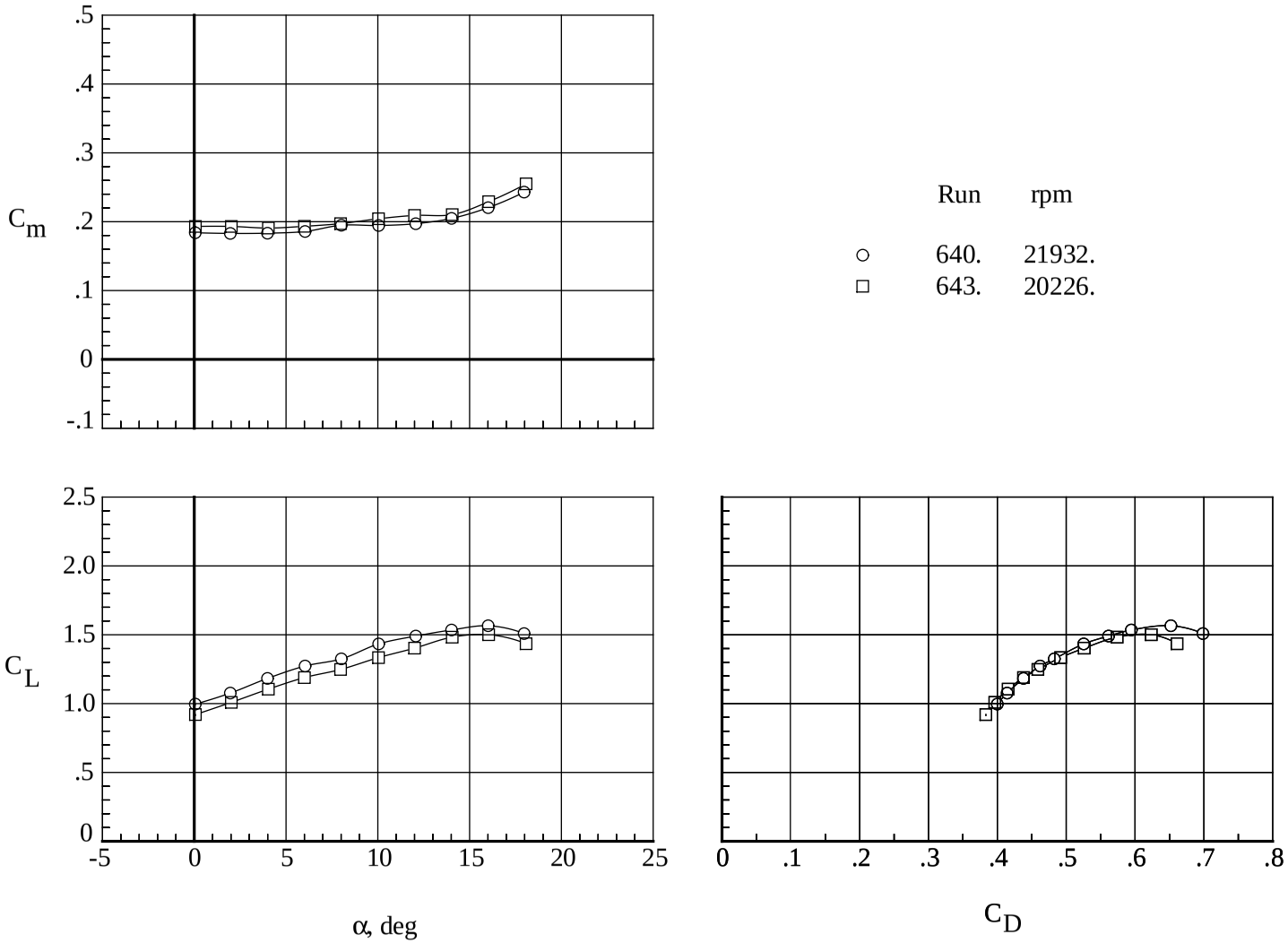

(b) *H/D* = 4.0.

Figure 23. Continued.

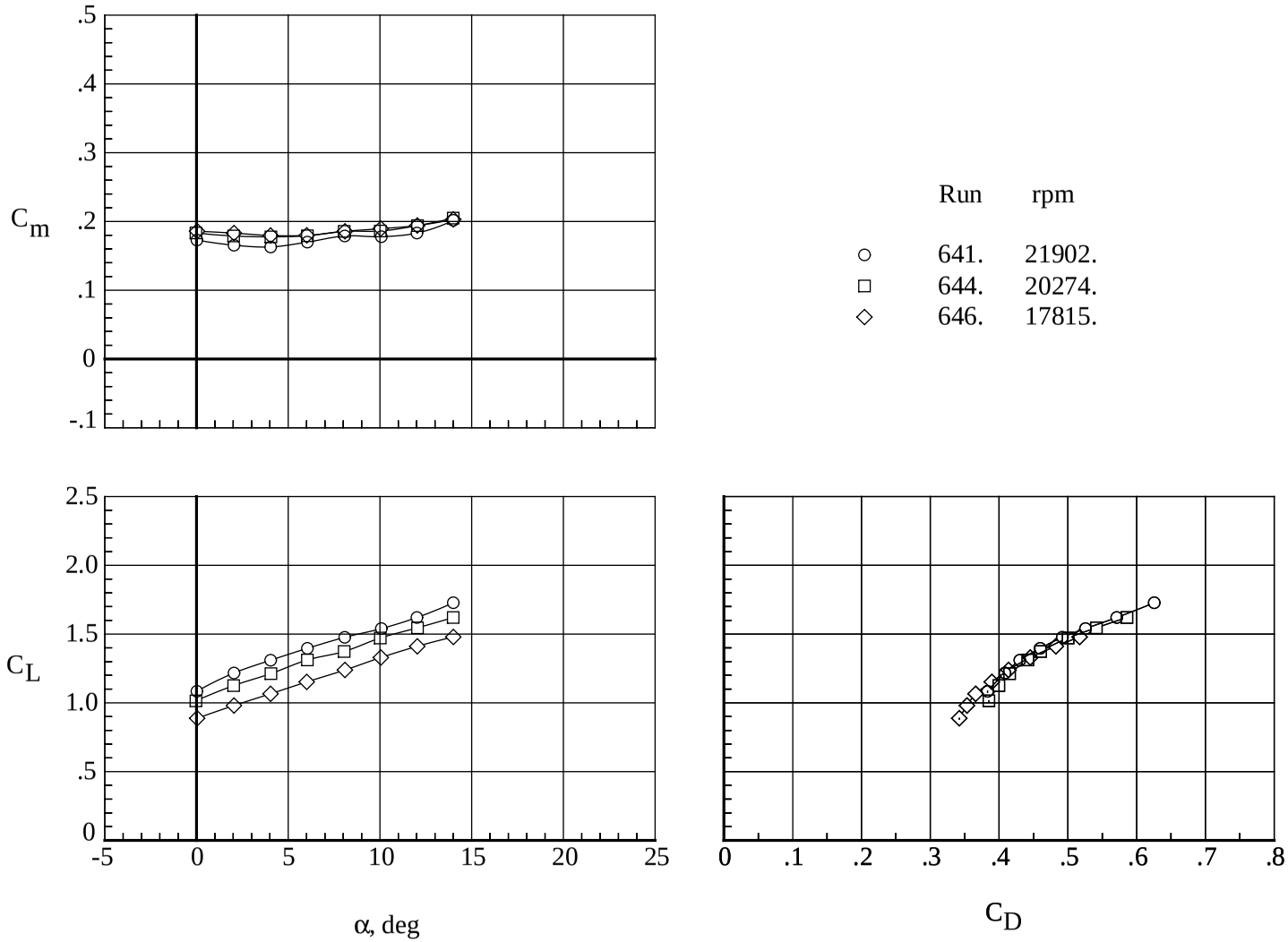

(c) *H/D* = 2.5.

Figure 23. Continued.

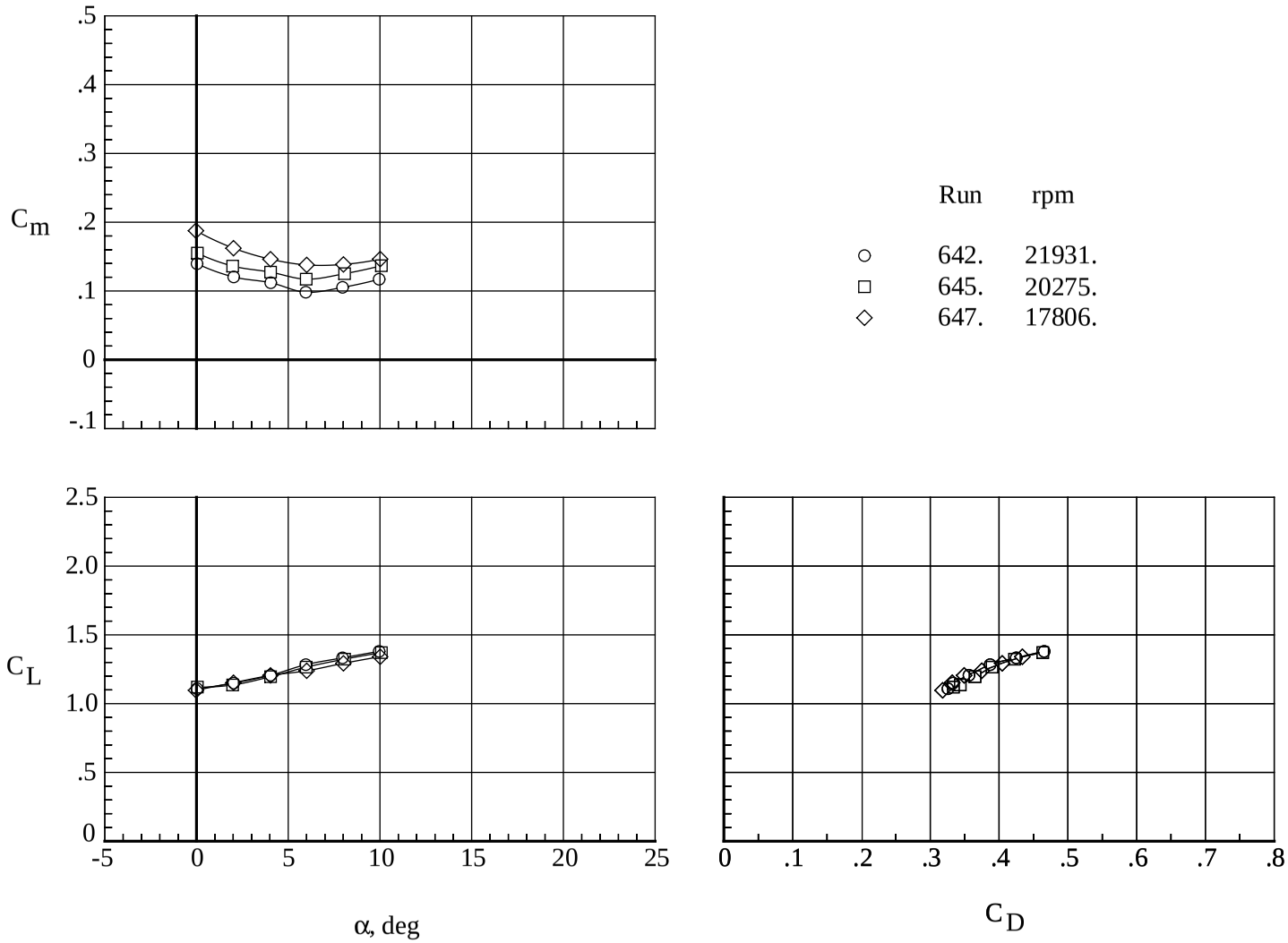

(d) *H/D* = 1.3.

Figure 23. Concluded.

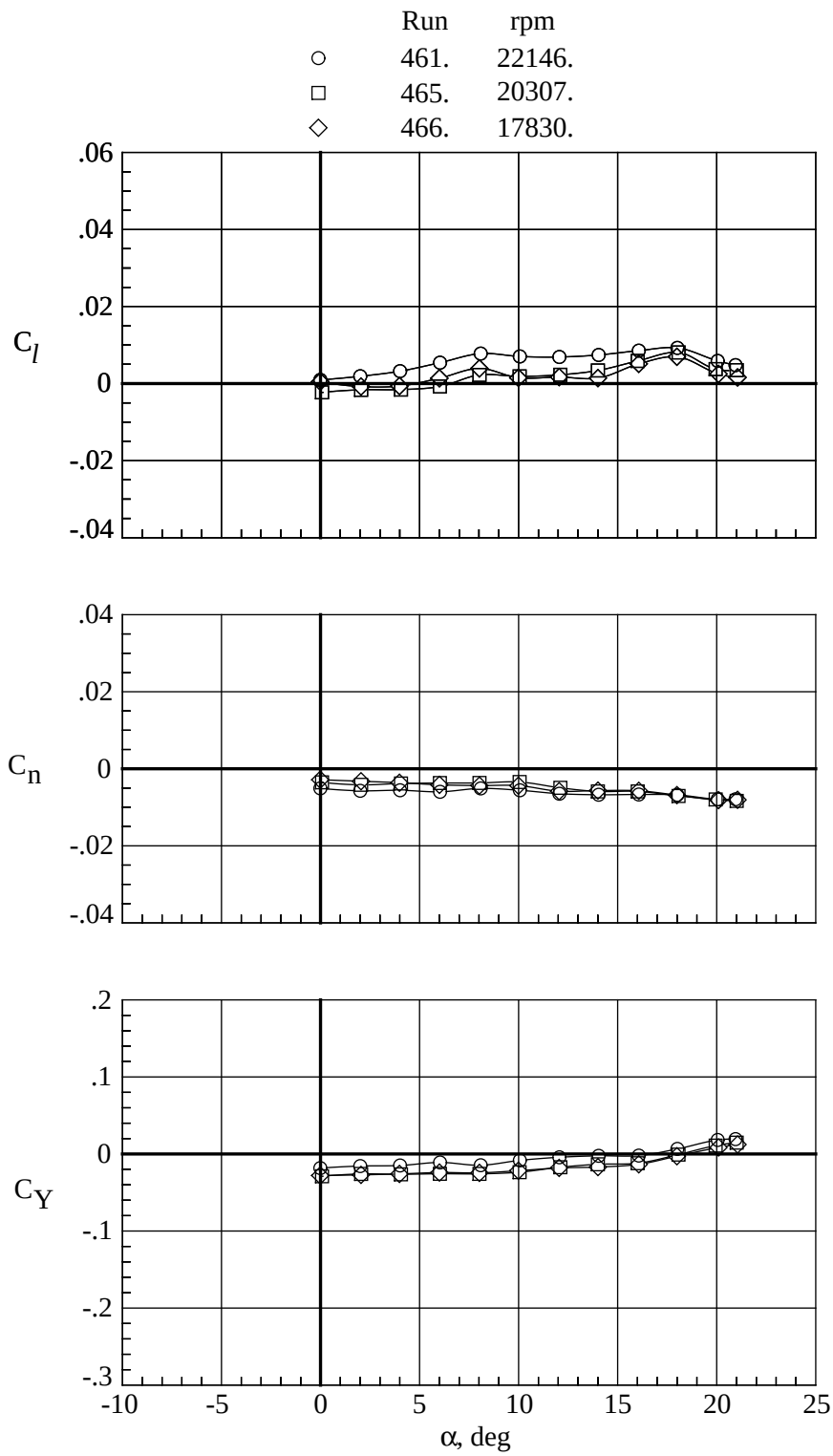

(a) *H/D* = 5.4.

Figure 24. Effect of fan rpm on variation of C_l, C_n, and C_Y with angle of attack for four values of *H/D* for B* G D1 T EV(15/15).

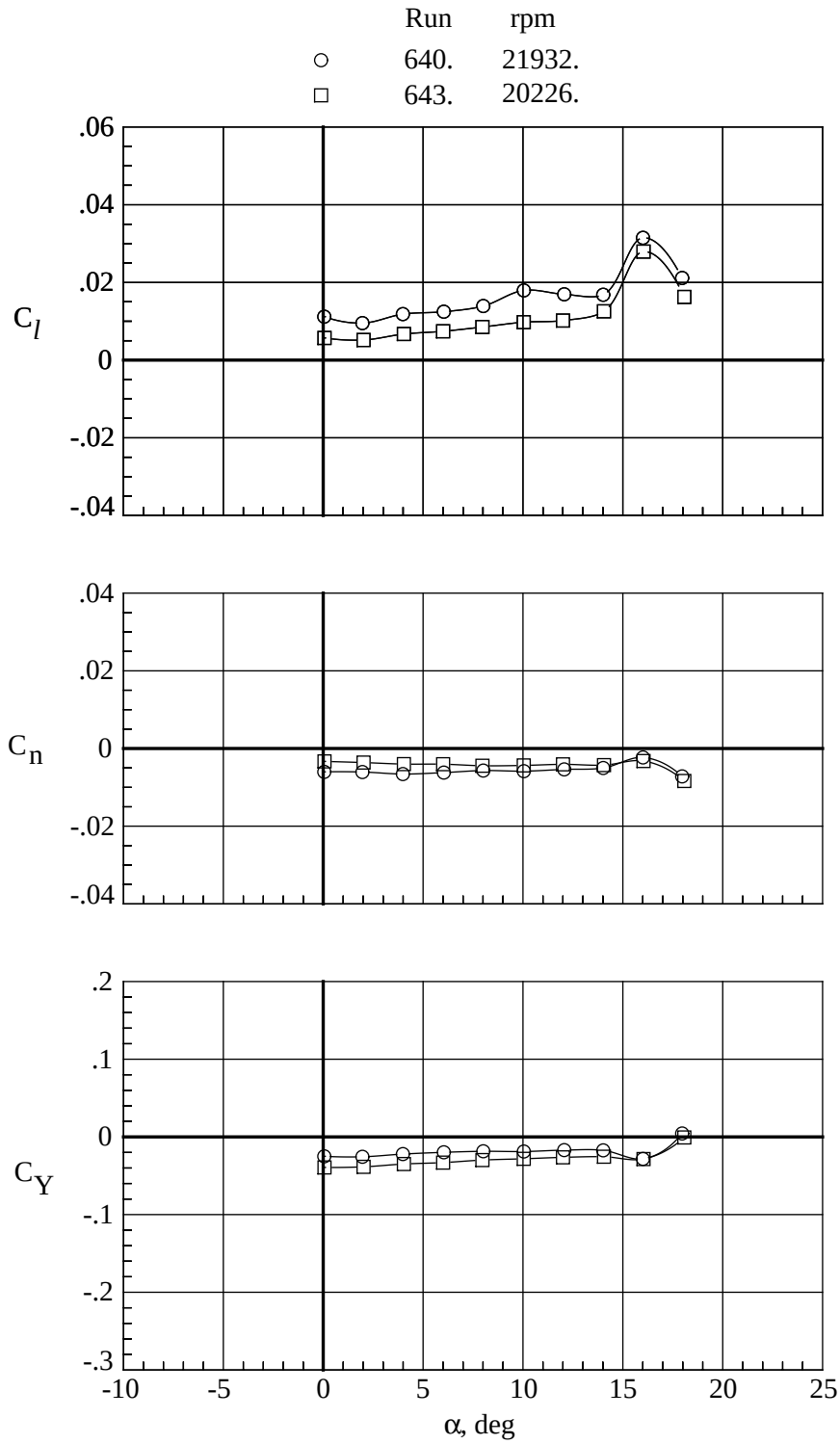

(b) *H/D* = 4.0.

Figure 24. Continued.

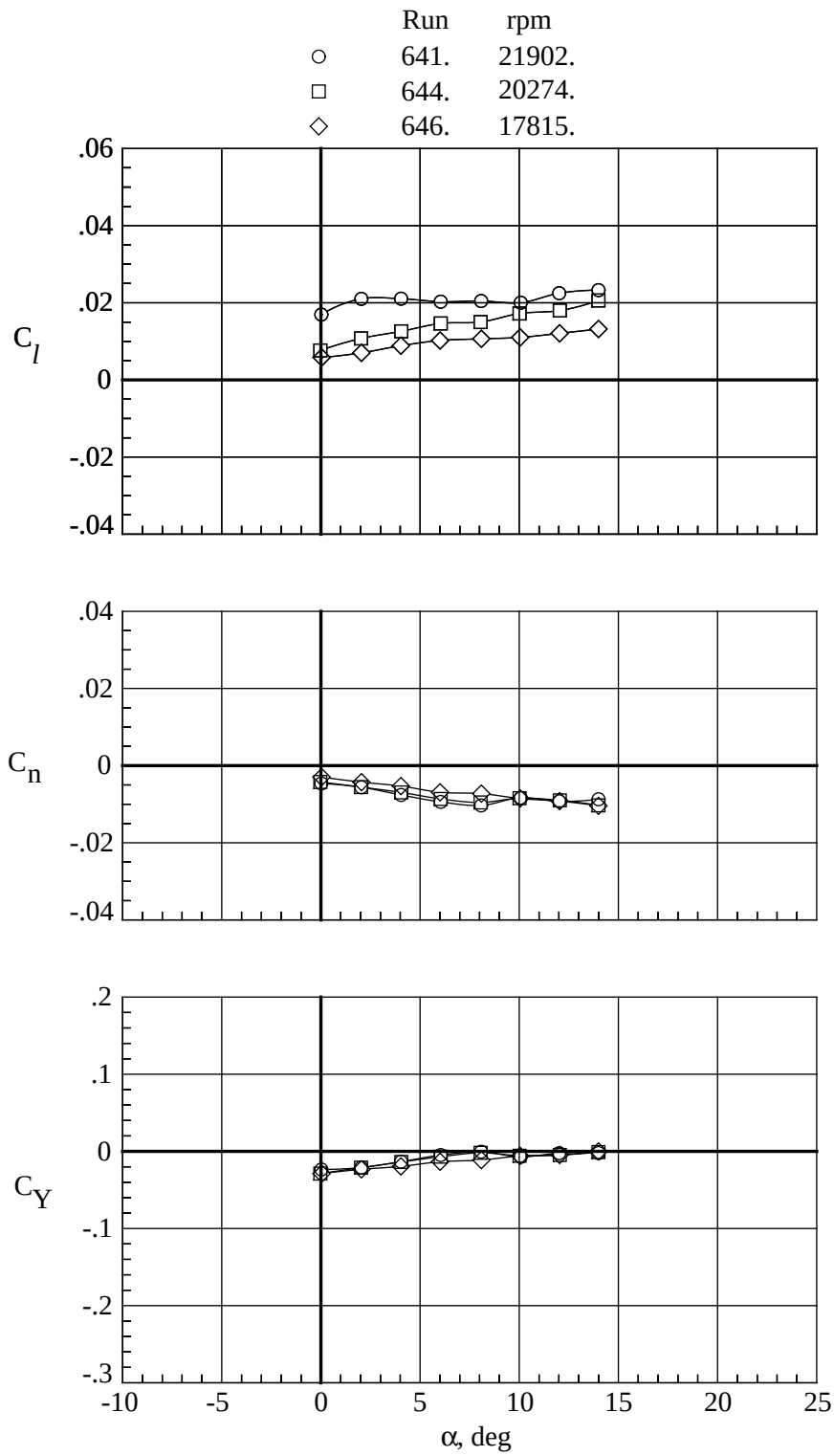

(c) *H/D* = 2.5.

Figure 24. Continued.

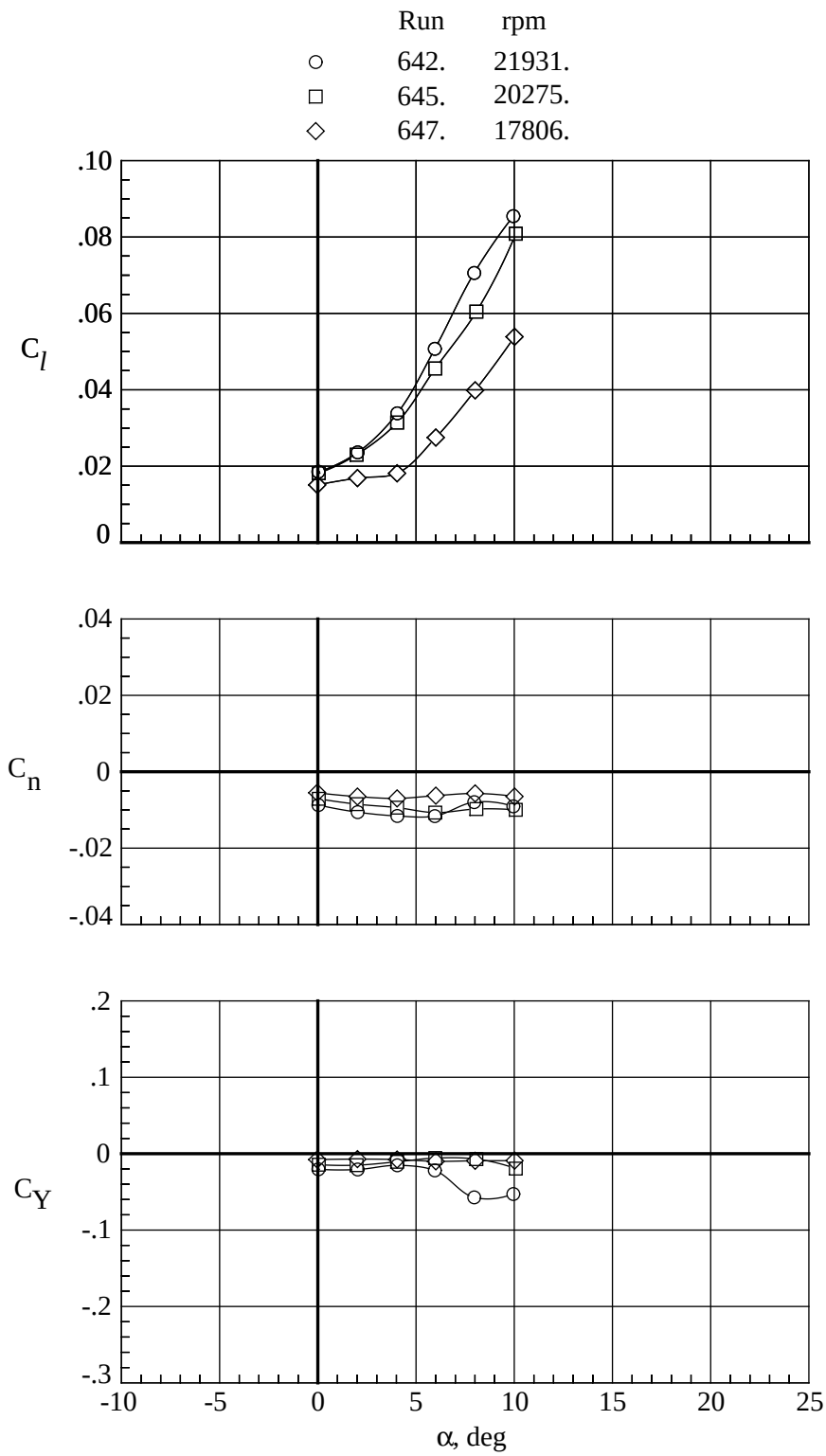

(d) *H/D* = 1.3.

Figure 24. Concluded.

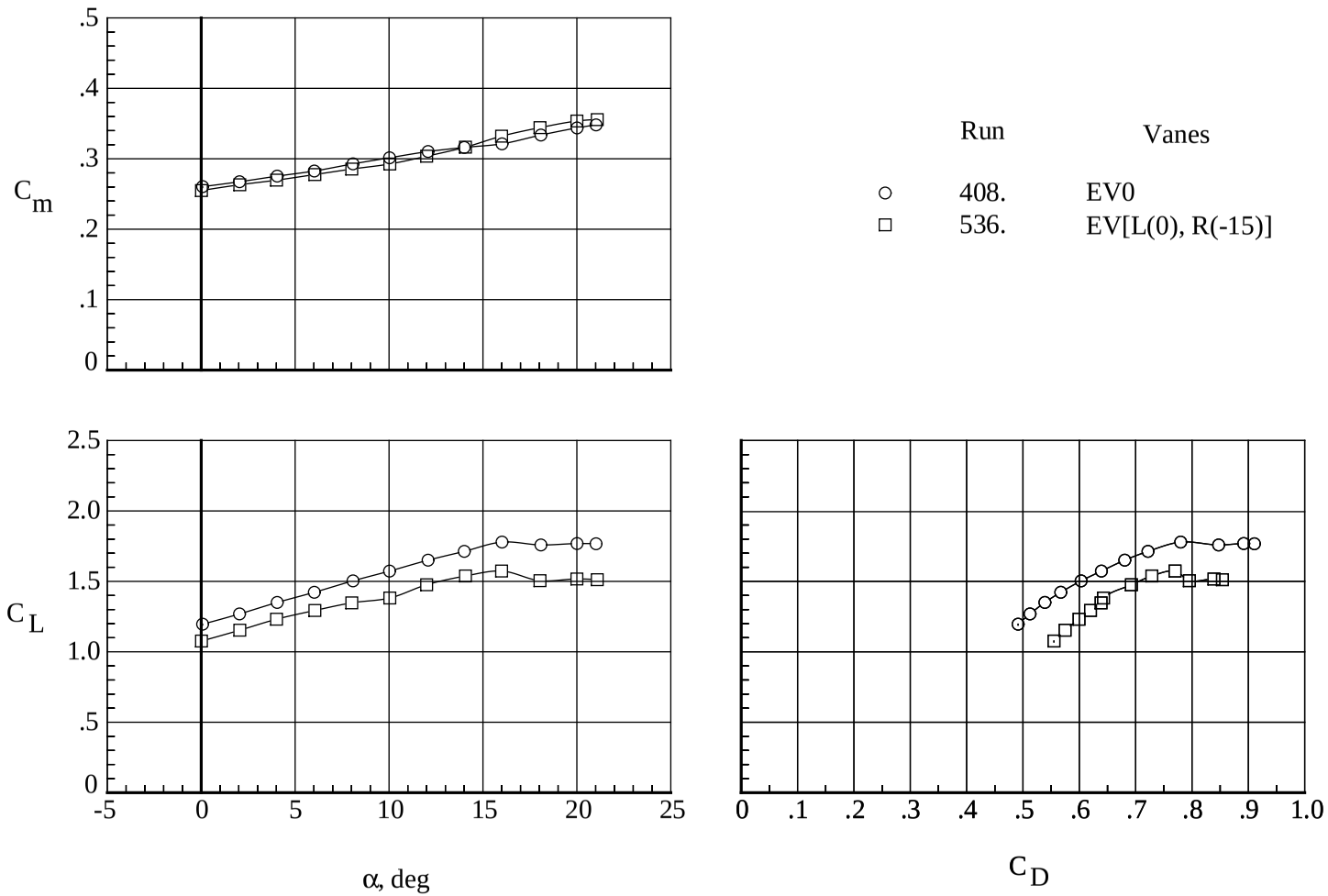

(a) C_m, C_L, and C_D.

Figure 25. Effect of vane configurations EV0 and EV[L(0), R(−15)] on variation of C_m, C_L, C_l, C_n, and C_Y with angle of attack and C_L with C_D (22000 rpm and H/D = 5.4).

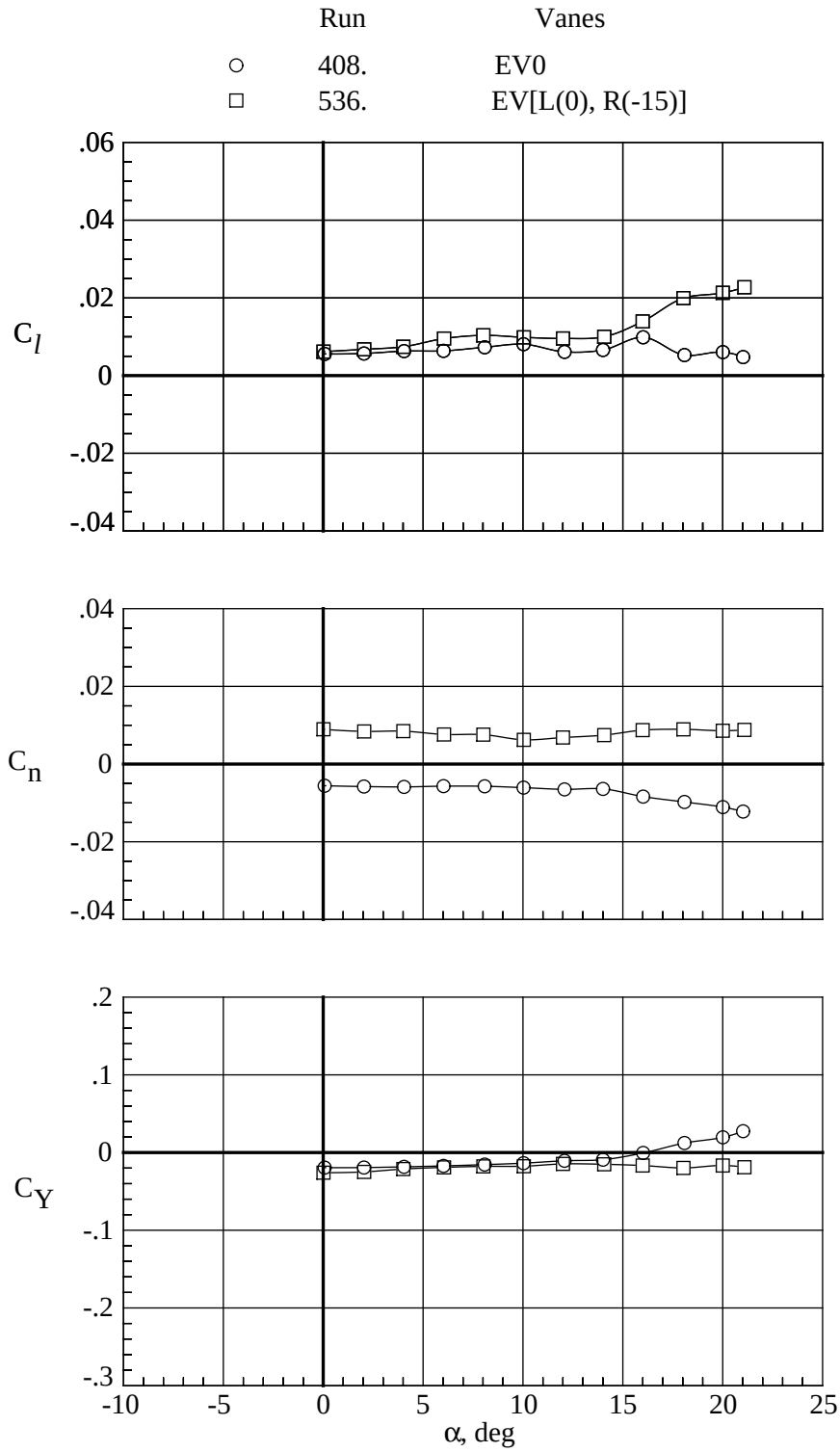

(b) C_l, C_n, and C_Y.

Figure 25. Concluded.

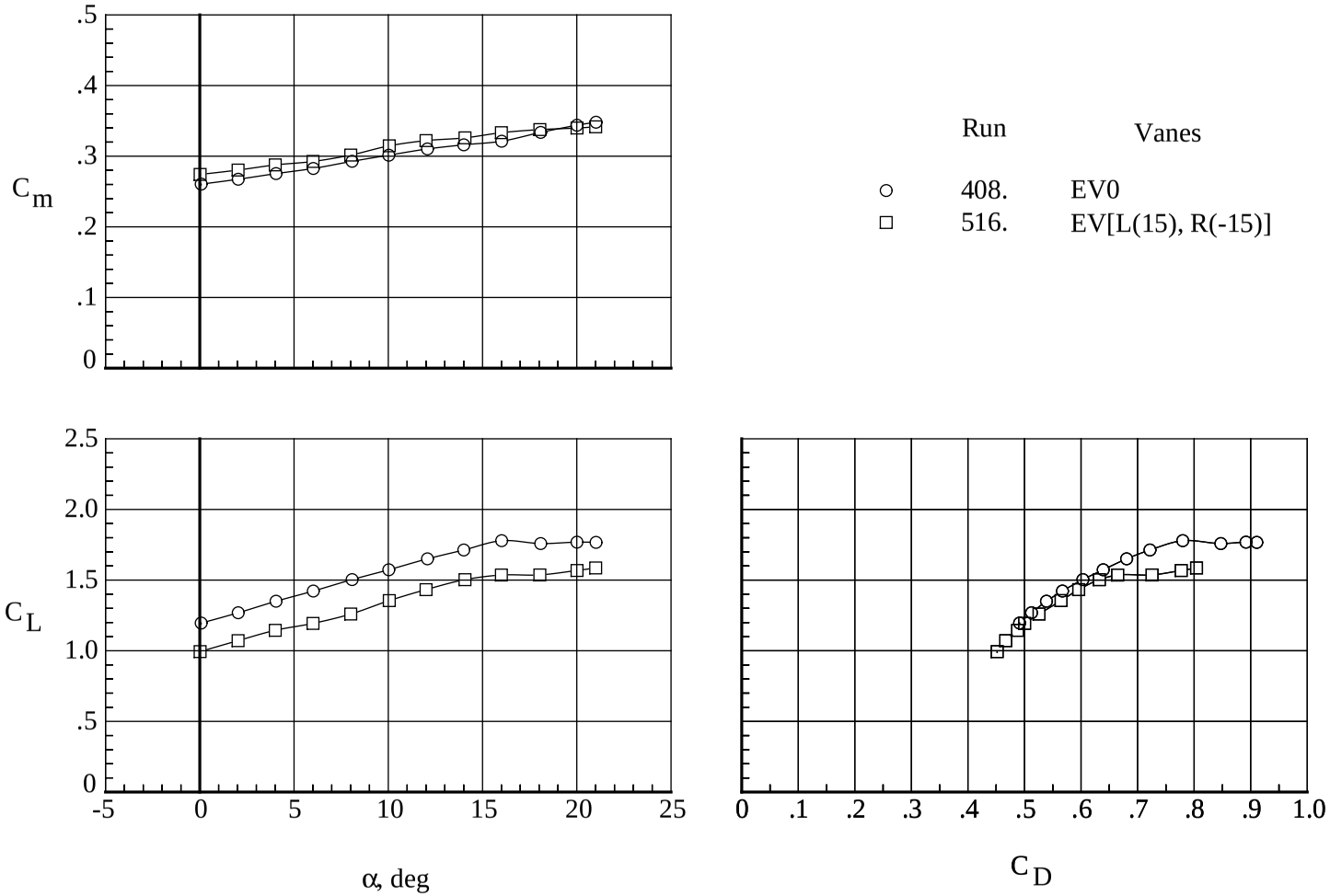

(a) C_m, C_L, and C_D.

Figure 26. Effect of vane configurations EV0 and EV[L(15), R(−15)] on variation of C_m, C_L, C_l, C_n, and C_Y with angle of attack and C_L with C_D (22 000 rpm and H/D = 5.4).

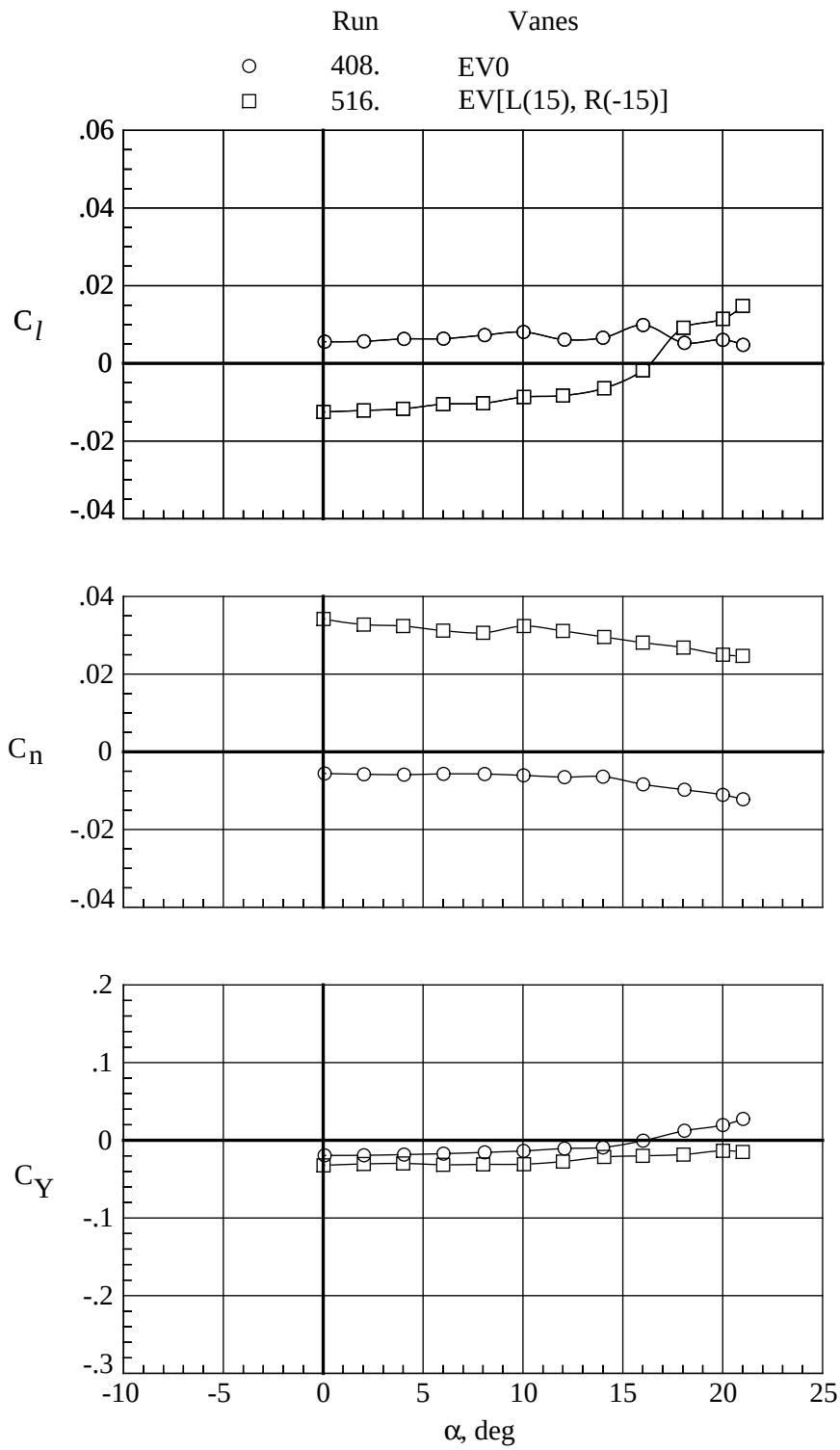

(b) C_l, C_n, and C_Y.

Figure 26. Concluded.

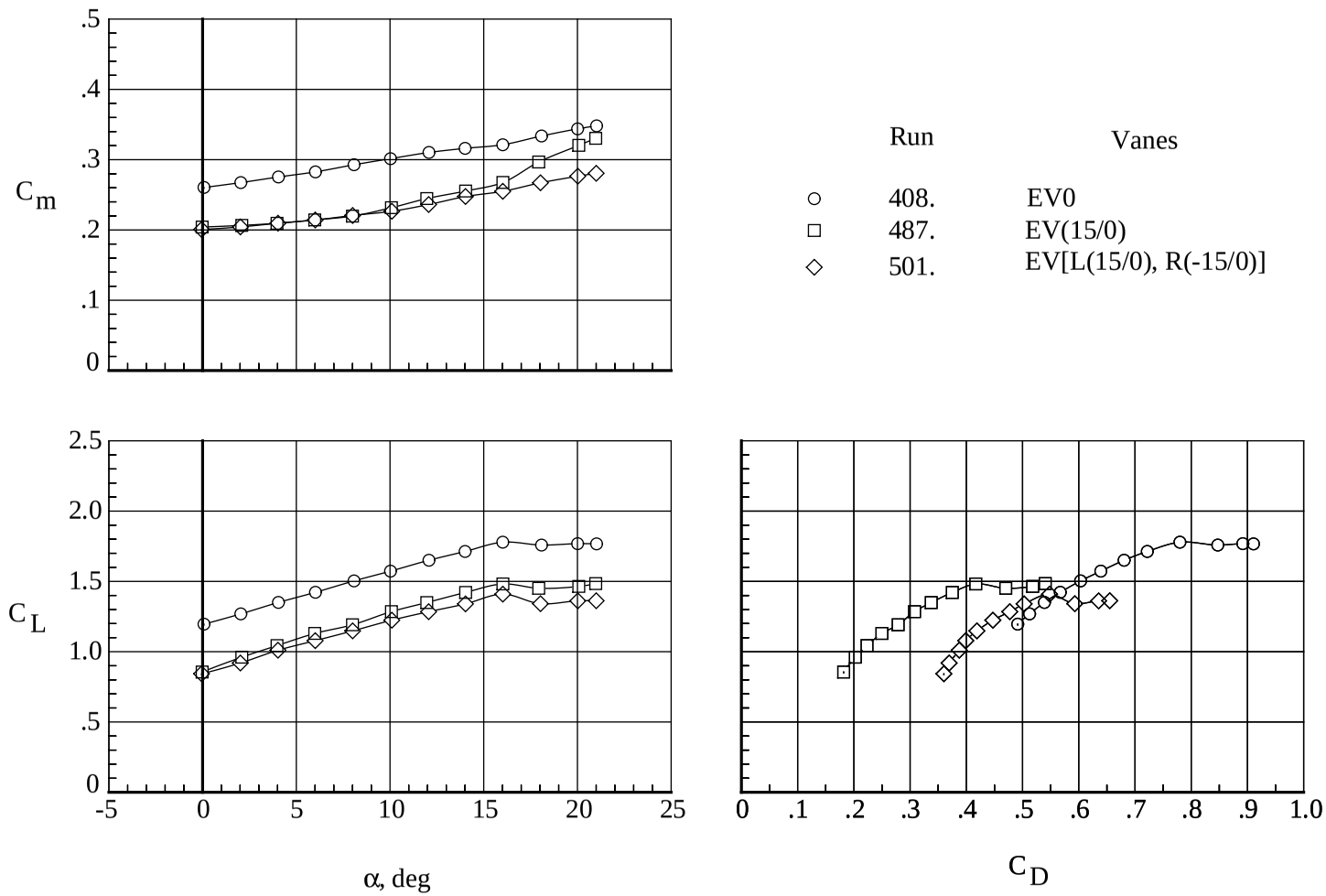

(a) C_m, C_L, and C_D.

Figure 27. Effect of vane configurations EV0 and EV[L(15/0), R(−15/0)] on variation of C_m, C_L, C_l, C_n, and C_Y with angle of attack and C_L with C_D (22000 rpm and H/D = 5.4).

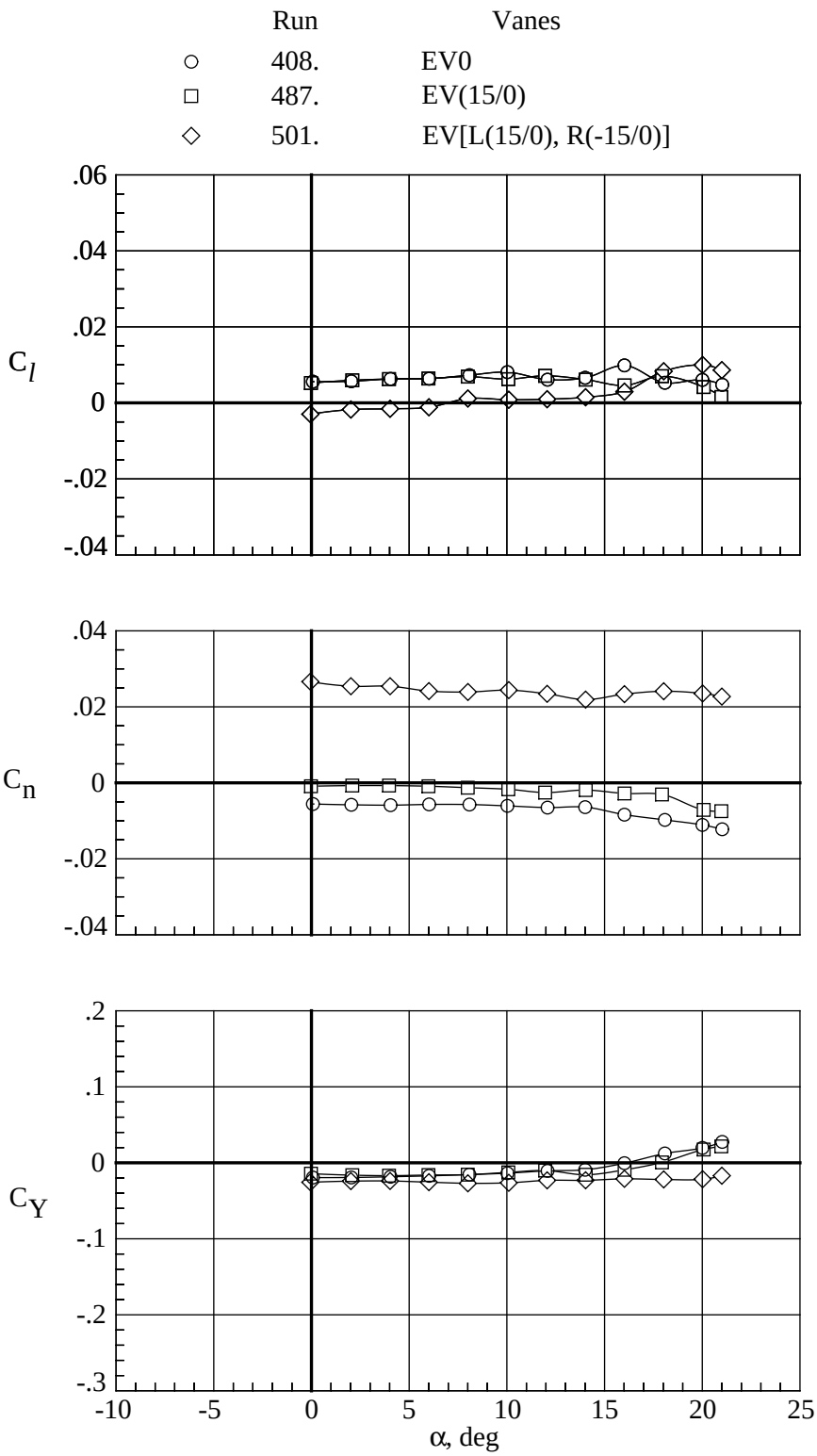

(b) C_l, C_n, and C_Y.

Figure 27. Concluded.

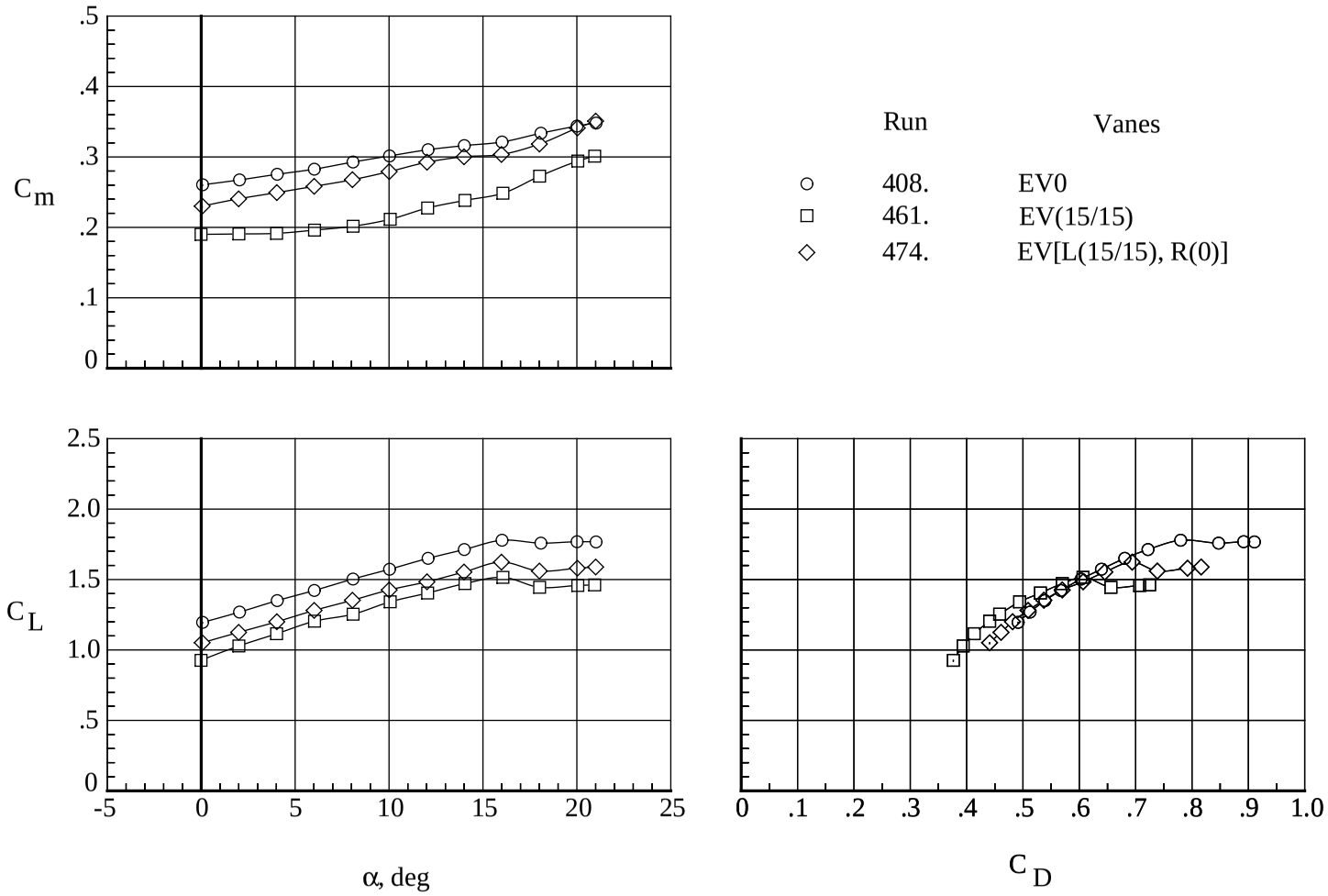

(a) C_m, C_L, and C_D.

Figure 28. Effect of vane configurations EV0, EV(15/15), and EV[L(15/15), R(0)] on variation of C_m, C_L, C_D, C_l, C_n, and C_Y (22000 rpm and H/D = 5.4).

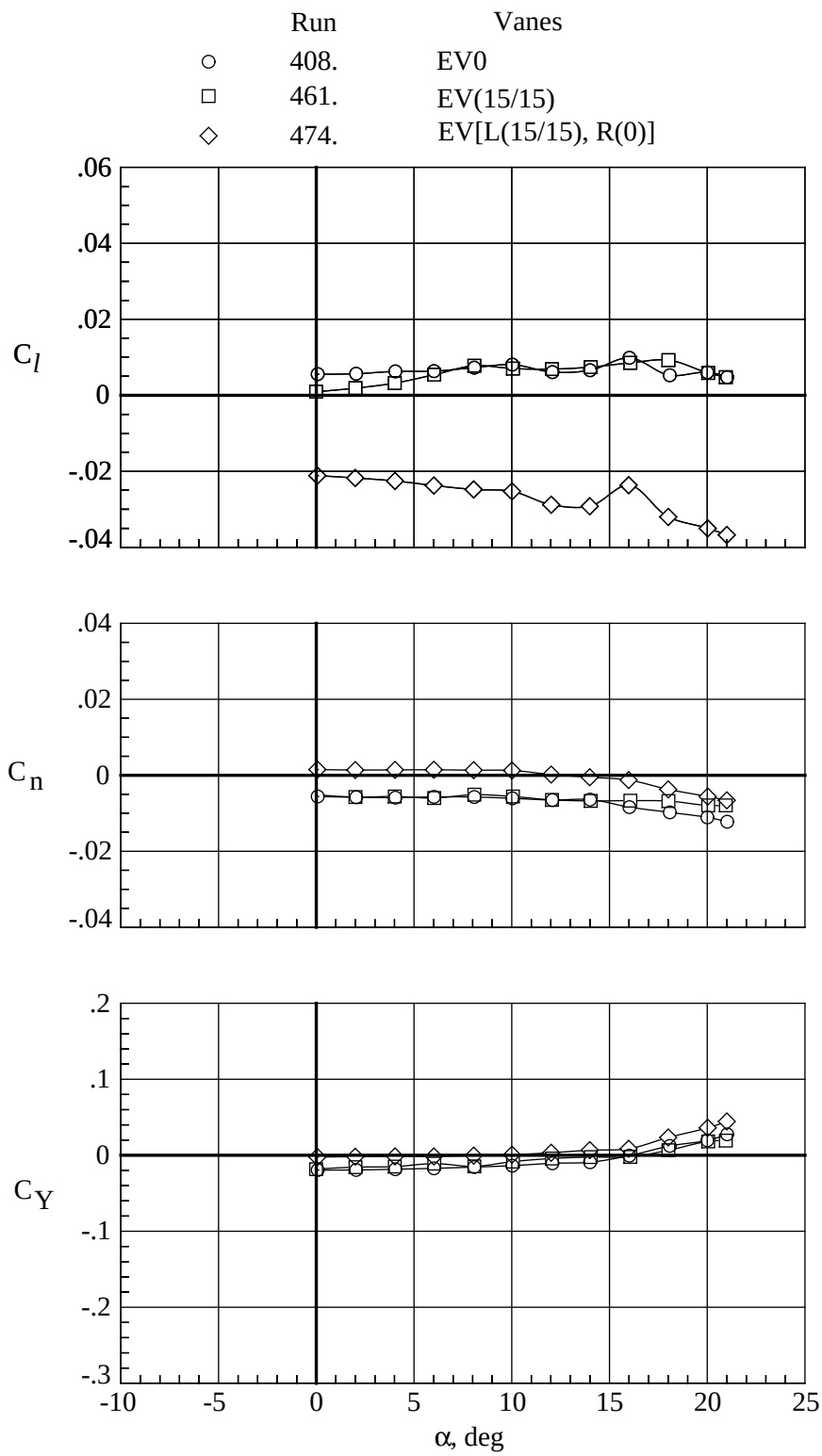

(b) C_l, C_n, and C_Y.

Figure 28. Concluded.

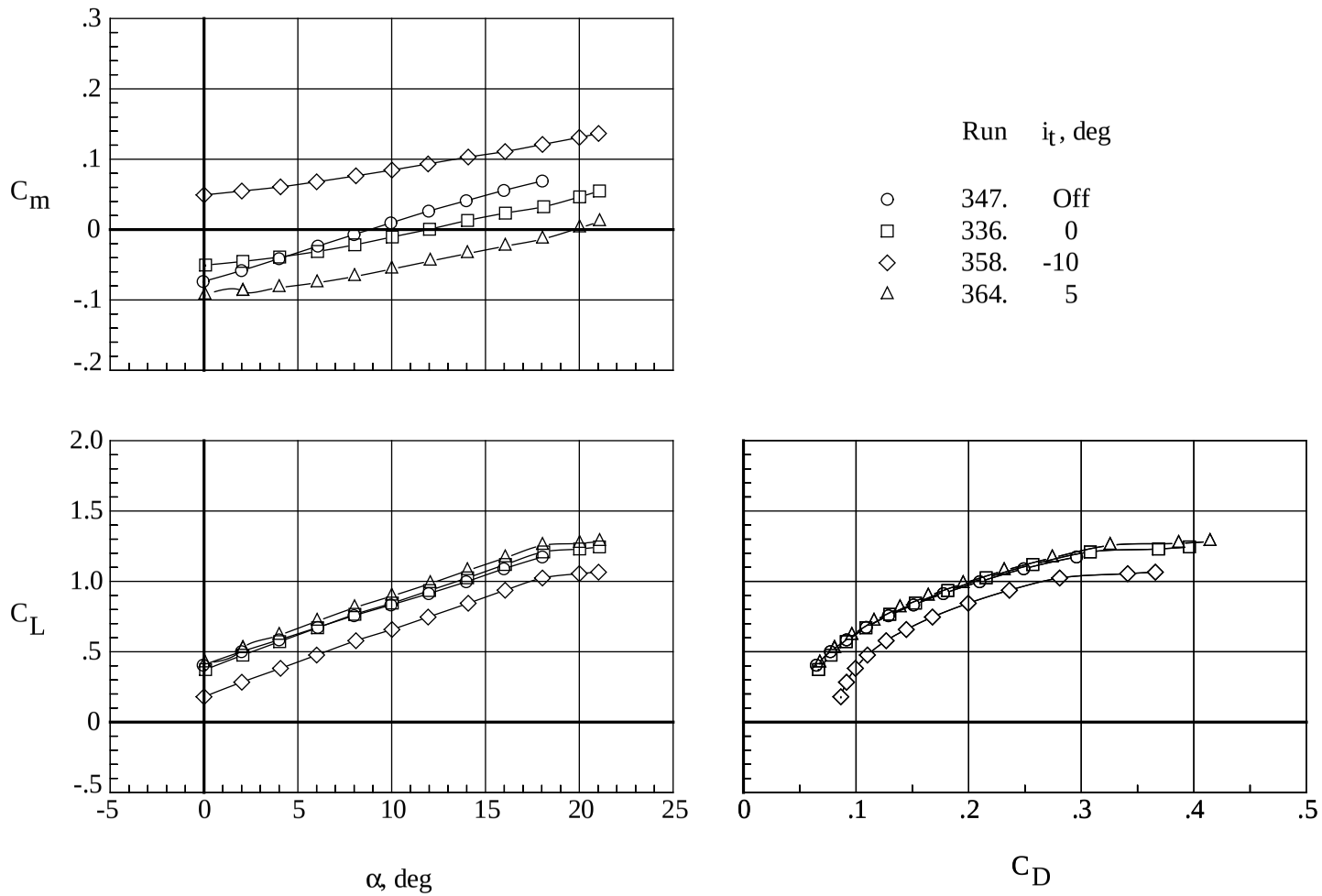

(a) *H/D* = 5.4.

Figure 29. Effect of tail incidence on variation of C_m and C_L with angle of attack and C_L with C_D for six values of *H/D* for B* G D1(c).

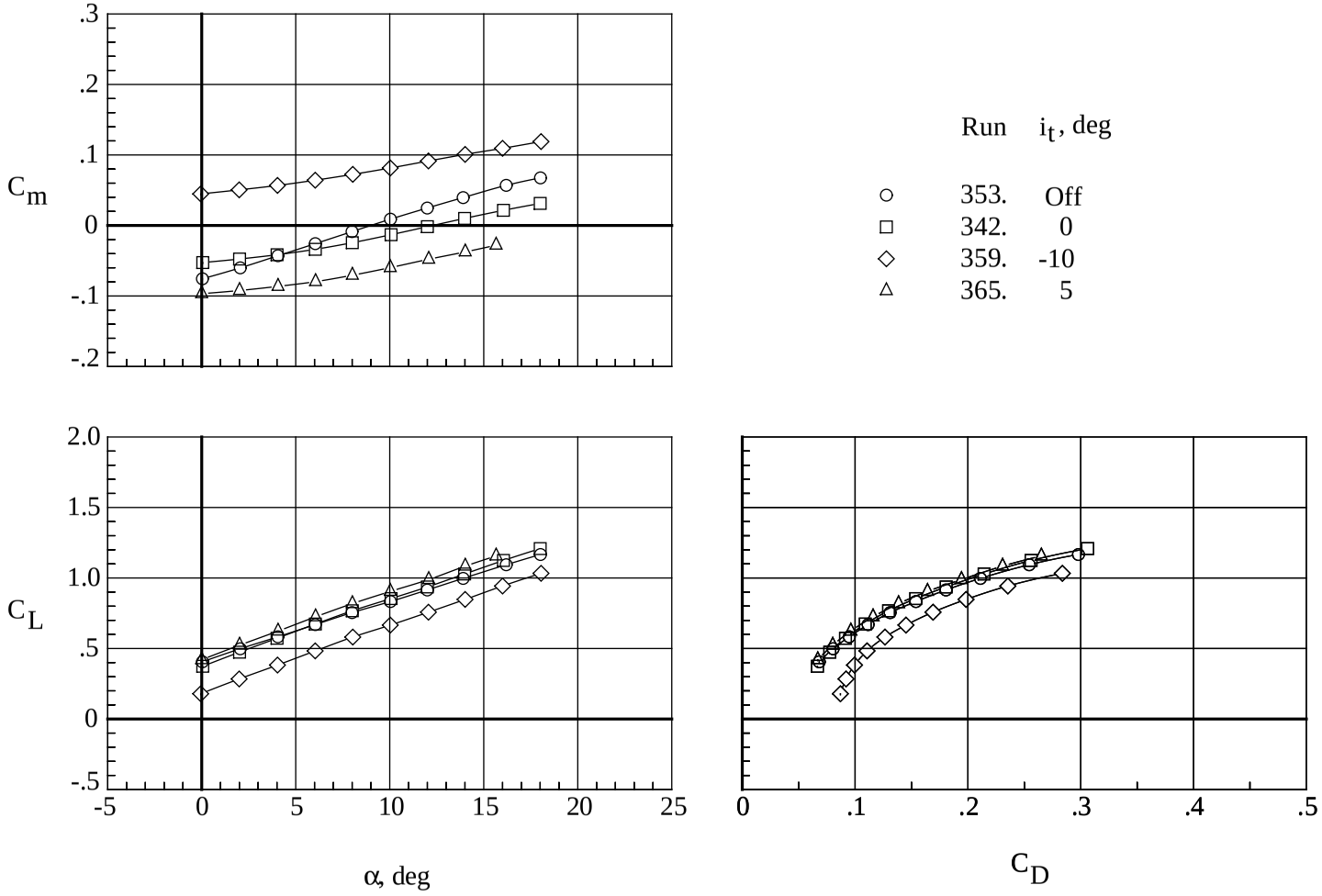

(b) *H/D* = 4.0.

Figure 29. Continued.

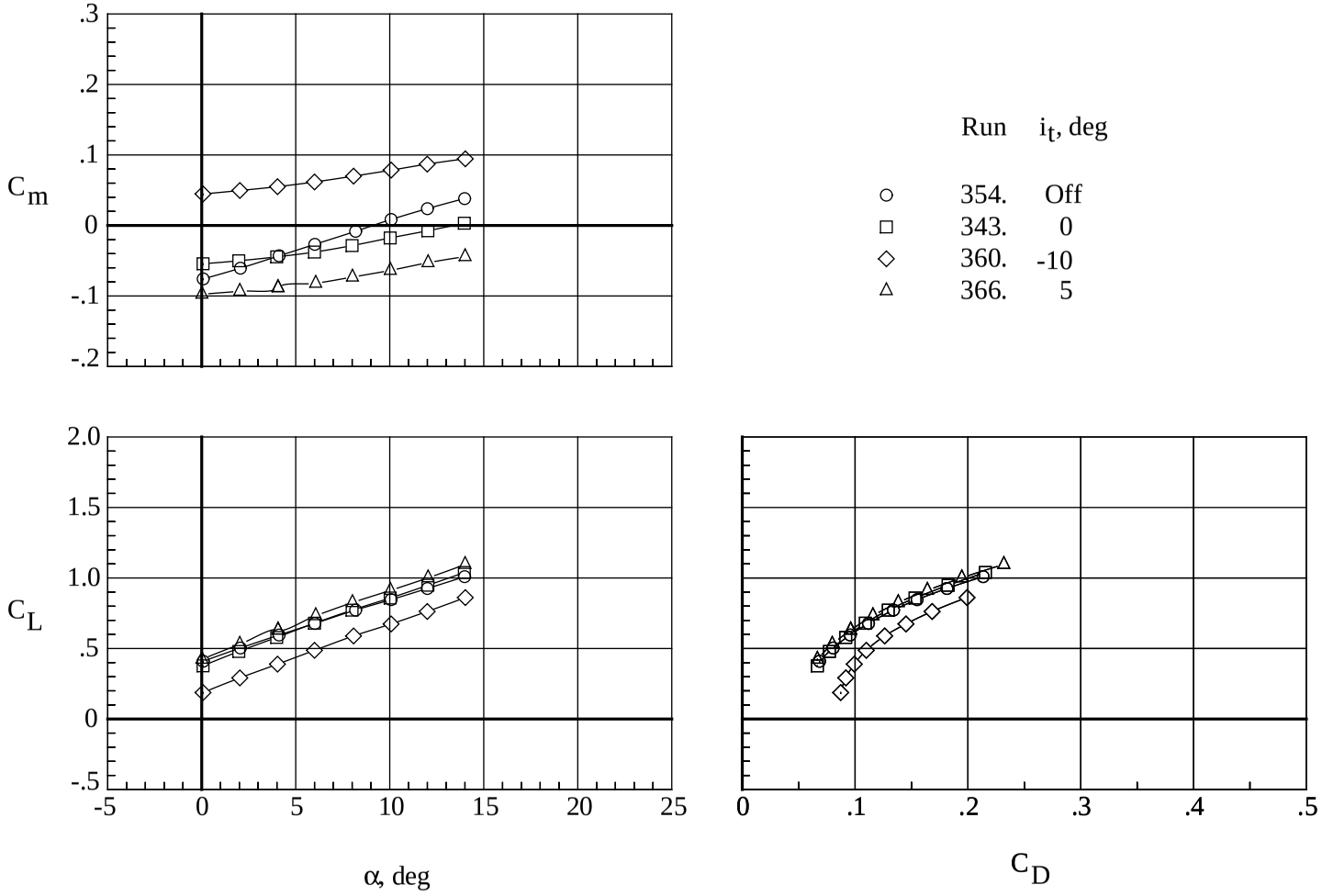

(c) *H/D* = 3.0.

Figure 29. Continued.

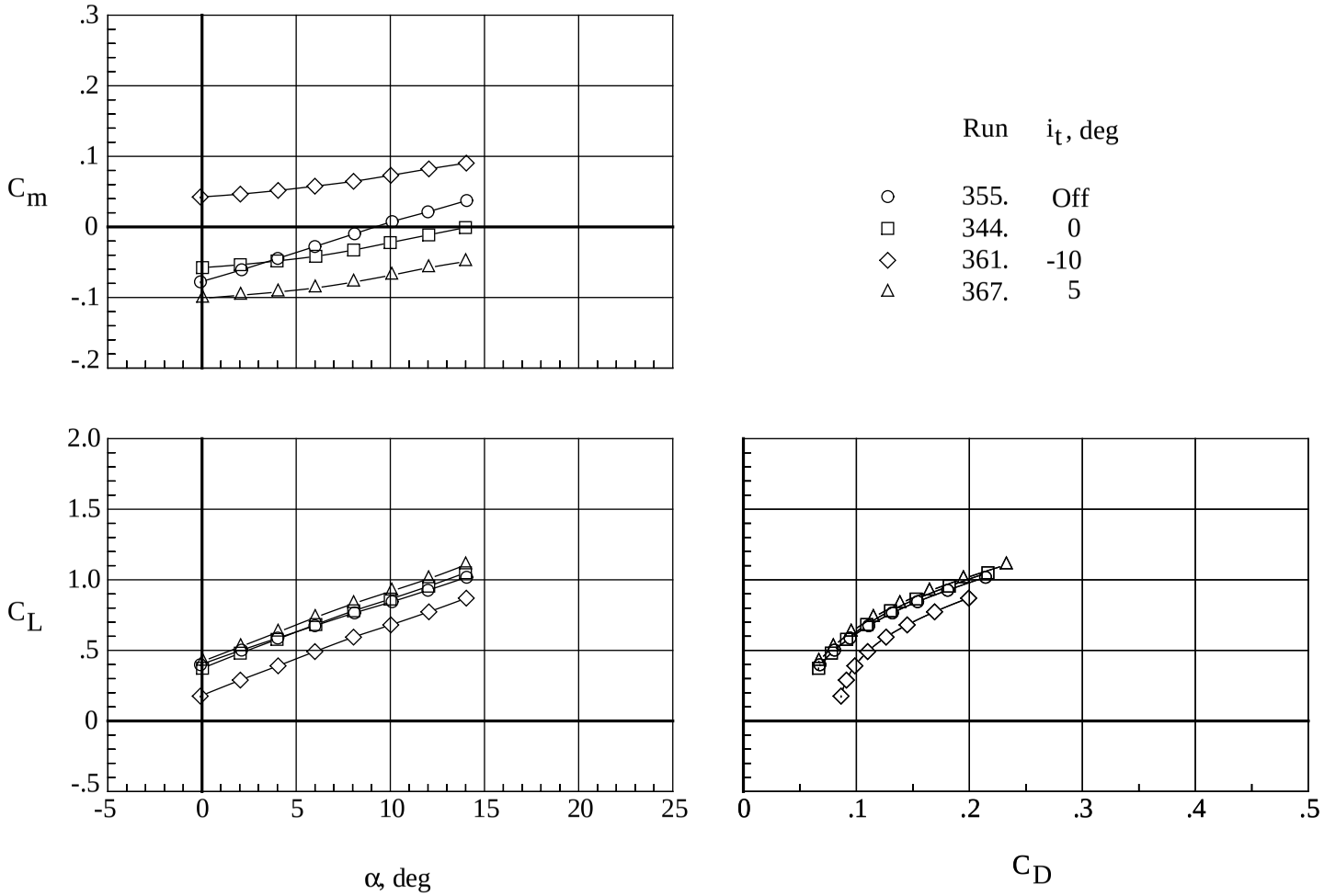

(d) *H/D* = 2.5.

Figure 29. Continued.

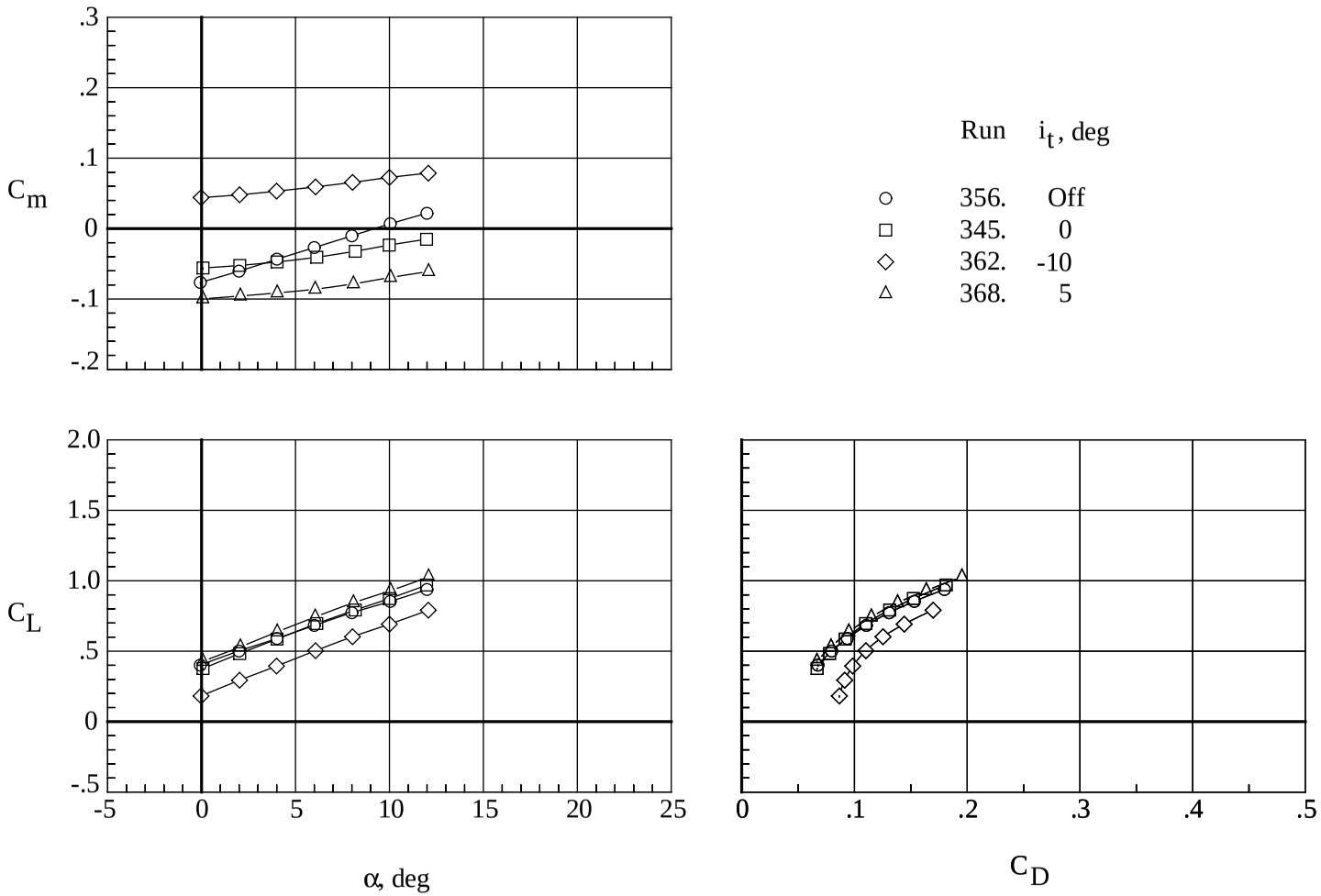

(e) *H/D* = 2.0.

Figure 29. Continued.

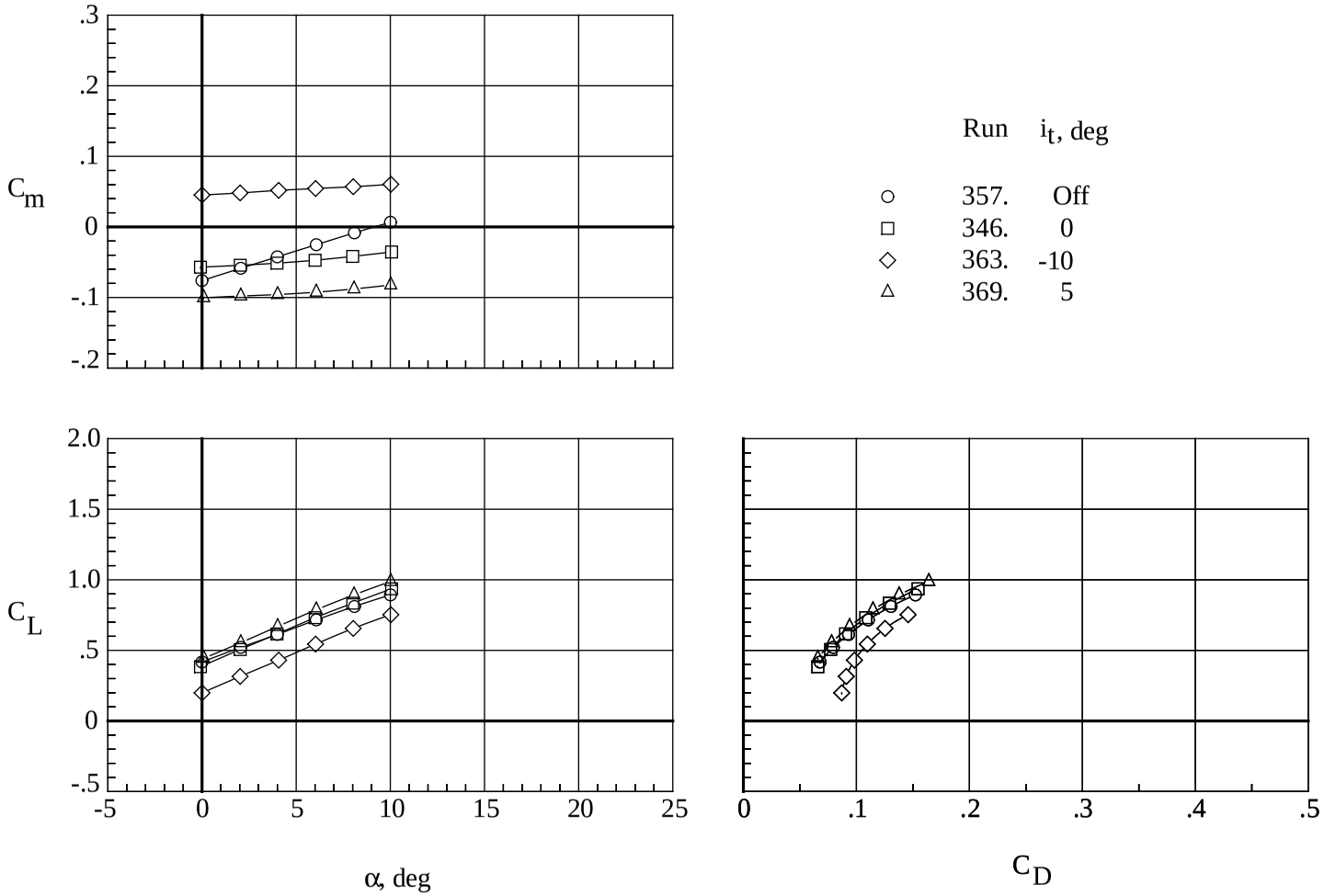

(f) *H/D* = 1.3.

Figure 29. Concluded.

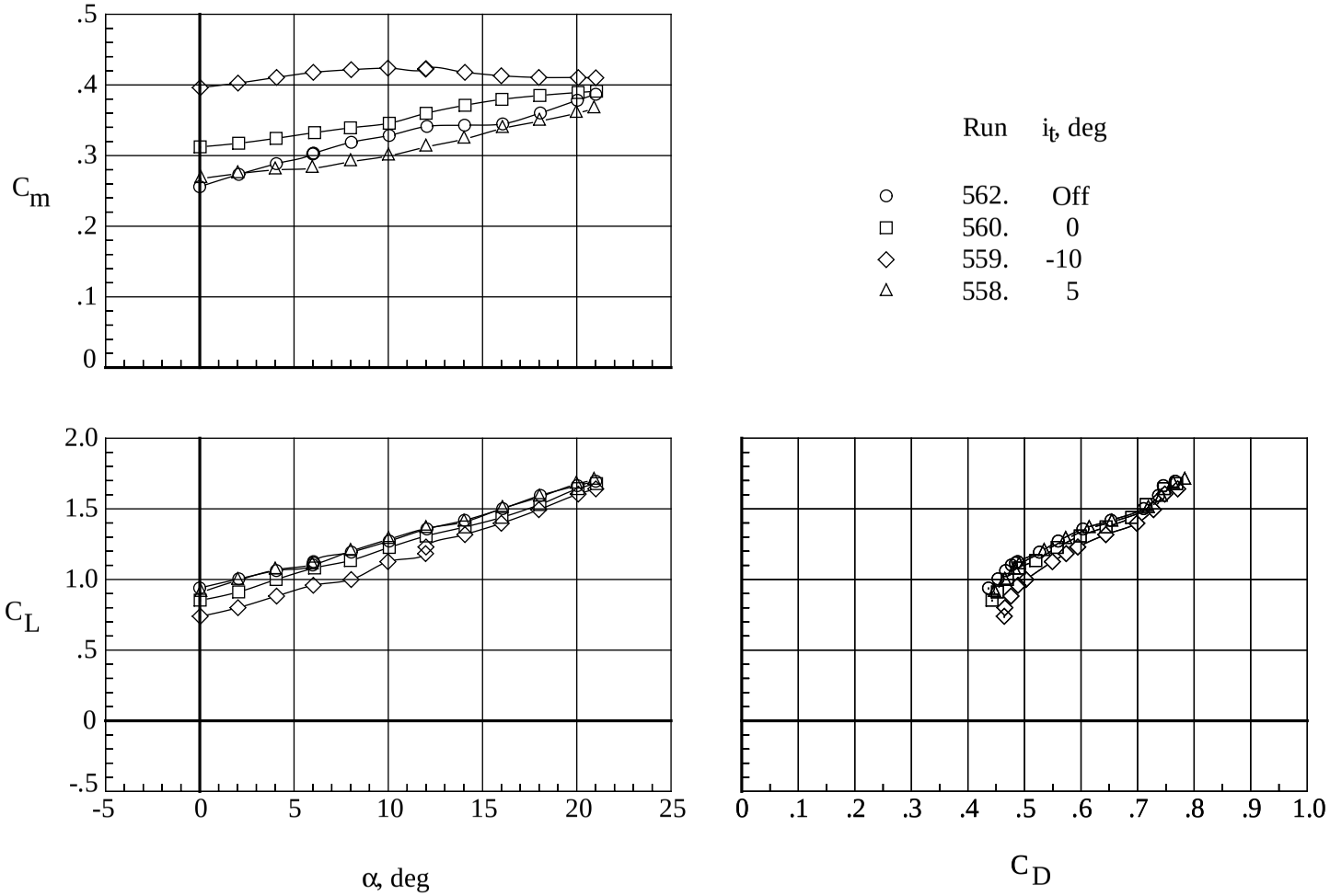

Figure 30. Effect of tail incidence on variation of C_m and C_L with angle of attack and C_L with C_D for W5 B6 D1 (22000 rpm and H/D = 5.4).

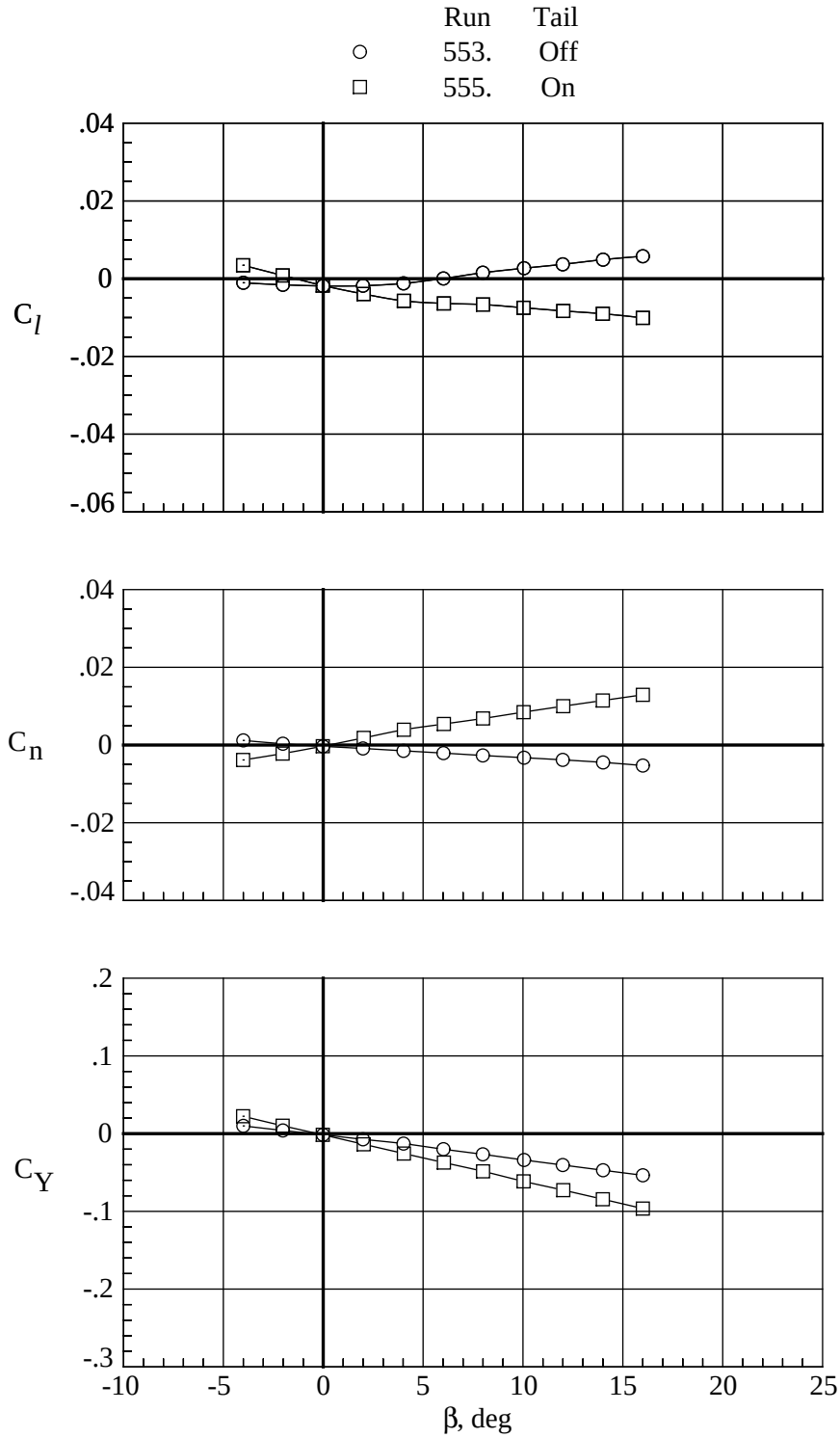

Figure 31. Effect of tail incidence on variation of C_l, C_n, and C_Y with angle of sideslip for W5 B6 D1(c) (H/D = 5.4 and $\alpha = 0°$).

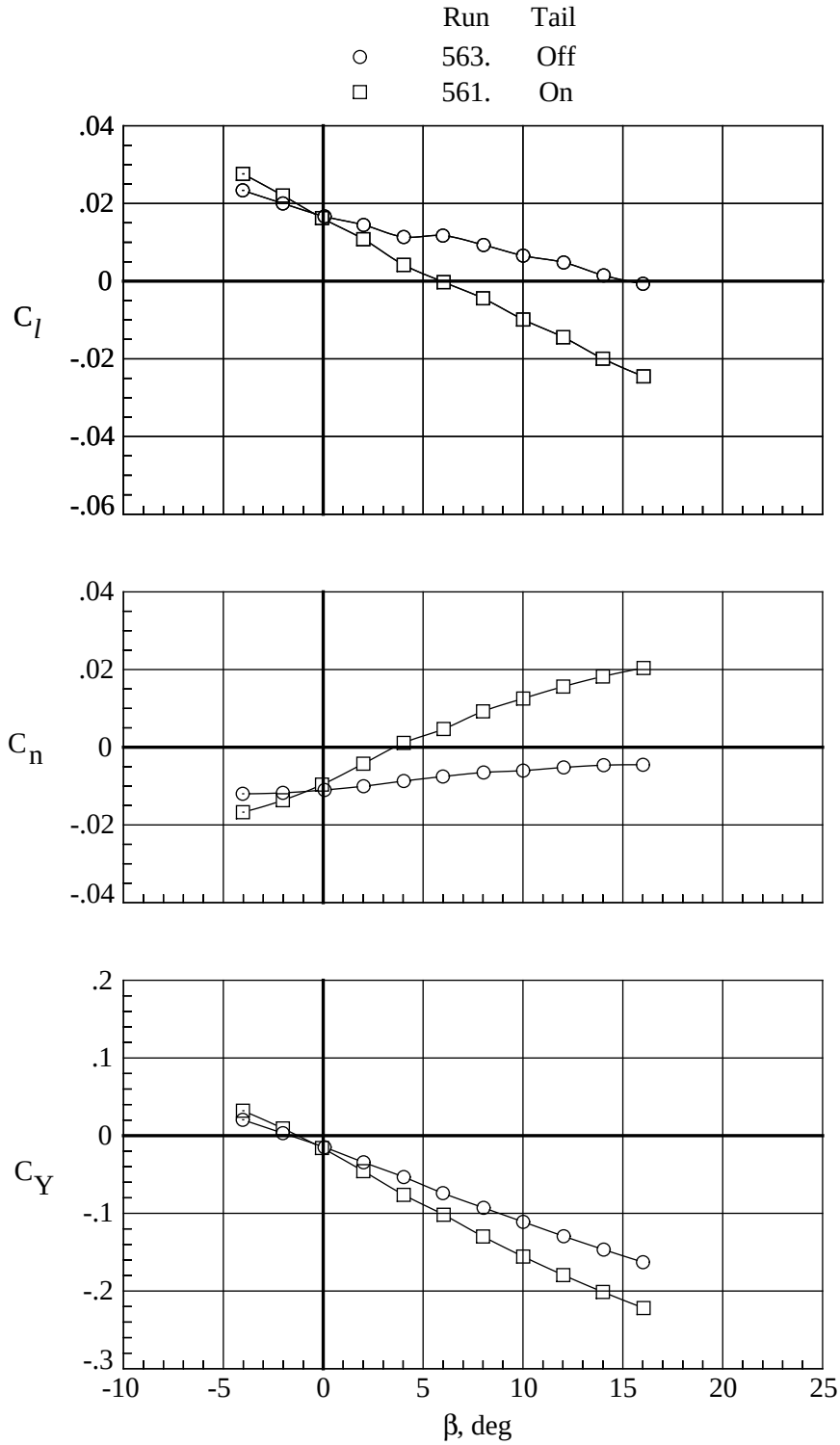

Figure 32. Effect of tail on variation of C_l, C_n, and C_Y with angle of sideslip for W5 B6 D1 EV0 (H/D = 5.4, α = 0°, and 22000 rpm).

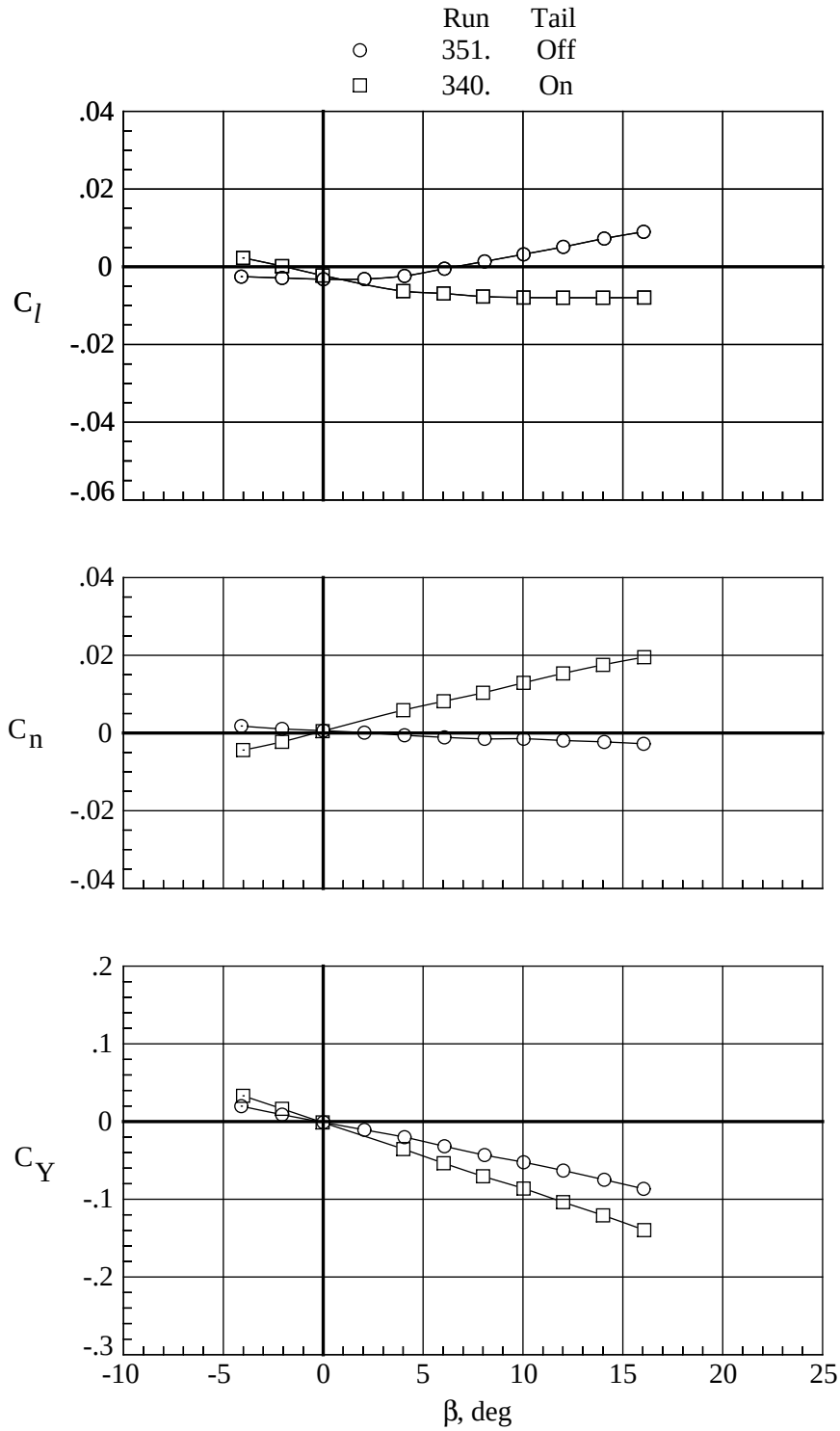

Figure 33. Effect of tail on variation of C_l, C_n, and C_Y with angle of sideslip for B* G D1(c) (H/D = 5.4 and α = 0°).

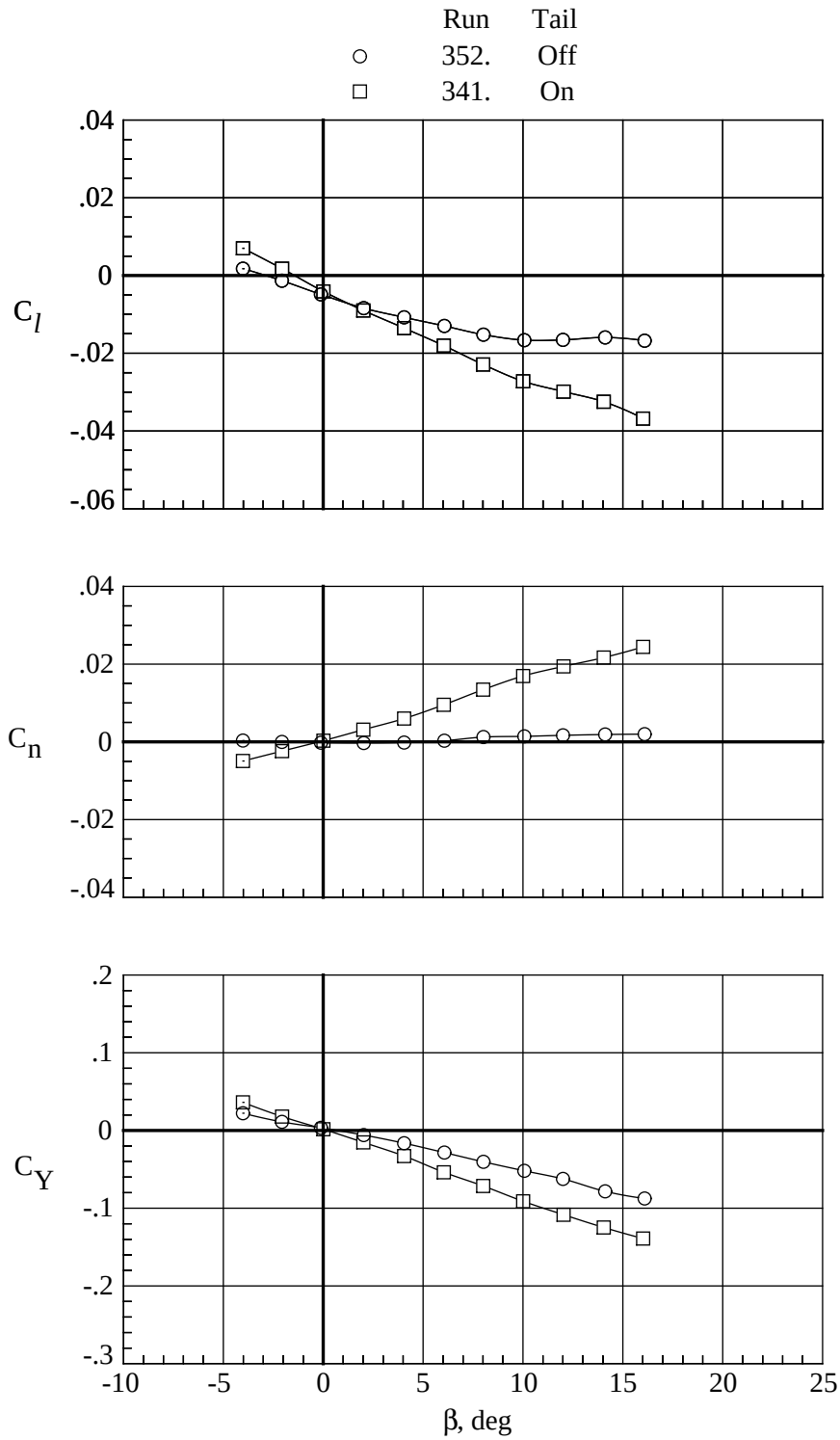

Figure 34. Effect of tail on variation of C_l, C_n, and C_Y with angle of sideslip for B* G D1(c) (H/D = 5.4 and α = 15°).

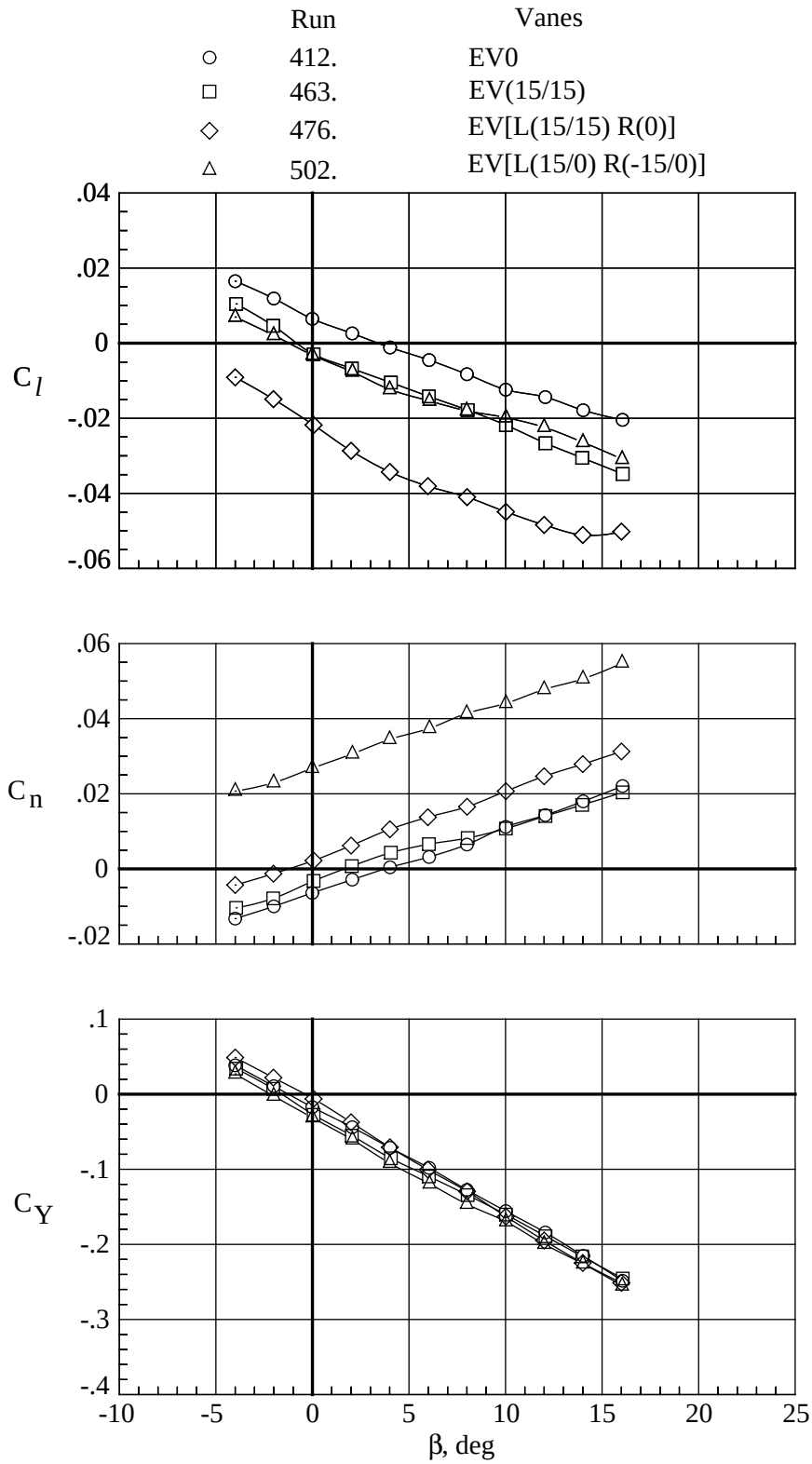

Figure 35. Effect of several vane configurations (EV0, EV(15/15), EV[L(15/15), R(0)], and EV[L(15/0), R(−15/0)]) on variation of C_l, C_n, and C_Y with angle of sideslip for B* G D1 T (22000 rpm, H/D = 5.4, and α = 0°).

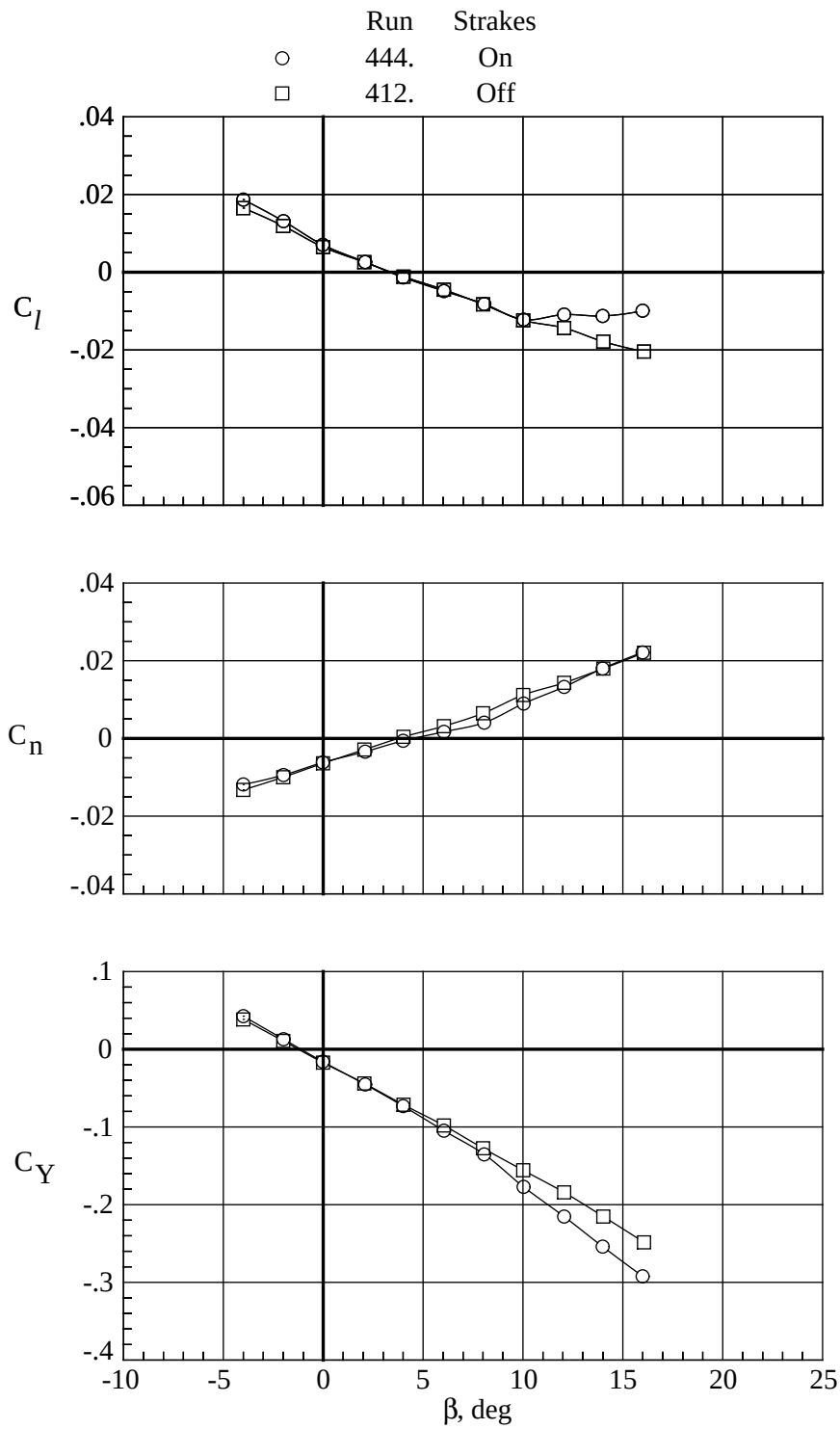

Figure 36. Effect of strake FS2 on variation of C_l, C_n, and C_Y with angle of sideslip for B* G D1 T FS2 EV0 (22000 rpm, H/D = 5.4, and α = 0°).

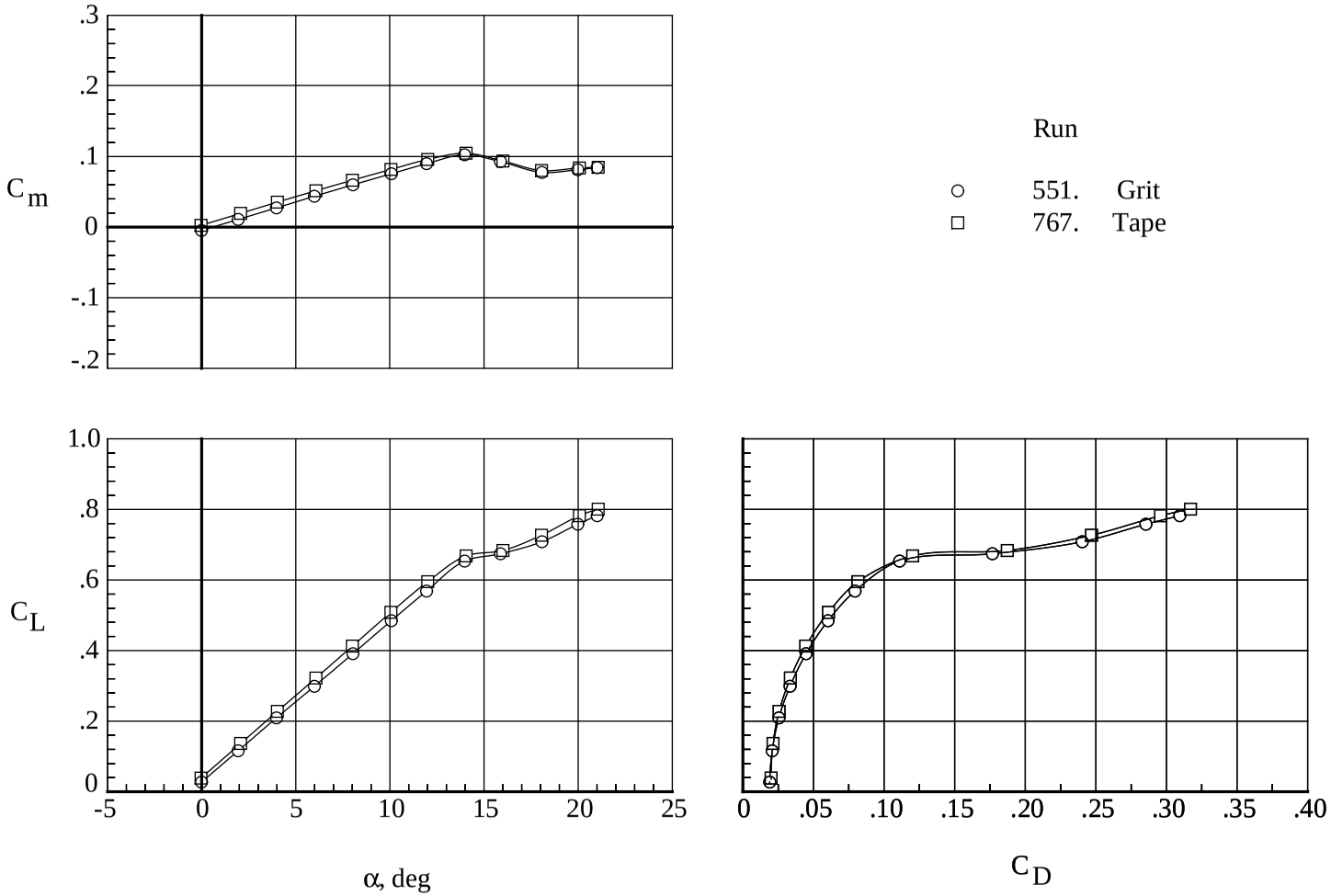

Figure 37. Comparison of boundary layer tripping with #80 grit and “pinked” tape for variation of C_m and C_L with angle of attack and C_L with C_D for W5 B6 D1(c).

REPORT DOCUMENTATION PAGE

Form Approved
OMB No. 0704-0188

1. AGENCY USE ONLY *(Leave blank)*

2. REPORT DATE
May 1996

3. REPORT TYPE AND DATES COVERED
Technical Memorandum

4. TITLE AND SUBTITLE
Wind Tunnel Test Results of a 1/8-Scale Fan-in-Wing Model

5. FUNDING NUMBERS
WU 505-59-87-92
PR 1L161102AH45

6. AUTHOR(S)
John C. Wilson, Garl L. Gentry, and Susan A. Gorton

7. PERFORMING ORGANIZATION NAME(S) AND ADDRESS(ES)
NASA Langley Research Center
Hampton, VA 23681-0001

Joint Research Program Office
Aeroflightdynamics Directorate
U.S. Army Aviation and Troop Command
NASA Langley Research Center
Hampton, VA 23681-0001

8. PERFORMING ORGANIZATION REPORT NUMBER
L-17448

9. SPONSORING/MONITORING AGENCY NAME(S) AND ADDRESS(ES)
National Aeronautics and Space Administration
Washington, DC 20546-0001
and
U.S. Army Aviation and Troop Command
St. Louis, MO 63120-1798

10. SPONSORING/MONITORING AGENCY REPORT NUMBER
NASA TM-4710
ATCOM TR-96-A-005

11. SUPPLEMENTARY NOTES
Wilson and Gorton: JRPO, Aeroflightdynamics Directorate, ATCOM, Langley Research Center, Hampton, VA; Gentry: Langley Research Center, Hampton, VA.

12a. DISTRIBUTION/AVAILABILITY STATEMENT
Unclassified–Unlimited
Subject Category 02
Availability: NASA CASI (301) 621-0390

12b. DISTRIBUTION CODE

13. ABSTRACT *(Maximum 200 words)*
A 1/8-scale model of a fan-in-wing concept considered for development by Grumman Aerospace Corporation for the U.S. Army was tested in the Langley 14- by 22-Foot Subsonic Tunnel. Hover testing, which included height above a pressure-instrumented ground plane, angle of pitch, and angle of roll for a range of fan thrust, was conducted in a model preparation area near the tunnel. The air loads and surface pressures on the model were measured for several configurations in the model preparation area and in the tunnel. The major hover configuration change was varying the angles of the vanes attached to the exit of the fans for producing propulsive force. As the model height above the ground was decreased, there was a significant variation of thrust-removed normal force with constant fan speed. The greatest variation was generally for the height-to-fan exit diameter ratio of less than 2.5; the variation was reduced by deflecting fan exit flow outboard with the vanes. In the tunnel angles of pitch and sideslip, height above the tunnel floor, and wind speed were varied for a range of fan thrust and different vane angle configurations. Other configuration features such as flap deflections and tail incidence were evaluated as well. Though the V-tail empennage provided an increase in static longitudinal stability, the total model configuration remained unstable.

14. SUBJECT TERMS
Fan-in-wing; Ducted fan; Powered lift; Ground effects

15. NUMBER OF PAGES
83

16. PRICE CODE
A05

17. SECURITY CLASSIFICATION OF REPORT
Unclassified

18. SECURITY CLASSIFICATION OF THIS PAGE
Unclassified

19. SECURITY CLASSIFICATION OF ABSTRACT
Unclassified

20. LIMITATION OF ABSTRACT